UNIVERSITY OF MALTA

Faculty of Engineering

Department of Metallurgy and Materials Engineering

FINAL YEAR PROJECT

B.ENG. (Hons.)

A Study on the Firing of Sourced Maltese Clay into a Usable Product

by

Luke Xuereb

A dissertation submitted in partial fulfilment of the requirements of the award of Bachelor of Engineering (Hons.) of the University of Malta

Copyright Notice

Abstract

The aim of this dissertation is to study the production of pottery from sourced Maltese clay through experimental firing. The clay sample was sourced from Il-Qolla hill in the vicinity of Rabat, Malta. The samples were then sieved through two different mesh sizes: 63 μm and 125 μm. The briquettes were manufactured from the sieved and dried clay and subsequently fired at temperatures of 500, 700 and 900 °C, with soaking times of 30 and 120 minutes, in both oxidising and reducing conditions. The mineralogical and structural modifications to the fired clay were examined by X-ray powder diffraction (XRPD) as well as optical and scanning electron microscopy (SEM). Finally, a Knoop hardness test was conducted to evaluate the hardness of the fired clay samples.

The colour, porosity and voids, microstructure, mineralogy, and material hardness, were all observed to alter with increasing firing temperature. This highlights that firing temperature is the parameter which affects the outcome of the fired clay more than all other criteria considered in this study. An increase in firing temperature resulted in sintering and transformation to a more compact structure. Calcite was observed to decompose in the temperature range of 900 °C, forming calcium oxide, which reacted with the quartz present in the microstructure to form wollastonite in the process. Briquettes fired at higher temperatures exhibited a harder microstructure, showing that the ceramic transformation has occurred more completely. Ceramics fired in oxidising conditions exhibited higher hardness results than those fired in reducing conditions.

Acknowledgements

I would firstly like to express my deepest appreciation to my tutor, Dr. Daniel Vella and co-supervisor, Dr. Ing. John Betts for their constant support, guidance and patience throughout this study. Without their help I would never have brought this study to fruition.

I am also grateful to Ms. Emma Richard-Tremeau for her massive help, encouragement and patience throughout this journey. Thanks for all the time you have dedicated despite having other work to do. Special thanks also goes to Ms. Maria Vella from the Department of Classics and Archaeology for always offering a helping hand when needed.

I would like to acknowledge the assistance of Mr. Daniel Dimech, Mr. Noel Tonna, Ing. James Camilleri, Mr Andrew Agius, Mr Nicholas Gingell and Ing. Mary Grace Micallef from the Department of Metallurgy and Materials Engineering for their lending hand throughout the experiments. Thank you all for your patience! I would also like to recognize the assistance of Ing. John Paul Borg from the Department of Industrial and Manufacturing Engineering for preparing the mould for the experiment.

Special thanks goes to my friends and girlfriend. You made University bearable throughout these four years, and I am sure our friendship will last a lifetime. Thanks a lot!

Last but not least, I am extremely grateful to my parents, Moira and Stephen, for your constant and endless support throughout this journey. Thanks for all the encouragement when times were rough, thanks for proof-reading the study and for always believing in me. I promise you that all your efforts will help me achieve something great in the near future.

Thanks to my brother, Jake, for your support and for bearing with my mood swings. Thanks Bro! Finally, to my Maltese Terrier Ollie, the entertainer during the many short breaks and always at the receiving end of my constant pestering!

Table of Contents

List of Figures

List of Tables

List of Abbreviations

%WP	Water of Plasticity percentage
%LDS	Linear Drying Shrinkage percentage
XRPD	X-Ray Powder Diffraction
ERA	Environment and Resources Authority
SOP	Standard Operating Procedure
PTFE	Polytetrafluoroethylene
VCC	Visual Comparison Chart
SEM-EDS	Scanning Electron Microscopy-Energy Dispersive Spectroscopy
ASTM	American Society for Testing and Materials

List of Symbols

$Weight_{wet}$	Weight of the wet sampled clay
$Weight_{dry}$	Weight of the dry sampled clay
$Length_{wet}$	Length between the slab marks of the wet clay
$Length_{dry}$	Length between the slab marks of the dry clay
n	Integer
λ	Wavelength of the electrons
d	Spacing of the crystal planes
θ	Angle between incident wave and scattering planes
P	Applied load
d_{max}	Maximum indentation length

1. Introduction

This Chapter describes the background to the process of firing clay to produce a ceramic. This Section also presents the research question, aim and objectives of this dissertation.

1.1 Background

Clays have been used for the manufacture of pottery since the Neolithic period, dating back to approximately 4000 to 2200 BC [1-3]. One of the important phases of this procedure is firing, a thermal process by means of which raw clay is transformed into ceramics. This firing process transforms the physical, chemical and mineralogical properties of the material [4, 5]. The dissertation focus will be on the study of clays for the manufacture of pottery.

The properties of the final ceramic product are dependent not only on the mineral composition, but also the parameters of the stages of production including drying, manufacture and firing. A number of studies have reported on the mineralogical transformation during the firing procedure [6]; there are, however, no such studies on clays from the Maltese Islands. This dissertation focuses on the process of firing sourced Maltese clay from one location at various firing parameters including, different firing temperatures and furnace soaking times, under both oxidising and reducing conditions. The ceramic obtained is then characterised to determine its mineralogical, chemical and physical properties.

This dissertation is part of the “Compiling Fabric Identity for Pottery from Maltese Sites” or CoFIPoMS Project, which is a wider project launched in May 2020. This project researches local archaeological pottery production and clay found in the Maltese Islands [7]. This thesis will look into the behaviour of potential raw materials, which will assist archaeological research by developing a better understanding of the potential and constraints of using raw material from Malta, and would allow archaeologists to gain insights into the technological choices and actions of ancient potters.

1.2 Aims and Objectives

The research question of this thesis is:

'Can clay sourced from the Maltese Islands be converted into pottery?'.

The aim of this dissertation is to study the production of pottery from sourced Maltese clay through experimental firing. This aim is to be achieved through the following objectives:

- Collecting a clay sample from a site in the Maltese Islands;
- Manufacturing and drying briquettes for firing;
- Designing an experiment with various firing parameters; and
- Analysing and characterising the produced ceramic.

2. Literature Review

This Chapter provides a brief description on the geological formation of the Maltese Islands, followed by an introduction to clay minerals with special emphasis on kaolinite clay. Included in this literature review is the process of sieving, the manufacturing of briquettes, the different firing studies and characterisation techniques utilised in this experiment.

2.1 Geological Formation

2.1.1 Introduction

The Maltese Islands, situated in the middle of the Mediterranean Sea, consist of the islands of Malta, Gozo and Comino and other small islets such as Filfla and St. Paul's Islands [8]. The geology of the Maltese Archipelago forms a marine sedimentary rock sequence which has a thickness of approximately 250m [9].

The landscape and flora of the Maltese Islands reflect the geological formations as well as distinguish the lithologic sequence [10]. The Maltese Islands geology consist of five horizontal formations, each having different characteristics of both erosion resistance and hardness [8, 11].

The geological formation from top to bottom are:

1. Upper Coralline Limestone Formation
2. Greensand Formation
3. Blue Clay Formation
4. Globigerina Limestone Formation
5. Lower Coralline Formation

Since this dissertation concentrates on ceramics which are derived from clay, the extraction of clay itself might have within it, eroded material from the Upper Coralline Limestone, Greensand and Blue Clay formation, together with wind-blown debris.

2.1.2 Greensand Formation

The Greensand layer usually has a thickness between 0.5 and 11m, however in Malta, the thickness is less than 0.5m or completely missing. In Gozo, studies show that this formation can reach the maximum thickness of 11m at Gelmus Hill [9, 12].

This layer is made up of a glauconitic sand bed and consists of very dark glauconitic marly limestone. It is black in colour because it is unexposed, however, due to the presence of iron oxides and oxidation, pale-yellow spots are noticed in exposed areas [9].

According to Pedley et al. [11], the grains most likely started as faecal pellets. The green potassium-iron-aluminium silicate was formed from a rich organic mineral. However, in the Maltese Islands, the colour turns to brown whenever these grains are exposed to air and rain water due to iron oxidation. The Greensand formation is a layer full of fossils, sometimes containing large thick-shelled sea urchins [11].

2.1.3 Blue Clay Formation

The thickness of the Blue Clay formation varies a great deal across the Maltese Islands. In the western part of the island, the Blue Clay formation was found to be over 70m thick, whilst totally absent in the eastern part [11].

The Blue Clay layer, which is the softest of all the layers, has very fine-grained sediment containing inorganic minerals and skeletal material consisting of a composition of macrofauna such as the remains of fish and mammals, molluscs, echinoids, and solitary corals. This means that like the Greensand formation, the Blue Clay formation also contains fossils made up of very small planktonic organisms, however, the majority of the bigger fossils were crushed and destroyed during the consolidation stage [9, 11, 13].

According to Pedley [14], the Blue Clay layer consists of light and dark-grey banded marls, where the light grey bands contain a high proportion of carbonate. However, Murray [15] argues that this formation never exceeds 30 per cent carbonate material. The top part of this formation exhibits brown phosphatic sand grains together with green grains of Glauconite. The top part of this layer is easily entwined with the layer above, that is, the Greensand formation. According to Soldati et al. [11] and Pedley et al. [13], the Blue Clay layer in the Maltese Archipelago was mainly composed of the kaolinite mineral.

In Malta, the Blue Clay is known as ‘*tafal*’ which, since the prehistoric era, has been an important raw material for the manufacturing and processing of pottery [9, 11, 13].

2.2 Clay

Rice [16] describes clay as a fine-grained earthy material that becomes plastic or malleable when moistened. Cuomo di Caprio [17] defines clay in a similar manner emphasizing that it is a non-metallic and a non-organic solid mixture, although it may include some organic materials. When in the raw state it is easily shaped. It is strengthened through the firing process.

Clay has two main characteristics [18]:

1. It is constituted of very small particles, typically < 2μm in diameter and,
2. Contains a high amount of inorganic minerals which is present in the mixture.

These two characteristics provide the clay with both its chemical and physical properties, allowing the clay to be manufactured and eventually fired, to create ceramics [18].

Pottery consists of a clay matrix which is an uninterrupted phase containing inclusions and tempers. Inclusions are non-plastic elements which are naturally present in the clay matrix, while tempers are intentionally added non-plastic elements to avoid shrinkage in both the drying and firing stages. Tempers such as quartz can also affect the thermomechanical properties of the material [19].

Clay minerals have two main behaviours in ceramics. When combined with water, clay becomes very plastic, which is in fact known as, hydroplasticity. Furthermore, when exposed to high temperatures during the firing stage, a strong ceramic is produced [20].

Clay minerals are categorized as hydrous aluminous sheet silicates that varies in both water content and structure. They mostly consist of alumina and silica, but contain small amounts of calcium, magnesium, potassium, iron, sodium and hydrogen. These can be classified in the form of oxides: Al_2O_3 (alumina), SiO_2 (silica), CaO (calcium oxide), MgO (magnesium oxide), K_2O (potassium oxide), FeO, Fe_2O_3, Fe_3O_4 (iron oxides) and Na_2O (sodium oxide) [17].

Kaolinite, Illite and Chlorite are examples of clay types. The Blue Clay layer of the Maltese Archipelago consists of the kaolinite mineral [11, 13]. For this reason, in this literature review, focus will be directed towards kaolinite type clay.

2.2.1 The Mineral Kaolinite

Kaolinite clay [$Al_2^{6+}(Si_2O_5)^{2-}(OH)_4^{4-}$] is made up of two layered-sheets: alumina octahedral sheets and silica tetrahedral sheets, see Figure 2.1. When water interacts with kaolinite, the water molecules enter between the layered sheets, creating a thin layer surrounding the clay particles. These particles, whose size ranges from one to a few microns, are free to mix and settle over other particles, resulting in plasticity [16, 17, 20].

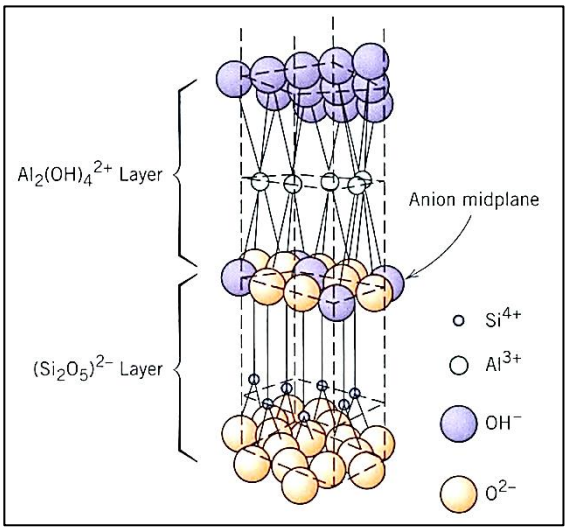

Figure 2.1 – Kaolinite clay structure [20].

2.3 Sieving

Different techniques of sieving have been created depending on the composition of the clay [18]. Sieving may be carried out on either wet or dry clay. Wet sieving tends to be favoured because it helps break down the chunks of clay into finer particles prior to separation [16, 18, 21, 22]. Wet sieving is performed by suspending a known mass of clay in water which is then passed through a number of sieves of different mesh sizes [16]. Orton and co-workers [18] suggested another effective method in the wet sieving process, namely using hydrogen peroxide. This peroxide is added to remove any organic material; however, this method is costly when dealing with large amounts of clay.

Rice [16] recommends using the sedimentation technique for very fine particles. Beuselinck et al. [23] used a combination of both wet sieving and sedimentation techniques to separate their clays. The former was used for clay fractions > 63 μm, whilst the latter was used for very fine clay fractions between c. 2-63 μm.

Cordell et al. [21] also mentioned that Rice had used a different technique where samples of clay were dried and crushed before sieving. Grech [24] employed a dry sieving procedure to separate his clay into fractions.

2.4 Briquette Manufacturing

2.4.1 Forming the Green Vessels

2.4.1.1 Types of Water

Clays generally consist of three types of water; 'water of plasticity', 'interlayer water' and 'chemically combined water' [16, 17, 19].

Water of plasticity is an important component in pastes which permits the clay to be formed into any shape and retain it. When water is added to the clay particles, a liquid film is formed, and this binds the particles together through surface tension. Water also serves as a lubricant and allows the clay particles to move over/against each other [16, 17, 19].

The clay must be combined with the right amount of water to obtain plasticity. Rice [16], Cuomo di Caprio [17] and Santacreu [19] state that there needs to be between 15% to 25% by weight of water to produce the right amount of plasticity in clay. Clay parts into small lumps if the required amount of water is not added. On the other hand, if more water is added than required, the clay becomes too watery, and shape is not retained. Di Caprio [17] proposed an empirical test to help verify the correct weight of water. This is done by rolling a small portion of clay into a rope and bending it to form a loop. If the loop cracks, this indicates that more water has to be added to the clay since it is not plastic enough.

Plasticity and particle size are inversely proportional. Thus, on decreasing the clay's particle size, the amount of water required to give rise to plastic behaviour needs to increase. This is due to the large surface area of the smaller particles [16, 17, 19]. This theory was proven by Bernal et al. [25] and Ferrari and Gualtieri [26].

The interlayer water present in clay evaporates when it is subject to low-temperature heating. This is a reversible process, however, if water is again added to the clay, a loss in plasticity is noted [16, 17, 19].

Chemically combined water, also known as crystal lattice water, is characterised by "apical hydroxyl groups in the octahedra of sheet silicates" [17, p.50]. These OH^- ions present in the crystal structure form strong chemical bonds and can be driven out at temperatures between 550 and 650 °C. When this occurs, an irreversible process takes place, and the clay will no longer regain plasticity when water is added. This shows that the clay has changed into a ceramic [16, 17, 19].

2.4.1.2 Assessing Plasticity

It is a fairly straight-forward procedure to assess the water required for plasticity of clay. It is assessed by slowly adding water to a known weight of dry clay. It is important to take note of the amount of water necessary to form initial plasticity and record the amount it needs to obtain its full plasticity. The upper limit of the working range is obtained when the clay becomes pasty and runny. The range of workability is the range between the upper and the lower quantities of water added [16].

Rice [16] and Cordell et al. [21] measured the percent water of plasticity by evaluating the wet clay's weight with its dry weight as follows:

$$\%WP = \frac{weight_{wet} - weight_{dry}}{weight_{dry}} \times 100 \tag{2.1}$$

2.4.1.3 Briquette Manufacturing

Lee and Yeh [6], Cordell et al. [21], Alonso Alcade et al. [27], Harry et al. [28], Karaman et al. [29], Webb and de Laguna [30] and Žuŝihovskaâ [31] all used the same technique to manufacture clay briquettes. The technique used by these authors consisted of forming test bars after the correct wedging and kneading of the clay. This was done to ensure that the clay and water combination were as homogeneous as possible. To obtain the proper shape, a mould was used for the test bars.

All the above authors, however, had a difficulty in extracting the clay from the mould. Hence, Cordell et al. [21], solved this problem by using parchment paper to line the mould. A wood block extruder was then used to extract the plastic and loose clay from the mould. For the ease of splitting the test bars into briquettes, a pointed tool was used to create five equal indents in the test bar before drying in the oven. After this process, the test bars were labelled and two points, 10cm apart, were indented with the same pointed tool. This helped to facilitate measuring the linear drying shrinkage of the test bar.

Manufacturing is affected by climatic conditions and "weather and climate may place constraints on production" [32, p.90]. The Arctic is not suitable to manufacture pottery since the climate is both cold and humid. As a result, clay is extracted in the wet state and plastic and is allowed to dry before it is worked into pots. This creates a considerable number of difficulties for the clay manufacturers. Harry et al. [28] outlined that humidity alters from time to time, which according to them caused more problems than consistent and high humidity.

Skibo et al. [33] also remarked that climatic conditions are important because clay extractions in Arctic regions will be very wet and plastic. Hence, to eliminate these difficulties, manufacturers dry the clay before forming them into their desired shape [28].

Harry et al. [28] stated that time was an important factor in the manufacturing of clay in these climatic conditions because this process entails that the pots are dry enough to support their own weight. When the conditions of the climate are warm and dry, the pots will quickly dry, and thus time no longer remains the key factor. This is the situation in the Maltese Islands, where the climate is characterised by warm and dry weather.

2.4.2 Drying and Shrinkage

2.4.2.1 Drying

In the previous Section, it was indicated that climatic conditions have an effect on the drying of clay. The factors affecting drying are humidity, air currents and temperature. These may lead to defects in the manufactured clay, or it may weaken the clay form. Varying temperatures and the evaporation rate may have a drastic effect on the moisture gradients between the surface of the manufactured clay and its interior. This causes diverse drying rates and as a result, warping occurs [16, 18, 19].

Drying occurs more rapidly when manufactured clay is left to dry in direct sunlight. Moreover, Rice [16] stated that air which is heated can absorb more water from the clay than a cooler air. However, the author argued that too much heat can cause defects on the surface of the manufactured clay due to a high rate of surface evaporation.

Cuomo di Caprio [17] explained that when drying is steady and slow, water which is evaporated from the surface is restored by water present in the interior of the clay. Thus, clay dries evenly. However, the author pointed out that if drying occurs rapidly, the

water found inside the clay will not manage to evaporate to the surface. As a result, the surface shrinks at a faster rate than the core of the clay, leading to cracking and warping. If the shape is uneven and irregular in thickness, drying will not be consistent. Thus, Rice [16] and Cuomo di Caprio [17] suggest to eliminate shrinkage water by drying clay slowly and in a uniform manner. Rice [16] recommends that drying should be monitored very carefully.

Harry et al. [28] discovered a negative correlation between drying time and number of cracks. The clay pots cracked more in dry conditions than in humid ones when the drying procedure was accelerated. However, when clay was left to dry slowly in humid conditions, the samples did not crack so much.

Rice [16] and Santacreu [19] give importance to the drying time needed when manufacturing clay. They state that this procedure can generally take either a few days or weeks depending on the clay's characteristics and thickness.

Rice [16] states that the size of the clay particles have an effect on the drying behaviour. Coarser clay particles dry at a faster rate than the finer ones, with reduced shrinkage.

Different authors used various drying temperatures, times and techniques to dry their clay greens. Cordell et al. [21] dried the briquettes at a temperature of 105 °C for roughly an hour in a drying oven. Lee and Yeh [6] dried the samples in a drying oven at a temperature of 110 ºC for four hours, whereas Carter [34], left the samples to dry in an oven for two hours at the same temperature. Jordán et al. [35] eliminated the water content at a temperature of 65 °C through infra-red heating for a period of three days. However, whereas Cordell et al. [21] and Carter [34] left the samples to dry at room temperature after drying them in the oven, Tencariu et al. [36] allowed the samples to dry in controlled laboratory temperatures (~18-20 °C) for two weeks. On the contrary, Albero [37] and Papadopoulou et al. [38] both agreed that the temperature for drying should be between 50 and 110 °C so as to completely eliminate the water absorbed by the clay's structure.

2.4.2.2 Drying Sequence

In the drying procedure, clay particles slide over each other so as to fill the empty space created during the process of evaporation of water, known as water of shrinkage. When the particles are close together, there is a decrease in volume. The leather-hard stage occurs when clay particles cannot get any closer, causing a loss in plasticity and the clay turns into a stiff mass [16, 17, 19].

After this stage, the form of the clay cannot shrink in size even after drying at room-temperature or low-temperature heating (105-110 °C). Additional shrinkage occurs only during the firing procedure [16, 17, 19]. Pores are small spaces in the clay that are present after the evaporation of water of shrinkage. Water trapped inside these pores is known as water of porosity. Carter [34] and Khalfi and Blanchart [39] were in agreement that the volume of water of porosity in the clay depended on the amount of humidity in the atmosphere.

Rice [16] recommends that drying clay at room temperature should take 144 hours to remove all the water except chemically combined water, which evaporates when the firing process takes place. On the contrary, Santacreu [19] argues that not all the water present in clay is evaporated and insisted that water of porosity is still present inside the clay after drying. Worrall [40] agreed with Santacreu, that water of porosity can be totally eliminated after the firing process, resulting in the formation of micro-pores in the clay.

2.4.2.3 Shrinkage

Cuomo di Caprio [17, p.85] describes shrinkage as “the contraction of volume which occurs when the water of plasticity is removed from clay”. The author states that shrinkage occurs at two different stages; during drying and firing at high temperatures. The latter causes the elimination of chemically combined water. When this water evaporates, the hydroxyl groups present in the clay structure are eliminated as the clay turns into a ceramic [17]. In agreement with di Caprio, Karaman et al. [29] states that the higher the firing temperature, the greater the shrinkage.

Finer clays exhibit more shrinkage as more water is required to create plasticity due to the large surface area to volume ration of these clay particles where many pores are present. On the other hand, Cuomo di Caprio [17] states that low plasticity results in less shrinkage but higher porosity.

2.4.2.4 Measuring Drying Shrinkage

Rice [16] gives an insight on how to measure linear drying shrinkage (%LDS). This is calculated by creating an indent with an equidistant length apart in the wet clay samples by using a pointed tool. This needs to be done after drying the clay at a temperature of 105 °C. Once this is done, this distance is re-measured and subtracted from the original length recorded. The result is then divided by the measurement of the wet length and is subsequently multiplied by a 100 to convert it into a percentage, as can be seen in the equation below [16]:

$$\%LDS = \frac{length_{wet} - length_{dry}}{length_{wet}} \times 100 \quad (2.2)$$

The same procedure was adopted by Cordell et al. [21] and Alonso Alcade et al. [27].

2.5 Firing

2.5.1 Introduction

In the production of pottery, firing is a crucial stage since there is a transformation from the raw material into a ceramic. Through this transformation, it is possible to distinguish the physical and mineralogical properties of the material [5].

According to Cuomo di Caprio [17], firing starts at ambient temperature and ends when the temperature has cooled back to ambient temperature. For the ceramic change to occur, a temperature varying between 550 °C and 650 °C is needed. After this transformation, the clay will not regain plasticity and thus, becomes a 'fired clay body' also known as a hard ceramic [16, 17].

Firing includes the chemical-physical transformations which alters the briquettes. A number of important factors affect this process, namely, the highest firing temperature, firing time, also known as soaking time, and firing atmosphere, either oxidising (in the presence of oxygen) or reducing atmosphere (in the absence of oxygen/in the presence of CO and CO_2). Other factors affecting this process are the heating rate, cooling time and cooling atmosphere. The latter have an effect on the colour of the surface of the briquettes [16, 17].

2.5.2 Experimental Firing

Experimental firing helps to determine the connection between the firing factors and the properties of both the raw materials and ceramic products. Experimental firing determines the influence on the chemical, physical, mechanical properties and composition of the fired products [5].

Experimental firings can be categorized as either experimental archaeology which is conducted on site, or laboratory-controlled which, as the name implies, is conducted inside a laboratory [5].

2.5.2.1 Experimental Archaeology Firing

Thér and Gregor [41] stated that experimental archaeology firings were conducted to test firing structures and methods, however, Harrison [42] argued that these experiments were done to reproduce pottery artefacts.

By running these types of experiments, one has the possibility of testing the effects that different variables have both on the firing method and on the fired briquettes [5]. Thér and Gregor [41] and Maggetti et al. [43] suggest that the temperature needs to be monitored. Thér [44] argued that using a certain method of firing structure can be applied to different procedures, such as kilns and bonfires. The author also stated that different products can be produced by controlling the rate of heating, cooling, firing duration, draft and type of fuel used.

Gosselain [45] and Livingstone-Smith [46] argued that in bonfires, temperature variation depends on the distribution, type and quantity of the fuel used, the way of stacking the objects in the fire and weather.

Sinopoli [5] emphasizes the importance of knowing the firing technology used to be able to interpret the results obtained from the studies.

2.5.2.2 Laboratory-Controlled Firing

Experiments conducted in laboratory furnaces are important to be able to control the firing procedure. This is done so as to study the effect varying conditions have on the physical, chemical and mechanical properties of the fired clay [5].

Sinopoli [5] stated that such experiments are more suited for the reproduction of kiln firings as both the cooling and heating rates of the oven can be adjusted to match those of archaeological kilns. Archaeometric studies are carried out in laboratory-controlled firing to fire a number of briquettes in a variety of temperatures. These briquettes differ in their physical and chemical characteristics, such as porosity, colour and composition of minerals present in the clay. This is due to the different parameters of firing temperatures, times, atmospheres and composition of the briquettes.

2.5.3 Stages of the Firing Process

As previously mentioned in Section 2.4.1.1, both water of plasticity and interlayer water evaporate when a firing temperature of up to 200 °C is reached [16, 17, 19]. It is of utmost importance that the heating process is gradual as water trapped inside the clay microstructure can lead to the breakage of the briquettes. Spalling may also occur if the briquettes are not dried properly, and heat is generated quickly. This leads to a scar or indentation or the flaking of clay at the surface of the briquettes [17].

When a temperature ranging from 300 and 600 °C is reached, organic materials present in the clay are pyrolyzed and evaporated as water vapour and carbon dioxide, creating an exothermic reaction producing heat in the process [16, 17, 19].

Combustion is not complete in a reducing atmosphere. When insufficient oxygen is present, carbon monoxide forms and organic materials do not combust, resulting in black coring in the middle of the briquette [16, 17, 19]. Cuomo di Caprio [17] reports that if cooling is very rapid and the briquettes are fired for a short period of time, incomplete oxidation occurs. The author also emphasizes that if organic materials are not completely volatilised, hot gases are entrapped within the clay microstructure, causing the formation of voids.

Clay minerals such as kaolinite, illite and montmorillonite, start to decompose when the temperature during firing reaches 450 to 650 °C. Also, at these temperatures, chemically-combined water evaporates, and hydroxyl groups are released. Once this

occurs, the crystal structure cannot retain its original form, confirming that the ceramic change has occurred [16, 17, 19].

According to Rice [16], Cuomo di Caprio [17] and Santacreu [19], the transition of quartz occurs when the temperature reaches 573 °C. Quartz increases in volume as it is transformed from alpha-SiO_2 to beta-SiO_2 form. At this stage, the briquettes are no longer soft but still not hard enough, thus, it is critical that temperature from 500 to 650 °C, is increased slowly [17]. Dehydroxylation occurs when the temperature reaches 550 °C and organic matter volatilises. The briquettes at this stage become red in colour due to the oxidation of the ferrous silicate [16].

At a temperature of approximately 800 °C, calcite starts to decompose to form calcium oxide and carbon dioxide, as seen in the chemical equation below [16, 17, 19]:

$$\boldsymbol{CaCO_3 \xrightarrow{800-870\,^{\circ}C} CaO + CO_2} \tag{2.3}$$

This chemical reaction is accomplished when a temperature of roughly 870 °C is reached, although this is affected by a number of parameters, including the firing atmosphere, the total time for the firing procedure and the size of the calcareous grains. The firing atmosphere is crucial because iron compounds present in the clay matrix are more reactive in a reducing atmosphere, rather than in an oxidising atmosphere, resulting in a rich black glossy appearance [17].

Cooling times rely on a number of factors, such as the size, shape and quantity of briquettes in the firing furnace. Cooling should not be rushed and should be allowed to happen slowly (furnace cooling) as the briquettes might experience fracture [16, 17, 19].

Different colours may be seen in the cross-section of the briquette, colours changing from light red to a red-brownish tinge and to a brownish-red. Each colour signifies a different phase in the process of re-oxidation. As previously stated, black coring occurs when cooling is quick and brief. On the other hand, if cooling takes place in a reducing atmosphere, carbonaceous particles are entrapped in the pores and the briquettes change to black [17].

2.5.4 Previous Experimental Firings

A number of authors who experimented with different firing parameters and techniques were selected, achieving a wide array of results.

In their experiment, Cordell et al. [21] used the lowest starting temperature, that of 400 °C, reaching 800 °C. They worked by firing five temperatures at 100 °C intervals in an oxidising atmosphere, with a soaking time of 30 minutes each. All briquettes were fired in an electric furnace.

De Bonis et al. [22] and Karaman et al. [29] used the same firing temperatures in their experiments, starting at 700 °C reaching a maximum temperature of 1100 °C at intervals of 100 °C in an oxidising atmosphere. Both these authors used an electric furnace [22, 29]. Soaking time was different; whereas De Bonis et al. [22] fired his samples at a soaking time of 90 minutes, Karaman et al. [29] used various soaking times starting from 120 minutes to a maximum of 480 minutes at two-hour increments.

Alcade et al. [27] chose to fire their samples at the shortest soaking time, namely for 10 minutes. Alcade et al. [27], like Tencariu et al. [36] and Pontikes and Angelopoulos [47], fired their samples at one constant temperature. Alcade et al. [27] and Tencariu et al. [36] fired their samples at a temperature of approximately 700 °C, whilst Pontikes and Angelopoulos [47] conducted their study at a temperature of 1000 °C. All three used a different firing technology, two of which were carried out under oxidising conditions, whereas Pontikes and Angelopoulos [47] conducted their experiment in oxidising and reducing atmospheres. Soaking time used by Tencariu et al. [36] and Pontikes and Angelopoulos [47] varied considerably as the former experimented with a two-hour soaking time, whereas the latter used one and four hours.

Lee and Veh [6] and Jordán et al. [35] both used an electric furnace in their experiments under an oxidising atmosphere. The authors used the same temperature ranging approximately from 900 to 1200 °C at different intervals, 100 and 50 °C, respectively. In their experiment, Lee and Veh [6] kept the samples at a maximum temperature, at approximately twice as long as the samples of Jordán et al. [35].

Table 2.1 summarises the different parameters and technologies used by various authors selected for this Literature Review.

Table 2.1 – Firing parameters and technologies used by various authors.

Authors	Firing Temperatures	Firing Times	Firing Atmospheres	Firing Technology
Cordell et al. [21]	400-800 °C at intervals of 100 °C	30 minutes soaking time	Oxidising	Electric Furnace
De Bonis et al. [22]	700-1100 °C at intervals of 100 °C	90 minutes soaking time	Oxidising	Electric muffle
Karaman et al. [29]	700-1100 °C at intervals of 100 °C	120, 240, 360 and 480 minutes soaking time	Oxidising	Electric Furnace
Alonso Alcade et al. [27]	705 °C	10 minutes soaking time	Oxidising	Furnace
Tencariu et al. [36]	650 °C	2 hours soaking time	Oxidising	Electric Kiln
Pontikes and Angelopoulos [47]	1000 °C	1 and 4 hours soaking time	Oxidising and reducing	Propane Firing Kiln
Lee and Veh [6]	900-1200 °C at intervals of 100 °C	60 minutes soaking time	Oxidising	Electric Furnace
Jordán et al. [35]	900-1150 °C at intervals of 50 °C	35 minutes soaking time	Oxidising	Electric Furnace

2.6 Characterisation Techniques

There are various ways in which clay can be characterised once it has gone through the firing process. In this Sub-Section, the main focus will be on Munsell Colour charts, X-ray powder diffraction (XRPD), light microscopy and hardness testing.

2.6.1 The Munsell Colour Chart

Orton and Hughes [18] report that Munsell produced a standard chart (Figure 2.2) for colour evaluations to be made. Although the data inputted is subjective, the Munsell chart helps to measure the likeness of similar colours. Photography and image analysis can also be used as an alternative to the Munsell chart. Cordell et al. [21], De Bonis et al. [22], and Jordán et al. [35] all used a Munsell chart for their macroscopic recording of colour.

Figure 2.2 – Munsell Colour Chart [48].

Rice [16] and Cuomo di Caprio [17] describe this chart as consisting of various colour chips, evenly spaced and placed according to three attributes of colour, namely hue, value and chroma.

Hue shows the colour of the sample. There are ten hues possible: five major and five intermediate, refer to Table 2.2. These colours are presented according to their position in the electromagnetic spectrum. Hues are categorized with the initials of the colour, ex. B = Blue, and are given a number which varies from 0 to 10 (also 0.5, 1.5, etc.), showing the position of the hue. Hues are placed in equal intervals so that there is uniformity between the two adjacent hues [16, 17].

Table 2.2 – Major and intermediate hues.

Major Hues	Intermediate Hues
R – Red	
	YR – Yellow-Red
Y – Yellow	
	GY – Green-Yellow
G – Green	
	BG – Blue-Green
B – Blue	
	PB – Purple-Blue
P – Purple	
	RP – Red-Purple

Value gives an indication on how light or dark a particular colour is. This value ranges from 0 (absolute black) placed at the bottom, to 10 (absolute white) placed at the top of the chart. Value 7/ indicates that the colour is lighter and more brilliant than Value 5/ [16, 17].

Chroma signifies the strength of a particular colour. Varying from left to right, chroma starts from 0 (neutral grey) up to approximately 20, which is the maximum saturation of the colour. A colour with a saturation of 7 is stronger than a colour with a saturation of 1. N indicates neutral and refers to greys and black that have a chroma of 0 [16, 17].

Cuomo di Caprio [17] states that colour charts help to introduce a common terminology and thus, remove ambiguous terms and reduces subjective descriptions. However, the author maintains that in ancient pottery these colour charts have not been widely accepted because in a single briquette there are variations of colour on the same sample. The author recommends that a description of the colour should be included with the code numbers as well as specifying both the chroma and value [17]. Through experience, Orton and Hughes [18], found it beneficial to describe the colour of the briquettes in different areas, starting with the core, being the farthest from the firing atmosphere, and moving on to the margins of the briquette, which is the area between the surface and the core. The surface colour of the briquettes is the last to be described.

Rice [16] states that it is difficult to find the right match on the Munsell chart because of the gaps in the three attributes (hue, chroma, and value). She thus recommends that more precision is needed by inserting decimals to distinguish the values and positions on the hue chart.

2.6.2 X-Ray Powder Diffraction (XRPD)

XRPD studies the mineralogical composition of both clays and ceramics in powder form. This is done using the Bragg equation [16, 19]:

$$n\lambda = 2d\sin\theta \tag{2.4}$$

By examining the sample through a variety of 2θ angles, all the diffracted directions should be reached because of the random orientation of the sample. Transformation of the diffraction peaks to d-spacings permits the identification of the phases since each mineral has a set of distinctive d-spacings [16, 19].

Karaman et al. [29], performed XRD on fired briquettes. No information was supplied with regards to the increment, step duration and rotational speed.

De Bonis et al. [22], Jordán et al. [35] and Santacreu and Mateu Vicens [49] used similar diffracting angles ranging from approximately 3-80° 2θ. As in Karaman et al. [29] experiment, no information was given except for Santacreu and Mateu Vicens [49] who programmed the XRD with a step duration of 3 seconds per step.

Grech [24] and Asciak [50] used the same increment of 0.02 and the same rotational speed of 15 revs per minute in their dissertations to study Roman pottery sherds. However, they used a different step duration and also a slightly different diffracting angle range.

Lee and Yeh [6] and Pontikes and Angelopoulos [47] characterised fired briquettes by using the exact same diffracting angle range, 10-70° 2θ, but like the other authors mentioned before, they did not supply any information on the increment, step duration and rotational speed.

For ease of reference, Table 2.3 summarises the different parameters used by various authors selected for my literature review.

Table 2.3 – XRD parameters used by various authors.

Authors	Diffracting Angle (°)	Increment (°)	Step duration (secs/step)	Rotational Speed (rpm)
Karaman et al. [29]	2-30	Not Specified	Not Specified	Not Specified
De Bonis et al. [22]	4-80	Not Specified	Not Specified	Not Specified
Santacreu and Mateu Vicens [49]	3-70	Not Specified	3	Not Specified
Jordán et al. [35]	4-70	Not Specified	Not Specified	Not Specified
Asciak [50]	5-60	0.02	2	15
Grech [24]	5-80	0.02	3	15
Lee and Yeh [6]	10-70	Not Specified	Not Specified	Not Specified
Pontikes and Angelopoulos [47]	10-70	Not Specified	Not Specified	Not Specified

2.6.3 Light Microscopy

Fired briquettes can be studied microscopically to assess the microstructural and physical changes that occur during the firing process, as well as particle size, frequency and shape of the inclusions [5, 16-18, 51]. Orton and Hughes [18] and Quinn [51] suggested to examine the samples at magnifications of x25. A hand-lens of magnification x8 or a high magnification microscope of up to x30 is not recommended to study the clay matrix and inclusions present.

According to Orton and Hughes [18], Santacreu [19] and Quinn [51] inclusions can be recorded by frequency, size, sorting and roundness. The frequency of the inclusions should be calculated by means of a visual percentage estimation chart. Size and sorting can be verified by the naked eye or by a light microscope. The Wentworth Scale Chart can be used to classify the inclusion size into its appropriate size category. Roundness indicates if the inclusions experienced any erosion and can be measured by using mainly an image-analysis technique.

Both Grech [24] and Asciak [50] used this characterisation technique to identify the inclusions present in the clay matrix in their dissertations.

2.6.4 Hardness

Hardness is a gauge of the behaviour of a material under stress from loading applied to the surface and can be established by means of a standard test which measures the resistance of a material to indentation. Hardness depends on both composition and microstructure of the ceramic which includes the type, form, size and inclusions present in the clay matrix [16, 17].

Rice [16] and Cuomo di Caprio [17] state that hardness usually increases with both soaking time and firing temperature. They also stress that atmosphere plays an important role as a reducing atmosphere increases hardness. Lee and Yeh [6] conducted a Vickers microhardness test whereby they confirmed that hardness increases with temperature.

Hardness is influenced by microstructural properties including the size of the grains, inclusions present in the clay matrix, and porosity of the ceramic. The finer the grains, the harder it is to penetrate the surface of the material [16, 17].

There are a variety of tests that can determine the hardness of ceramics. Orton and Hughes [18] recommend the Mohs hardness scale (Figure 2.3) to measure the hardness of pots. In the Mohs hardness test, the person conducting the test scratches the surface of the pot with a harder material. The hardness is determined by the number of the material that resists scratching the surface. Alternatively, a fingernail (Mohs 2 or 2.5), copper wire (Mohs 3), a window pane (Mohs 4.5) and a steel blade (Mohs 6) can be used to replace some of the materials, as suggested by Rice [16] and Orton and Hughes [18].

Scale	Mohs mineral	Substitute
1	Talc	
2	Gypsum	
2.5	–	Fingernail
3	Calcite	Copper wire
4	Fluorite	
4.5	–	Window glass
5	Apatite	
6	Orthoclase	Steel blade
7	Quartz	
8	Topaz	
9	Sapphire	
10	Diamond	

Figure 2.3 – Mohs hardness scale and substitutes [16].

Other hardness tests include the Knoop, the Vickers and Brinell hardness techniques which are conducted in similar ways. Rice [16] and Cuomo di Caprio [17] state the importance of polishing the sample prior to the test to be able to clearly see the indents under the microscope. Clinton and Morrell [52] argued that Knoop hardness is the most suitable hardness test since ceramics are brittle. Also, larger loads may be applied without fracturing the sample.

3. Methodology

This Chapter is a recollection of the flow-process undertaken for this dissertation as summarized diagrammatically in Figure 3.1. Each step is explained in detail in the following Sections.

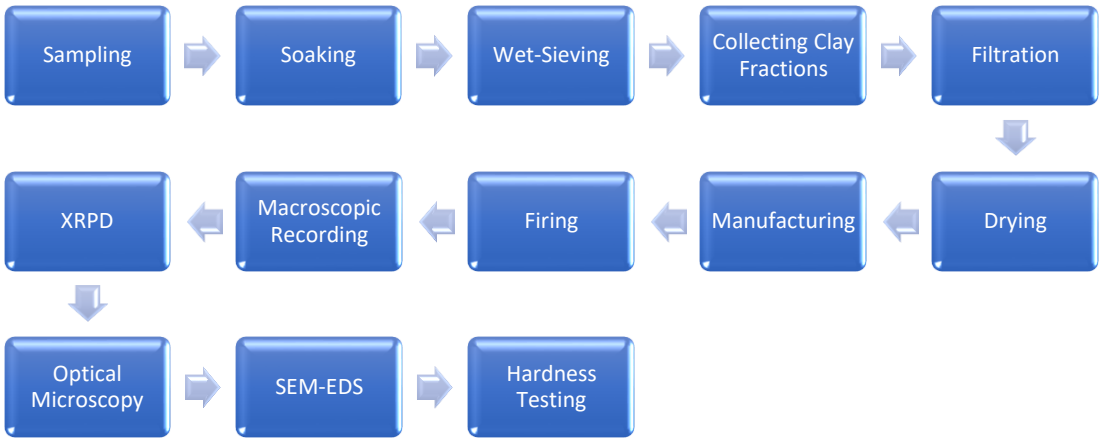

Figure 3.1 – Methodology flow-process.

3.1 Sampling

Arnold [53] suggested that clay was sourced at a distance between 1 km and 7 km from the centre of the town. According to Bonanno [54], Rabat is an area where pottery could have been manufactured, albeit there is no evidence to support this. Thus, Il-Qolla hill was the location selected to extract clay for this dissertation since it was within a reasonable walking distance from the centre of Rabat. Figure 3.2 shows the geographical location of Il-Qolla in Rabat.

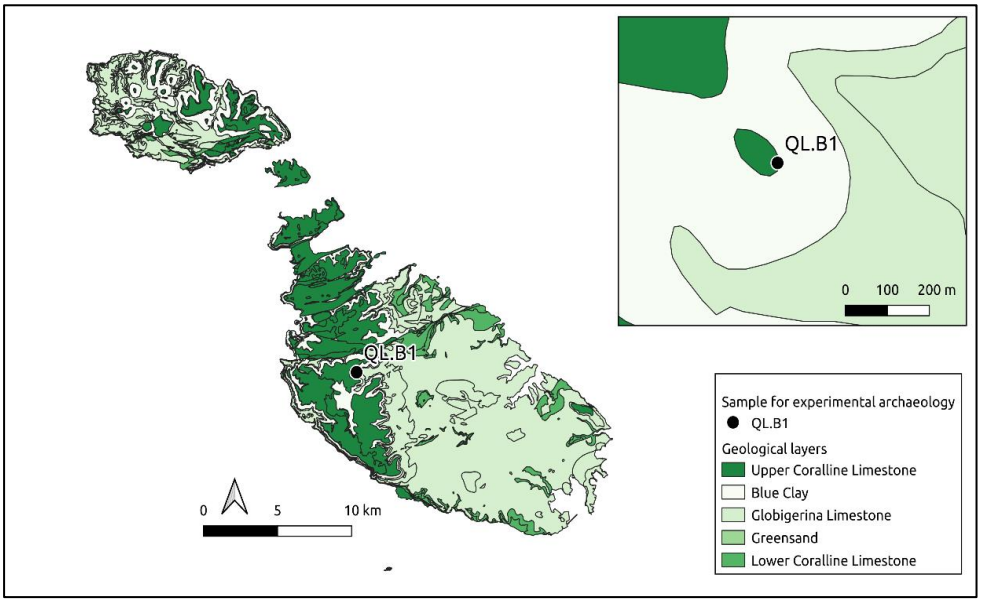

Figure 3.2 – Geological map of the Maltese Islands with Il-Qolla marked with a black marker (Image by Ms. Emma Richard-Tremeau).

Prior to the sourcing of clay, permission was requested from the Environment and Resources Authority (ERA).

A relatively flat surface on the hillside was chosen at Il-Qolla to provide better stability when using the spiral auger to be able to penetrate the layers of the soil. A GPS was used to give the approximate co-ordinates and the elevation from the ground of the sampling location.

A trowel and pick-axe were utilized to remove excess material from the surface such as thistles, rocks and flora to avoid any contamination of the sampled soil. A spiral auger was used to loosen the soil. This was then replaced by an Edelman auger to collect a total of approximately 3 kg of clay which was placed in a labelled sample bag. A hand-held weighing scale was used to weigh the extracted clay, which was damp and compact. A measuring tape helped to record the depth of the hole from the surface.

After extracting the required amount of clay, the sampling location was backfilled in the best possible way to restore the landscape.

3.1.1 Sample Labelling

Sample labelling was an important step to separate Il-Qolla sampling location from the other locations of the wider CoFIPoMS project. The name denoted for the Il-Qolla sample was QL.B. The data recorded on the sampling bags included sampling location, sample reference number, date of sampling, initials of researchers and mass of sample collected. Information on the sampling location is tabulated in Table 3.1.

Table 3.1 – Sampling location information.

Location of sample	Il-Qolla, Rabat, Malta
Sample Reference Number	QL.B
Date of sampling	29/08/2020
Co-ordinates of sampling location	35°53’59.4”N 14°23’06.6”E
Elevation where the sample was extracted	187 m above sea-level
Maximum depth of sample below surface	74 cm
Mass of sample collected	3.25 kg
Characteristics of site	Thistles, dried vegetation and seeds were present. A loose surface was noted. A high elevation was chosen because the hill was terraced.
Characteristics of clay	When digging deeper, compactness of the soil was evident. A knife was utilised to remove soil from the sampling tool.

3.2 Sample Soaking

The clay samples were soaked for a minimum of three days so as to facilitate sieving. The sample to be sieved was weighed on the weighing scale and recorded as unsieved weight (uw) and placed in a labelled container. The clay sample inside the container was completely covered with tap water, with the amount of water added also recorded.

3.3 Wet Sieving

The aim of the sieving procedure was to remove the larger particles and to obtain a material which is more suitable for the manufacture of briquettes. Various levels of sieving were used to produce batches of briquettes with different composition.

Section 6.5 of the Standard Operating Procedure (SOP) entitled "Wet Sieving of Clay Samples for Archaeological Research" was followed [55]. This procedure was conducted with the following sieves in this order: 1 mm, 500 μm, 250 μm, 125 μm and 63 μm. Figure 3.3 shows the clay, soil and rock particles collected in the different sieves. The sieves were then left to dry for a few days before extracting the particles from the mesh.

Figure 3.3 – Clay, soil, and rock particles in the different sieves. From left to right – 1 mm sieve, 500 μm sieve, 250 μm sieve, 125 μm sieve, and 63 μm sieve.

3.4 Collecting the Clay Fractions

The next step was to collect the fractions left in the sieves, by following Section 6.6 of the "Wet Sieving of Clay Samples for Archaeological Research" SOP [55]. These fractions were placed in labelled sampling bags and properly stored in case further analysis on the fractions was required. Interestingly, roughly 94% of the extracted sample was totally composed of clay particles, proving that the clay extraction was done efficiently.

3.4.1 Cleaning

Sieves were cleaned in an ultrasonic bath (Kerry Ultrasonics) to remove the fine residual clay and stored for future use, as per SOP Section 6.9 [55].

3.5 Filtration of the Clay Samples

The filtration process was used to minimize the loss of fine particles after the clay had sedimented in water. The procedure adopted was per SOP Section 6.7 [55].

3.6 Drying

After the removal of water from the top layer of the buckets, the sediments were ready to be dried. The drying procedure was carried out in a Memmert UF 160 drying oven. The steps of this procedure were followed from Section 6.8 of the SOP [55]. Table 3.2 shows the settings used in the drying procedure.

Table 3.2 – Drying oven settings [55].

Temperature	105 °C
Fan	50 %
Timer	8 hours
Flap	10 %

Figure 3.4 shows the clay after 8 hours of drying.

Figure 3.4 – Dried clay.

The dried clay was then collected, weighed and placed in a labelled sample bag.

3.7 Manufacturing of Briquettes

The mould used to manufacture clay slabs was manufactured from polytetrafluoroethylene (PTFE) due to its non-stick characteristics, hence, making it easier to eject the clay from the mould [56]. Figure 3.5 shows the engineering drawing with the dimensions of both the male (upper – A on the drawing) and female (lower – B on the drawing) parts.

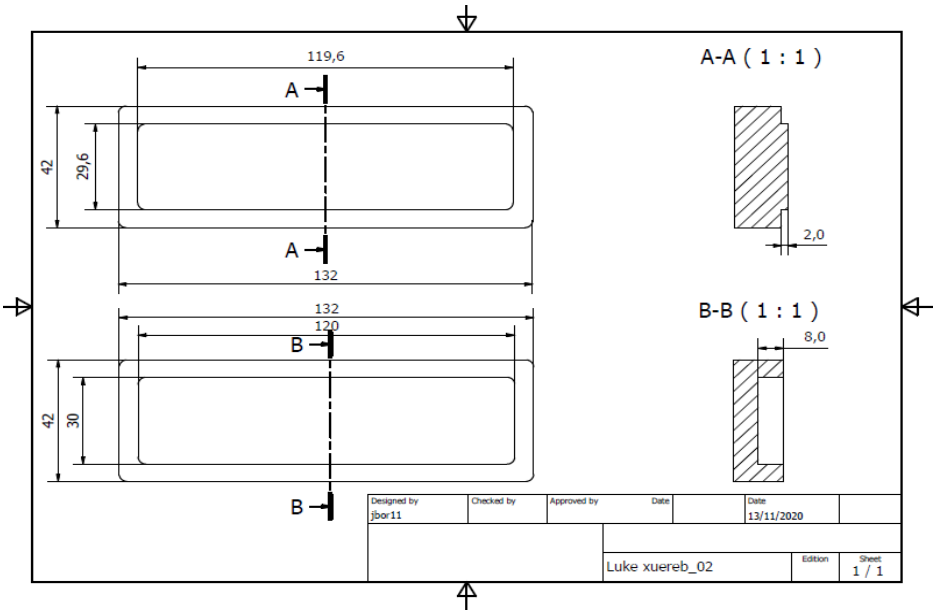

Figure 3.5 – Engineering drawing of the mould.

In this study, clay slabs were produced in four batches; two were sieved to 125 μm and the other two to 63 μm. The water of plasticity was maintained in the range of between 15 to 25% by weight of water, in accordance with the work of others [16, 17, 19].

The dry clay was weighed, then crushed into a fine powder using a pestle and mortar to improve its workability, and transferred to a container.

Water was poured in the sample in an amount equivalent to 15% w/w (lower limit) of the original weight of the crushed clay. Water was added to the dried clay in increments of roughly 10 g. This step was done until the clay was homogenized and was plastic enough to maintain a bent U-shape without breaking [17]. The total weight of the added water to the clay sample was calculated and compared to the water of plasticity range (15-25%) [16, 17, 19].

The next step was to cover both parts of the mould with cling film to easily remove the clay from the mould. The homogenized clay was pressed into the female part until it

was full. The male part of the mould was then used to press further the homogenized clay into the female part, flattening the surface of the slab in the process.

After the slabs were extracted from the mould, two shallow marks, ± 10 cm apart, were indented into the slabs with a blade and ruler. This was done to calculate the linear drying shrinkage of the slabs. Vernier calipers were used to measure the distance between the marks every 24 hours, for a week, as per procedure laid out by Cordell et al. [21]. The masses of the slabs were also recorded by using a KERN 440 electronic weighing scale.

The blade was also used to make transverse indents, 3 cm apart, to make it easier for the briquettes to be separated after firing. Each briquette was numbered by a number/letter punch while still soft. The slabs were assigned a letter (A, B, etc.) and marked into four divisions labelled 1 to 4.

The final step of this procedure was to leave the slabs to dry at room temperature. The slabs were not left in the same room during the drying process, hence, resulting in a change in environment. An important stage of this process was to flip the slabs once a day so that evaporation is constant on both sides throughout the drying process. At the same time, both the length of the indents and mass of the slabs were recorded at approximately the same time each day to accurately measure the shrinkage of the slabs every 24 hours. Graphs were then plotted showing the changes of both length between marks and mass with time.

After seven days of air drying, the slabs were dried in the Memmert UF 160 drying oven set at a temperature of 105 °C for 1 hour. The conditions of air and oven drying were taken from Cordell et al. [21]. Air drying followed by oven drying ensured that water was completely removed from the slabs.

The next step was to gently lay the slabs in containers filled with silica gel since the gel acts as a drying agent.

A briquette prepared from clay sieved to 125 μm and another briquette sieved to 63 μm were crushed to a fine powder with a pestle and mortar. These were then subject to XRPD analysis to see whether there were any differences in mineral phases between these two mesh sizes.

3.8 Firing

The manufactured slabs were then split into briquettes by breaking the slabs from the transverse indents made by the blade. Prior to firing, a briquette reference system was developed to give each briquette a unique name, as can be seen below, and is further explained in Table 3.3.

63_500_30_Oxi/Red

Table 3.3 – Briquette reference system.

63	Mesh size of the sieve
500	Temperature the briquettes were fired at
30	Duration of firing at maximum temperature
Oxi/Red	Atmosphere in which the briquettes were fired in

In the example above, the briquette was sieved to the 63 μm mesh size, fired at a temperature of 500 °C at a soaking time of 30 minutes in an oxidising/reducing atmosphere.

The next step of this procedure was the firing of the briquettes in a series of firing parameters, as evidenced in Table 3.4.

Table 3.4 – Firing parameters.

Temperatures	500, 700 and 900 °C
Soaking Times (time at maximum temperature)	30 and 120 minutes
Atmospheres	Oxidising and Reducing atmospheres
Heating Rate	200 °C/hour
Cooling Rate	Natural furnace cooling until it reaches room temperature

The above firing temperatures and soaking times were chosen to compare this study with the experiments conducted by Lee and Veh [6], Cordell et al. [21], De Bonis et al. [22], Alonso Alcade et al. [27], Karaman et al. [29], Jordán et al. [35], Tencariu et al. [36] and Pontikes and Angelopoulos [47]. An oxidising and reducing atmosphere was also applied in this procedure. The atmosphere in the furnace served as the oxidising atmosphere, whereas, for the reducing conditions, N_2-$5H_2$ reducing gas mixture was leaked into the furnace at a rate of 50L/h. Both the heating rate and cooling rate were set as constant parameters throughout this procedure.

The slabs were broken up into briquettes and divided into their subsequent firing parameters. These briquettes were placed in a stainless steel U-channel which was inserted inside the Nabertherm tube furnace. The parameters (Table 3.4) for the firing stage were pre-programmed. This procedure was repeated until all the briquettes were fired.

The briquettes were then left to cool in the furnace, the U-channel was extracted, and the briquettes were placed in labelled sample bags.

3.9 Macroscopic Recording

3.9.1 Photography

Photographs of both the unfired and fired briquettes were taken using a Nikon camera, model D7100 Digital SLR attached to a copy-stand. Lighting was provided by two LED light bulbs. Both the camera settings and light orientation were kept constant. The briquettes were photographed with a photography colour and dimension scale against a black background.

3.9.2 Munsell (Colour) Chart

The Munsell Soil Colour Book (HM-519) was used in this procedure (Figure 2.2). The colour of the surface of the briquettes was recorded by placing the sample behind the hue card. The hue, value and chroma of the colour chip that matched the sample were recorded. A colour name diagram, found on the opposite page of the Munsell Chart, described the colour of the briquettes. Cracks, blisters, voids or inclusions on the surface were also noted. All the recordings were taken in the same room under the same lighting conditions. Colour notation was documented in the following order:

Hue Value/Chroma Colour

For example: 5YR 5/4 reddish brown, where the hue is 5YR, the value is 5, the chroma is 4, and the colour is reddish brown.

The briquettes were then split into two with pincers. Half of the sample was crushed using a pestle and mortar to produce a finely powdered sample. This was placed in a labelled sample bag and stored for XRPD analysis.

The colour of both the core and the margin of the uncrushed briquettes were recorded, as shown in Figure 3.6. Before grinding and polishing them, these samples were viewed under a Meiji Techno Stereomicroscope at a magnification of x10. For the microscopic imaging of these cross-sections, the “Low Magnification Micrographs of Pottery with Meiji Techno Stereomicroscope and Microtec Camera” SOP (SOP No. CAR-RE-001-01) was followed [57]. This procedure was repeated with all the fired briquettes.

Figure 3.6 – A cross-section of one of the fired briquettes showing the different colours of the surface, core, and margin.

3.10 X-Ray Powder Diffraction (XRPD)

XRPD was conducted on the crushed and powdered fired clay samples with a Bruker D8 Advance machine to attempt to determine the mineral phases present. The powdered sample was placed in the pocket of the circular sample holder and was flattened for alignment purposes. The sample holder was then mounted onto the goniometer.

When changing samples, the sample holder was cleaned with compressed filtered air to remove any remaining particles. It was then rinsed with ethanol to ensure it was free from the previous material. Table 3.5 shows the X-ray diffraction parameters used to characterise the briquette samples.

Table 3.5 – X-ray diffraction parameters.

2 theta range	5-80 °
Increment	0.02 °
Step Duration	3 seconds/step
Rotational speed of sample holder	15 rpm
Voltage	45 kV
Current	40 mA

These parameters were selected to replicate X-ray procedures followed by De Bonis et al. [22], Grech [24] and Asciak [50].

The generated diffractograms were analysed using the PDXL software to identify the mineral phases present in the samples.

This procedure was applied for both the unfired and fired briquettes. It was noted that there was no difference between the unfired samples sieved to 63 μm and those sieved to 125 μm. Hence, for this dissertation, all the 63 μm briquettes were characterised and analysed together with the 125_900_120_Oxi briquette to determine if there were any differences between the mesh sizes when firing at high temperatures.

3.11 Preparation of the Fired Briquette Cross-Section

Adequate surface preparation was required for microscopy and hardness testing. This was done to ensure that the surface of the samples was adequately flat and levelled to view the indents when performing the microscopic analysis and hardness test. The samples were then embedded in cold-curing resin.

A Struers Tegramin-25 automatic grinding machine was used for the grinding process. The embedded briquettes were ground in sequence with 320, 600, 1200, 2500 and 4000 grit sizes of silicon carbide grinding discs. Water was used as a lubricant in this process. After each stage of grinding the samples were rinsed with water to eliminate any residual SiC particles or other grinding debris.

The embedded briquettes were polished with a porous neoprene polishing disc. The abrasive used for polishing was a polycrystalline diamond 1-micron in a water-base suspension. The samples were polished by rotating in a counter motion direction to the grinding machine.

After polishing, the samples were rinsed thoroughly with water. Pressurized air applied parallel to the surface of the embedded briquettes was used to dry them and to prevent excessive water from being trapped in the pores of the briquettes.

3.12 Microscopy

3.12.1 Optical Microscopy

The samples were observed with a Meiji Techno stereo microscope attached to a Microtec camera. Swift Imaging software was used to record micrographs and scale them. The embedded briquettes were viewed at magnifications of x10 and x50.

At x10 magnifications, the core thickness and briquette thickness of the oxidising samples were recorded at five different locations. The ratio of average core thickness over average briquette thickness was then generated. A bar chart depicting the relationship between soaking time and the thickness ratio was plotted for all the briquettes fired in an oxidising atmosphere, except the 63_500_30_Oxi sample since not a full cross-section was recovered since this briquette broke up during the grinding procedure.

The embedded samples were then viewed at a magnification of x50. Visual Comparison Charts (VCC) were used and the clay matrix frequency; sorting (size difference of the inclusions within the clay matrix), shape, size, frequency and colour of the inclusions; and the size and shape of the voids, were recorded.

Figure 3.7 shows the VCC used to estimate the frequency of inclusions in the clay matrix; Figure 3.8 illustrates the VCC used to describe the sorting of the inclusions; Figure 3.9 displays the VCC used to describe the shape of the inclusions, where equant (approximately spherical in shape) can be seen in the top row of the figure whereas elongate (longer in shape) are shown in the bottom row of the figure; Table 3.6 shows the Wentworth scale chart used to help determine the size of the inclusions; Table 3.7 indicates how the frequency of inclusions are classified; Table 3.8 determines how void sizes are classified; and Figure 3.10 depicts the VCC utilised in identifying the different void shapes [51].

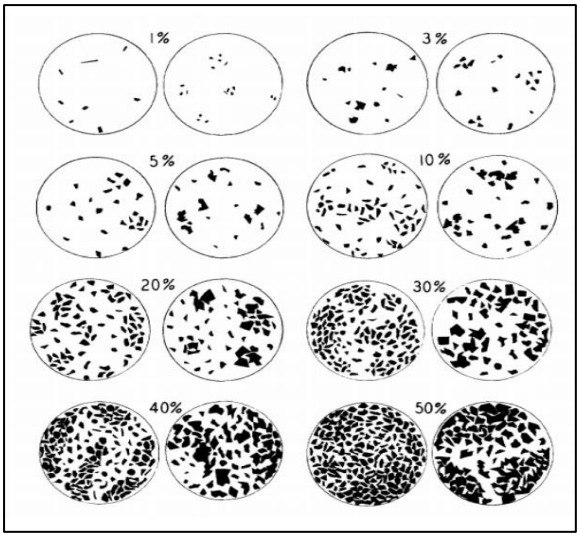

Figure 3.7 – VCC for inclusion frequency estimation in clay matrix [51].

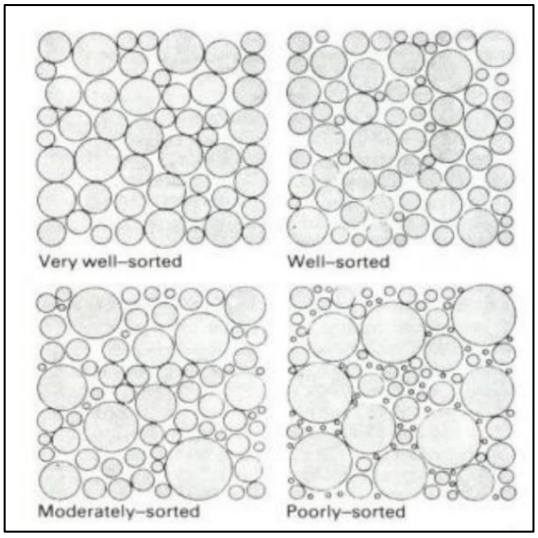

Figure 3.8 – VCC for inclusion sorting estimation [51].

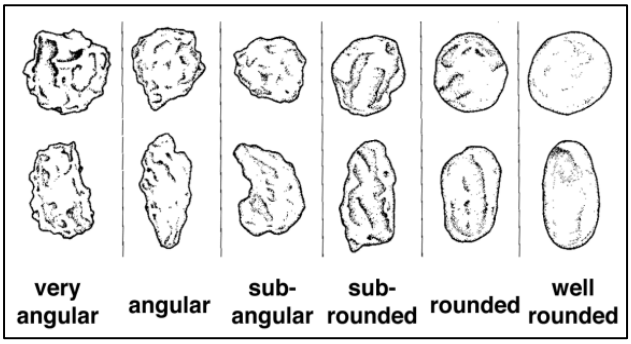

Figure 3.9 – VCC for inclusion shape estimation; Top row – equant; Bottom row – elongate [58].

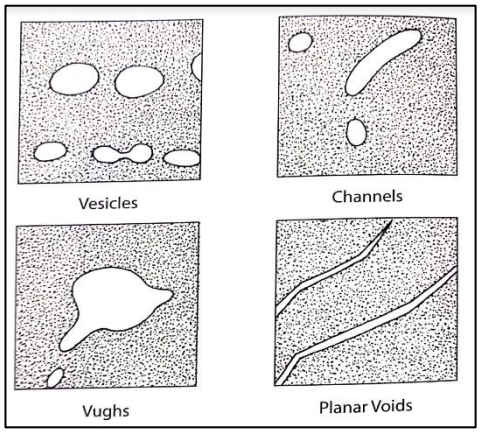

Figure 3.10 – VCC for void shape estimation [51].

Table 3.6 – Wentworth scale chart [51].

Inclusion Size Category	Inclusion Size (μm)
Extremely coarse	>2000
Very coarse	2000-1000
Coarse	1000-500
Medium-coarse	500-250
Medium-fine	250-125
Fine	125-62
Very fine	<62

Table 3.7 – Inclusion abundance frequency chart [51].

Frequency Labels (Inclusion Abundance)
Predominant (>70%)
Dominant (50-70%)
Frequent (30-50%)
Common (15-30%)
Few (5-15%)
Very Few (2-5%)
Rare (0.5-2%)
Very Rare (<0.5%)

Table 3.8 – Void scale chart [51].

Void Size Category	Void Size (mm)
Mega	>2
Macro	0.5-2
Meso	0.05-0.5
Micro	<0.05

The Swift Imaging software was also used to label and number the inclusions and voids of all the embedded samples. A table was then tabulated with all the inclusions and voids present in the clay matrix.

3.12.2 Scanning Electron Microscopy-Energy Dispersive Spectroscopy (SEM-EDS)

The embedded briquettes were observed using a Zeiss Merlin Field Emission Scanning Electron Microscope equipped with Energy Dispersive Spectroscopy (SEM-EDS) to view the samples at high magnifications and to determine the chemical composition of the inclusions present in the clay samples.

Prior to SEM-EDS analysis, the samples were placed in the airlock to remove air from the pores. Due to the non-conductive nature of the fired-clay samples, an Agar auto-sputter coater was used to deposit a thin film of gold on the surface of the embedded briquettes. The embedded samples were then attached to the double sided conductive carbon tape and onto aluminium stubs. However, for the unfired 63 μm and 125 μm samples, the powdered clay was attached to the double sided carbon tape and onto an aluminium stub.

The samples were viewed at magnifications of x100, x500, x5000 and x15000. The elemental X-ray spectrum of the fired clay inclusions were generated by performing point analysis. The elemental weight percentage (wt % or at%) of elements detected within the inclusions were presented in tables.

3.13 Hardness Testing

Hardness testing was conducted to evaluate whether hardness changes with firing conditions. This test was performed by using a Mitutoyo MVK-H2 machine. According to the ASTM C1326-13 standard, Knoop hardness tests are ideal for ceramics since they are brittle and larger loads may be applied without fracturing the sample [59]. This was corroborated by Clinton and Morrell [52]. The indenter was loaded with a 50 gf (gram-force) load for 10 seconds, as per ASTM C1326-13 standard [59]. A total of ten indents per sample were applied in order to have repeated readings. In the case of the oxidising samples, ten indents were made on the outer layer and ten other indents were incised on the core layer, whereas for the reducing samples only ten indents were made due to their homogeneous cross-section. Care was taken that no indents were indented on the visible voids.

An Axiocam 202 camera was attached to a Zeiss Axioscope 5 light microscope and was used at x50 magnification. The Zen software was utilized to measure the maximum indentation length of the indents.

The hardness value (HK) was calculated by substituting the maximum indentation length measured with the software and the applied load (0.05 kgf). The following equation was used (Equation 3.1):

$$HK = 14.229 \frac{P}{{d_{max}}^2} \tag{3.1}$$

where P is the force in kgf, d_{max} is the maximum indentation length in mm and 14.229 is the correction factor [59].

An average per sample was obtained and bar charts were plotted to show how hardness varies with both firing atmospheres and how hardness varies between the outer layer and core hardness of the briquettes.

4. Results

This Chapter encompasses the findings from the experiments carried out as explained in detail in Chapter 3 (Methodology). The results are presented in the following sequence; linear drying shrinkage, macroscopic documentation, XRPD, microscopy and hardness testing. A discussion on the findings can be found under Chapter 5 (Discussion).

4.1 Linear Drying Shrinkage

4.1.1 Clay sieved to 125 μm

Batches 1 and 2 were manufactured with clay particles sieved to 125 μm. From these batches of clay, four to five slabs were produced per batch. Batch 1 had water of plasticity of approximately **38%**, whereas batch 2 had water of plasticity of roughly **39.5%**, resulting in only a slight difference between these two batches. The linear drying shrinkage (%LDS) was then calculated on a daily basis by using equation (2.2).

Table 4.1 presents the average mass of the slabs in grams and average shrinkage measure in cm with respect to drying time in hours for batch 1. The average was determined from 5 readings.

Table 4.1 – Batch 1 average recordings.

Drying time (hours)	Avg mass of slab (g)	Length between marks (cm)	Linear Drying Shrinkage (%LDS)
0	63.90 ± 1.05	10.00	0
24	60.86 ± 1.13	9.87 ± 0.04	1.3
48	58.10 ± 0.94	9.63 ± 0.04	3.7
72	55.00 ± 0.64	9.39 ± 0.04	6.1
96	52.19 ± 1.07	9.19 ± 0.06	8.1
120	51.20 ± 0.98	9.18 ± 0.05	8.2
144	50.86 ± 0.98	9.15 ± 0.05	8.5
168	46.12 ± 0.87	9.10 ± 0.04	9

Table 4.2 presents the average mass of the slabs in grams and average shrinkage measure in cm with respect to drying time in hours for batch 2. The average was determined from 5 readings.

Table 4.2 – Batch 2 average recordings.

Drying time (hours)	Avg mass of slab (g)	Length between marks (cm)	Linear Drying Shrinkage (%LDS)
0	62.82 ± 2.58	10.00	0
24	60.77 ± 2.57	9.89 ± 0.02	1.1
48	57.95 ± 2.47	9.72 ± 0.08	2.8
72	55.39 ± 2.26	9.54 ± 0.07	4.6
96	52.61 ± 2.14	9.34 ± 0.05	6.6
120	50.62 ± 2.08	9.18 ± 0.02	8.2
144	49.82 ± 2.07	9.13 ± 0.04	8.7
168	44.95 ± 1.91	9.11 ± 0.05	8.9

Figures 4.1 and 4.2 show the graphs of mass of slabs (g) against drying time (hours) and length between marks (cm) against drying time (hours) for the averages of batches 1 and 2, respectively.

From these graphs, it can be seen that the same trend line for both batches applies. It is important to note that at 144 hours the samples were placed in a drying oven at a temperature of 105 °C for one hour. At this stage, the gradient of the graph increased which shows that more water evaporated from the briquettes. Also, batches 1 and 2 exhibit roughly the same linear drying shrinkage.

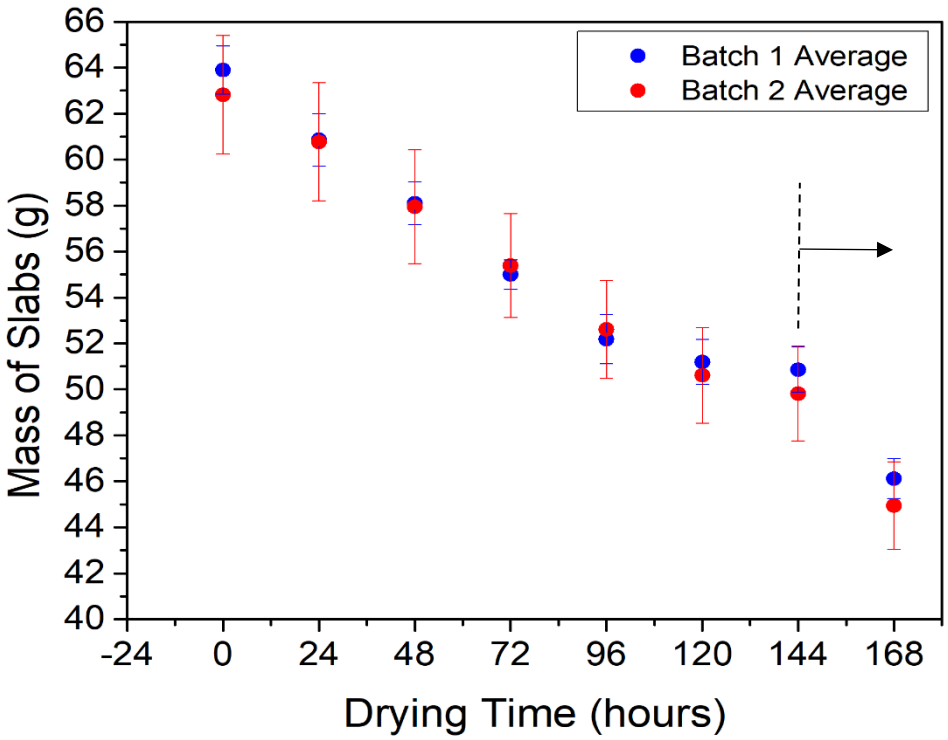

Figure 4.1 – Graph of avg mass of slabs (g) vs drying time (hours) for samples sieved to 125 μm. From dotted line onwards, the slabs were placed in a drying oven at a temperature of 105 °C.

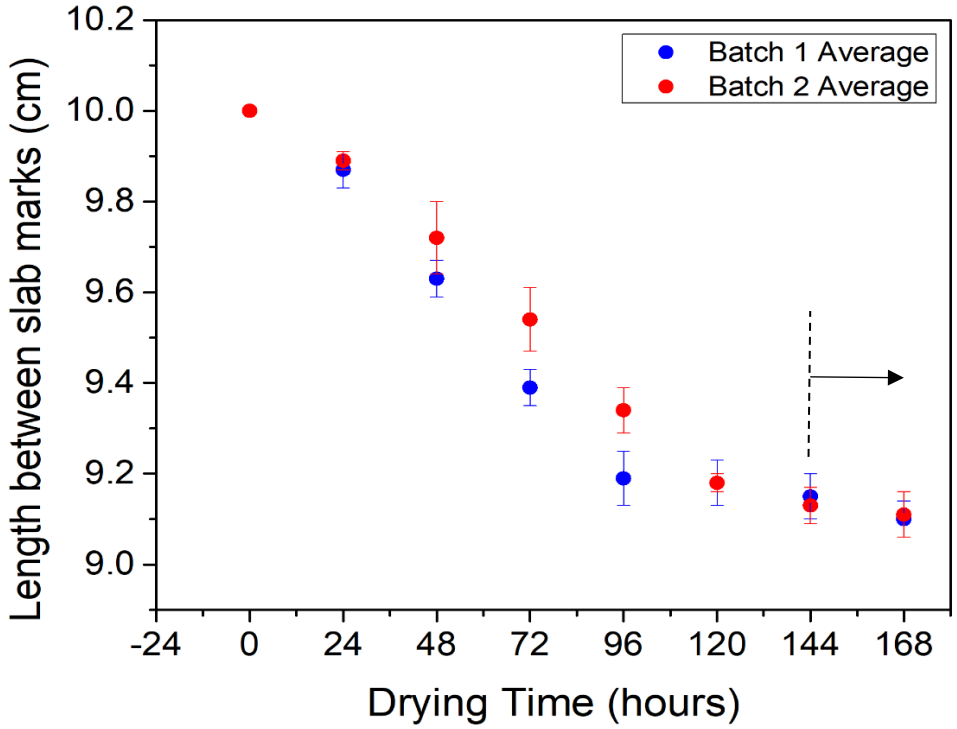

Figure 4.2 – Graph of avg length between slabs marks (cm) vs drying time (hours) for samples sieved to 125 μm. From dotted line onwards, the slabs were placed in a drying oven at a temperature of 105 °C.

4.1.2 Clay sieved to 63 μm

Batches 3 and 4 were manufactured with clay particles sieved to 63 μm. From these batches of clay, four to five slabs were produced per batch. Batch 3 had water of plasticity of approximately **41%** whereas batch 4 had water of plasticity of roughly **44.5%**. The difference in water of plasticity between the two batches was small, a mere ~ 3.5%. The linear drying shrinkage (%LDS) was then calculated on a daily basis by using equation (2.2).

Table 4.3 presents the average mass of the slabs in grams and average shrinkage measure in cm with respect to drying time in hours for batch 3. The average was determined from 5 readings.

Table 4.3 – Batch 3 average recordings.

Drying time (hours)	Avg mass of slab (g)	Length between marks (cm)	Linear Drying Shrinkage (%LDS)
0	62.87 ± 1.43	10.00	0
24	58.88 ± 2.29	9.76 ± 0.09	2.4
48	55.45 ± 1.92	9.49 ± 0.07	5.1
72	53.05 ± 1.68	9.28 ± 0.06	7.2
96	51.55 ± 1.45	9.22 ± 0.04	7.8
120	50.79 ± 1.30	9.17 ± 0.03	8.3
144	50.31 ± 1.19	9.15 ± 0.05	8.5
168	46.25 ± 1.04	9.11 ± 0.06	8.9

Table 4.4 presents the average mass of the slabs in grams and average shrinkage measure in cm with respect to drying time in hours for batch 4. The average was determined from 5 readings.

Table 4.4 – Batch 4 average recordings.

Drying time (hours)	Avg mass of slab (g)	Length between marks (cm)	Linear Drying Shrinkage (%LDS)
0	59.47 ± 2.43	10.00	0
24	56.06 ± 2.09	9.85 ± 0.04	1.5
48	52.19 ± 1.82	9.54 ± 0.06	4.6
72	49.50 ± 1.77	9.31 ± 0.07	6.9
96	46.87 ± 1.75	9.06 ± 0.04	9.4
120	45.70 ± 1.87	8.99 ± 0.04	10.1
144	45.00 ± 1.91	8.96 ± 0.06	10.4
168	41.11 ± 1.82	8.93 ± 0.06	10.7

Figures 4.3 and 4.4 show the graphs of mass of slabs (g) against drying time (hours) and length between marks (cm) against drying time (hours) for the averages of batches 3 and 4, respectively.

From these graphs, it can also be seen that the same trend line for both batches applies. However, batch 4 has a lower mass than batch 3. It is important to note that at 144 hours the samples were placed in a drying oven at a temperature of 105 °C for one hour. At this stage, the gradient of the graph increased which shows that more water evaporated from the briquettes. Also, batch 4 has a greater linear drying shrinkage than batch 3.

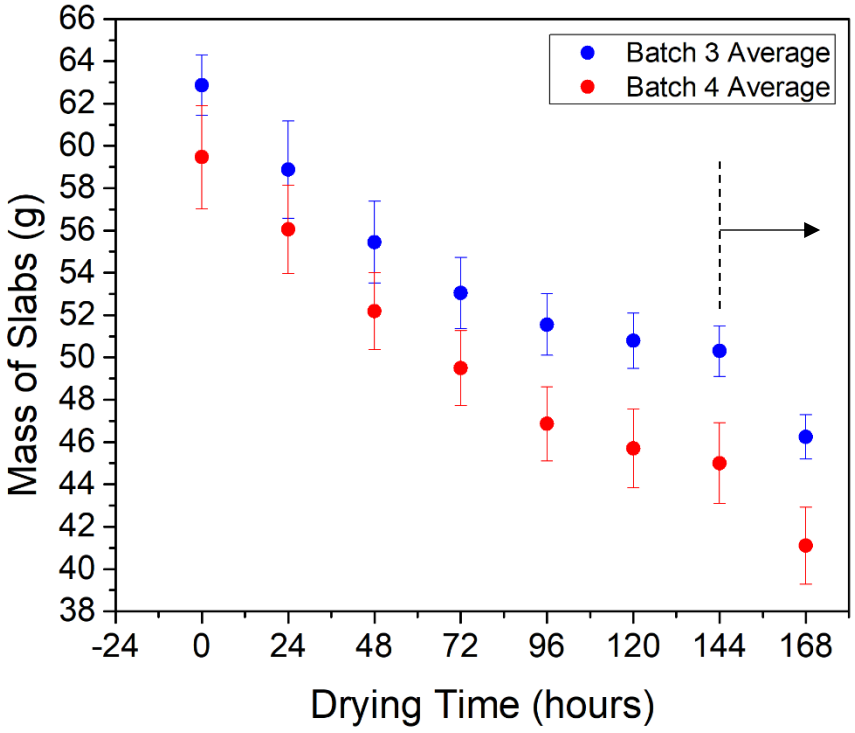

Figure 4.3 – Graph of avg mass of slabs (g) vs drying time (hours) for samples sieved to 63 μm. From dotted line onwards, the slabs were placed in a drying oven at a temperature of 105 °C.

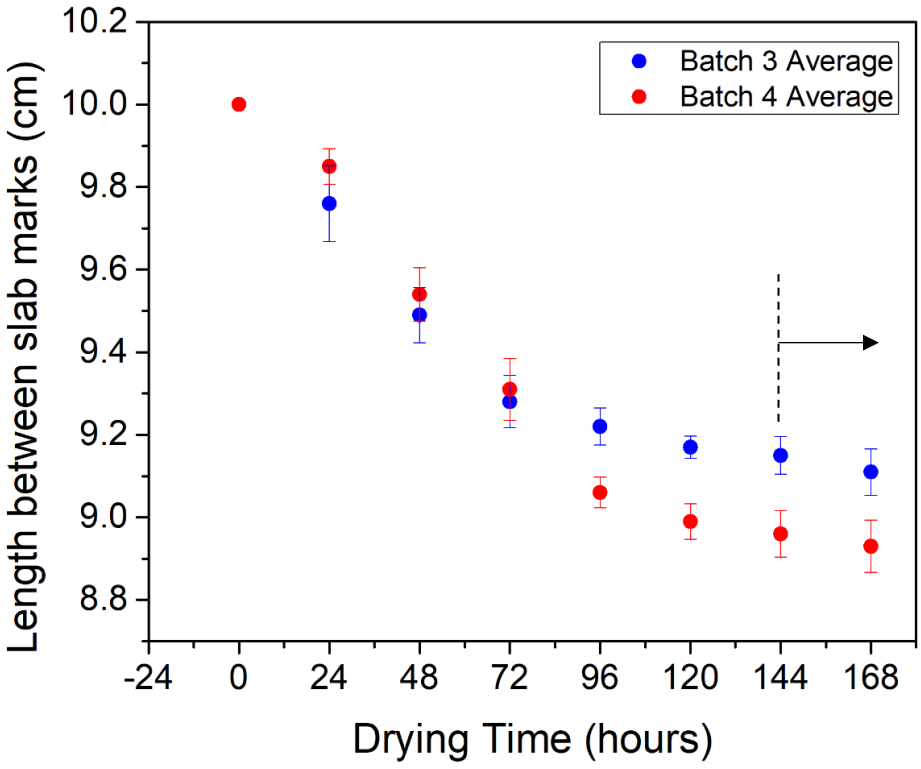

Figure 4.4 – Graph of avg length between slabs marks (cm) vs drying time (hours) for samples sieved to 63 μm. From dotted line onwards, the slabs were placed in a drying oven at a temperature of 105 °C.

4.2 Macroscopic Recording

4.2.1 Photography

Figure 4.5 shows the slabs after being manufactured and before being fired (green state). From this figure the two shallow marks can be clearly seen, as well as the transverse indents made to aid in the separation of slabs into briquettes. The number/letter punches are also visible on the slabs.

Figure 4.5 – Photograph of slab A and B (Batch 1) after manufacturing.

Figure 4.6a) presents the 63 μm briquettes fired at 500, 700 and 900 °C in an oxidising atmosphere for 30 minutes and 120 minutes. Figure 4.6b) presents the 63 μm briquettes fired at 500, 700 and 900 °C in a reducing atmosphere for 30 minutes and 120 minutes.

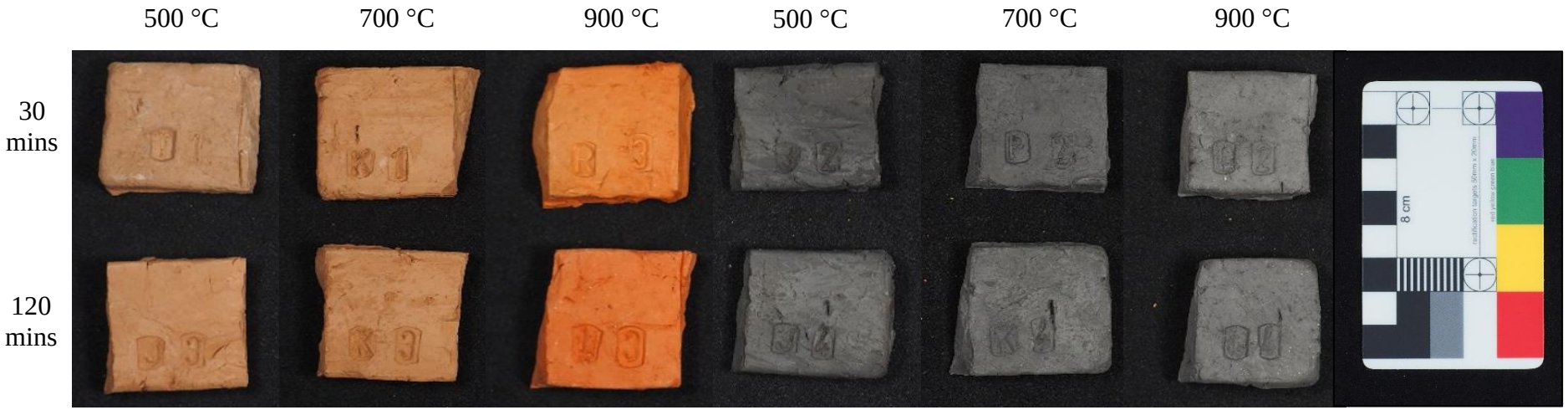

a) b)

Figure 4.6: a) From top left to bottom right: 63_500_30_Oxi, 63_700_30_Oxi, 63_900_30_Oxi, 63_500_120_Oxi, 63_700_120_Oxi, 63_900_120_Oxi. b) From top left to bottom right: 63_500_30_Red, 63_700_30_Red, 63_900_30_Red, 63_500_120_Red, 63_700_120_Red and 63_900_120_Red.

From this figure it can be seen that on increasing the temperature in an oxidising atmosphere, the colour of the briquettes tends towards a more reddish colour. However, in a reducing atmosphere, the briquettes are black at the lowest temperature and on increasing the firing temperature, they tend towards a greyish colour. There are only slight differences in colour when varying the soaking times.

Figures 4.7 and 4.8 show the cross-section of the embedded briquettes prepared from 63 μm clay particles and fired to 500 °C in an oxidising atmosphere for 30 and 120 mins, respectively. Figure 4.7 does not show a full cross-section as this briquette broke up during the grinding procedure and the whole cross-section was not recovered.

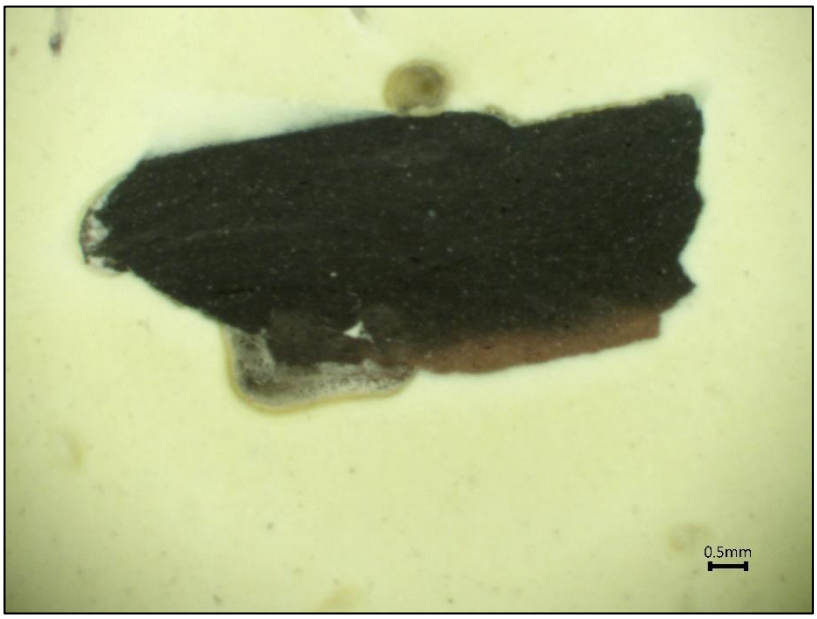

Figure 4.7 – 63_500_30_Oxi embedded briquette cross-section at a magnification of x10.

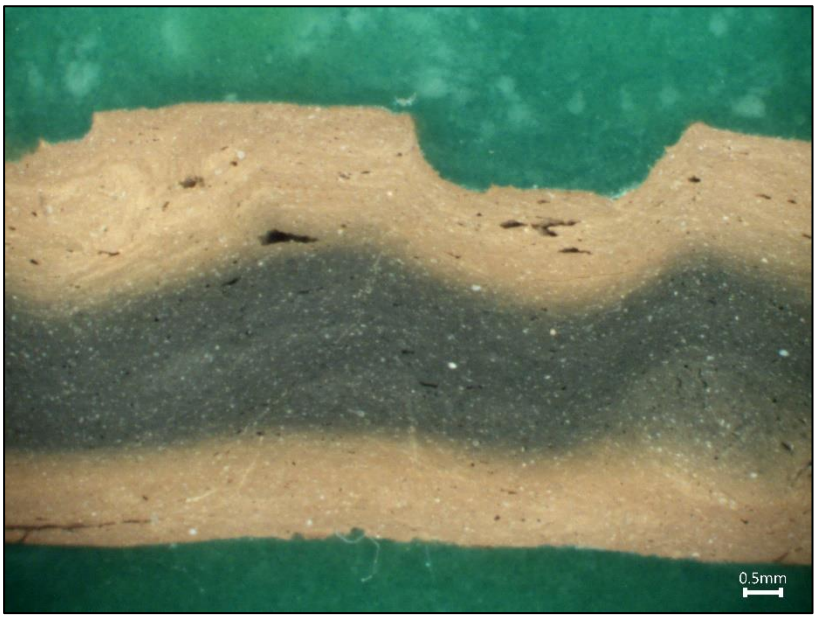

Figure 4.8 – 63_500_120_Oxi embedded briquette cross-section at a magnification of x10.

Figures 4.9 and 4.10 present the cross-section of the embedded briquettes prepared from 63 μm clay particles and fired to 700 °C in an oxidising atmosphere for 30 and 120 mins, respectively.

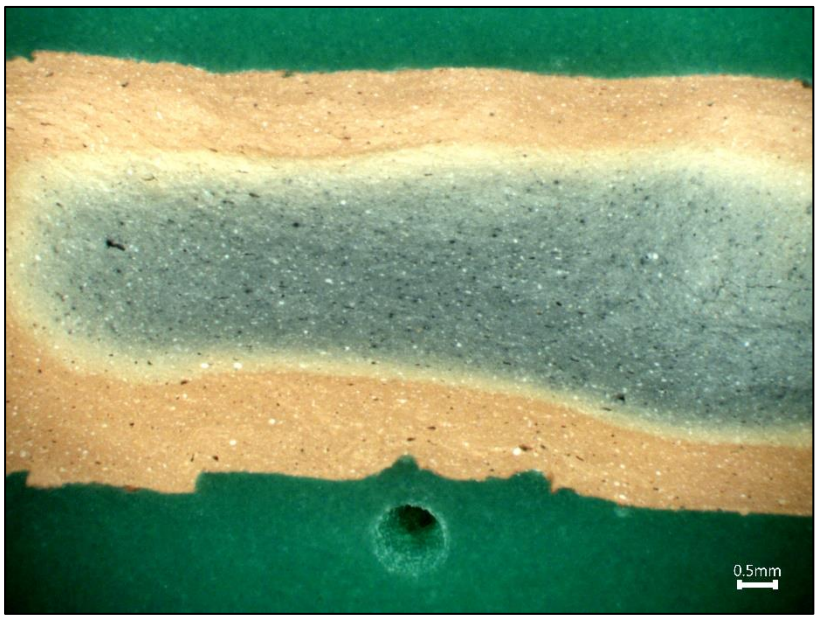

Figure 4.9 – 63_700_30_Oxi embedded briquette cross-section at a magnification of x10.

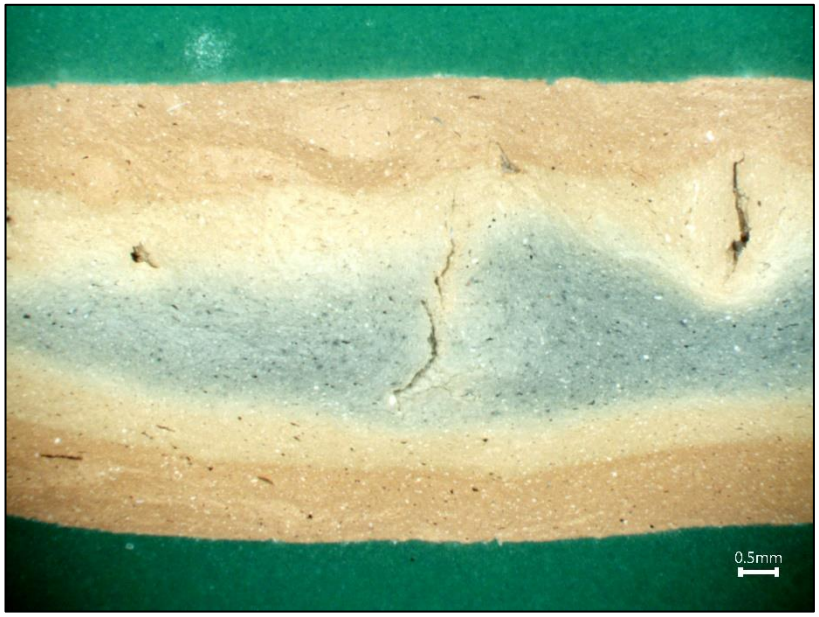

Figure 4.10 – 63_700_120_Oxi embedded briquette cross-section at a magnification of x10.

Figures 4.11 and 4.12 visualise the cross-section of the embedded briquettes prepared from 63 μm clay particles and fired to 900 °C in an oxidising atmosphere for 30 and 120 mins, respectively.

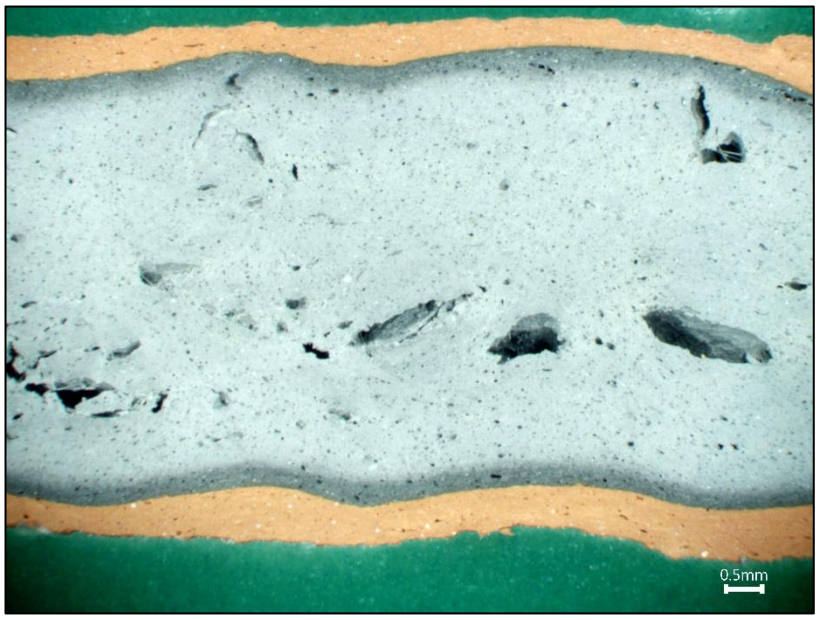

Figure 4.11 – 63_900_30_Oxi embedded briquette cross-section at a magnification of x10.

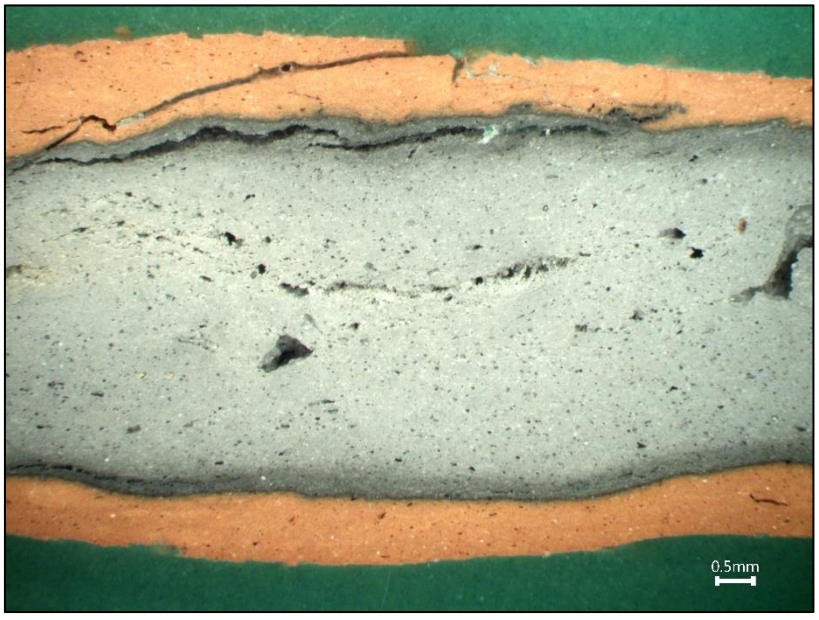

Figure 4.12 – 63_900_120_Oxi embedded briquette cross-section at a magnification of x10.

Figure 4.13 shows the cross-section of the embedded briquette sieved to 125 μm fired in an oxidising atmosphere at a soaking time of 120 minutes at 900 °C. This was done in order to see if there were any differences in the cross-sections when varying the mesh size the clays were sieved to.

Figure 4.13 – 125_900_120_Oxi embedded briquette cross-section at a magnification of x10.

From figures 4.8-4.13 it can be observed that on increasing the soaking time, the core thickness decreases. When the firing temperature is increased, the core colour changes, and more porosity and voids are present in the cross-section. In Figure 4.13, more visible inclusions are present in the microstructure than the other figures shown above.

Figures 4.14 and 4.15 present the cross-section of the embedded briquettes prepared from 63 μm clay particles and fired to 500 °C in a reducing atmosphere for 30 and 120 mins, respectively.

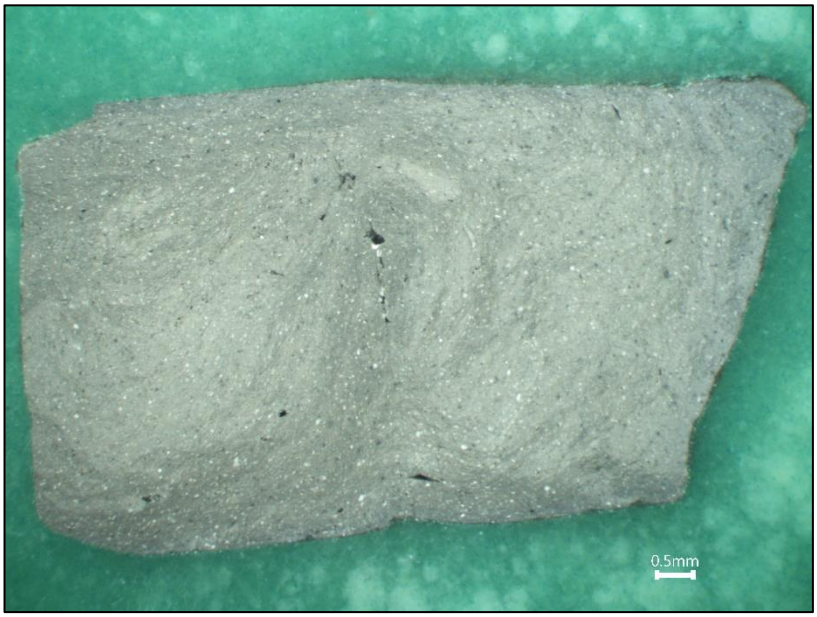

Figure 4.14 – 63_500_30_Red embedded briquette cross-section at a magnification of x10.

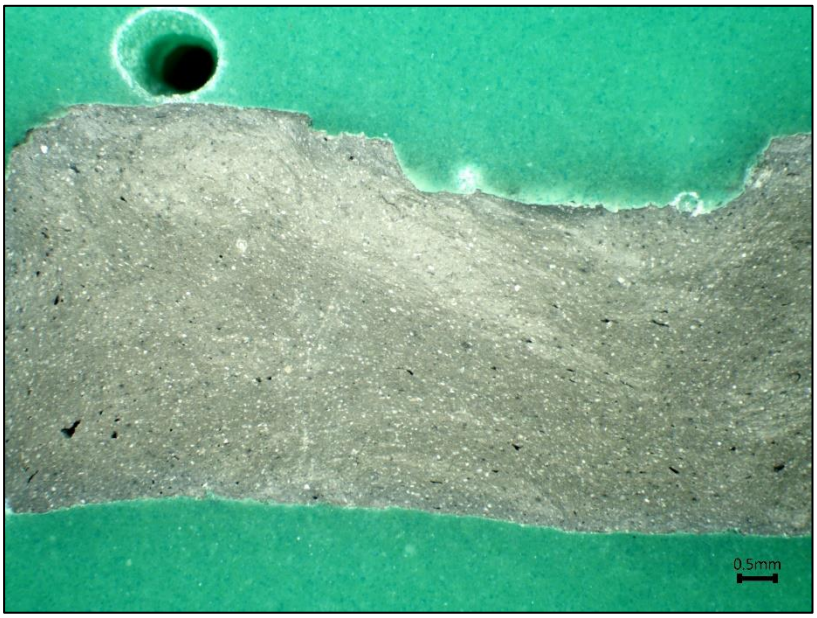

Figure 4.15 – 63_500_120_Red embedded briquette cross-section at a magnification of x10.

Figures 4.16 and 4.17 show the cross-section of the embedded briquettes prepared from 63 μm clay particles and fired to 700 °C in a reducing atmosphere for 30 and 120 mins, respectively.

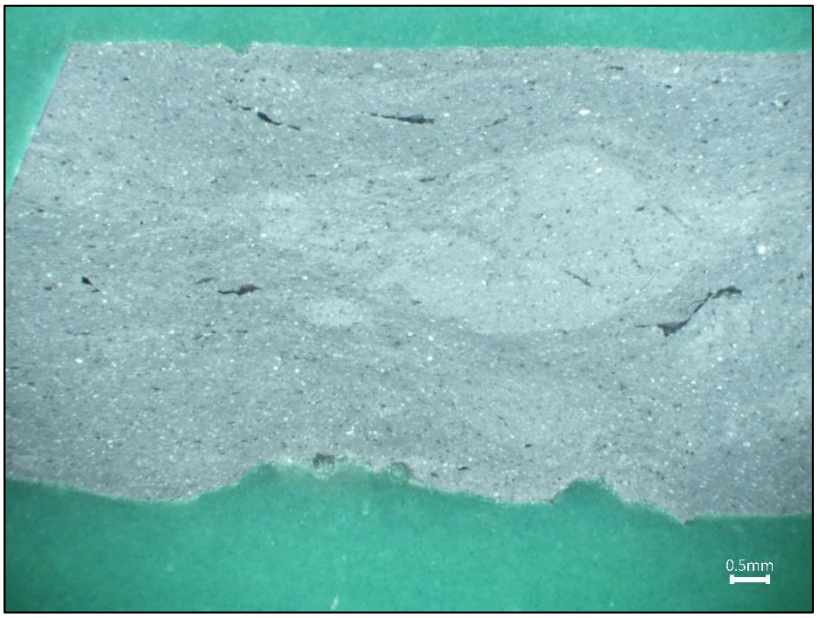

Figure 4.16 – 63_700_30_Red embedded briquette cross-section at a magnification of x10.

Figure 4.17 – 63_700_120_Red embedded briquette cross-section at a magnification of x10.

Figures 4.18 and 4.19 visualise the cross-section of the embedded briquettes prepared from 63 μm clay particles and fired to 700 °C in a reducing atmosphere for 30 and 120 mins, respectively.

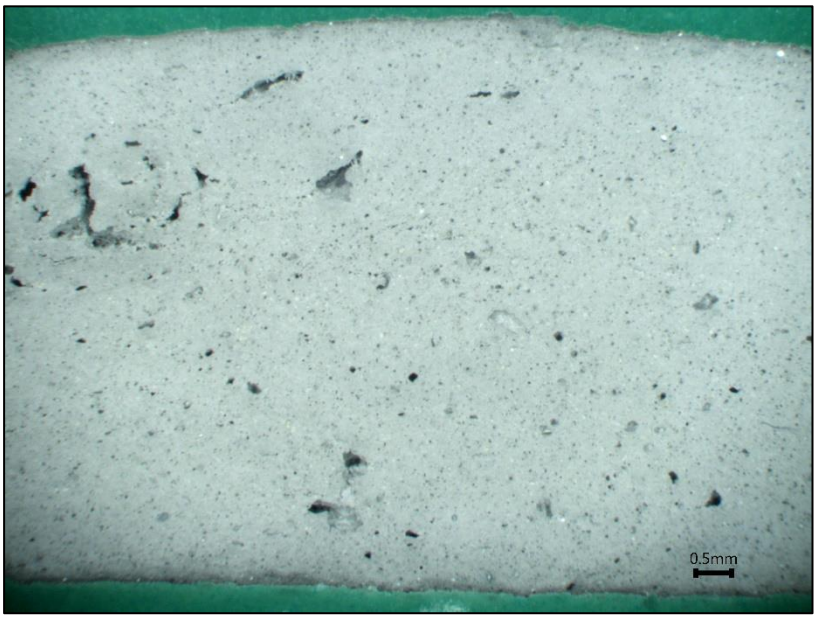

Figure 4.18 – 63_900_30_Red embedded briquette cross-section at a magnification of x10.

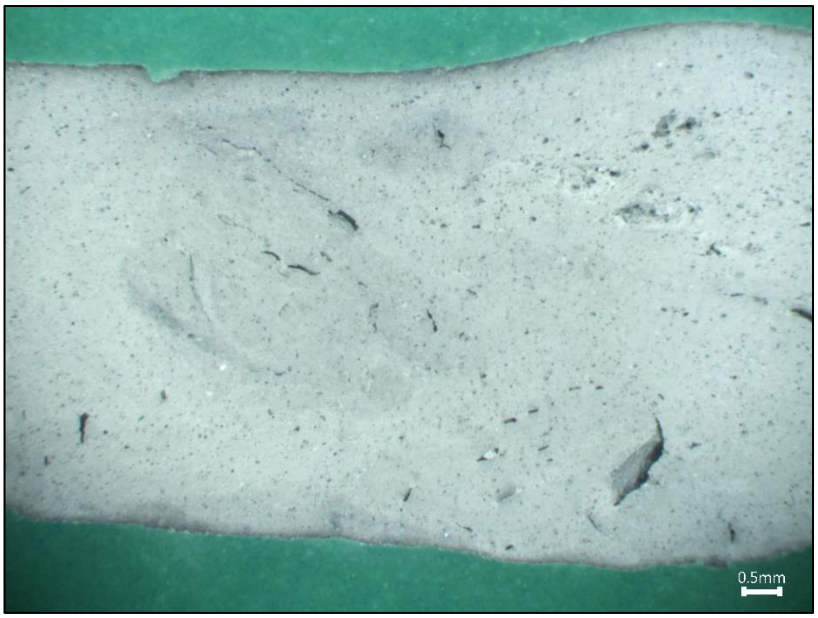

Figure 4.19 – 63_900_120_Red embedded briquette cross-section at a magnification of x10.

From figures 4.14-4.19 it can be observed that on increasing the soaking time, there are no significant differences. However, when the firing temperature is increased, the core colour changes, and more porosity and voids are present in the cross-section.

In Table 4.5 the average of the core thickness and briquette thickness obtained when measuring five different points together with the soaking time are observed. The ratio of average core thickness over average briquette thickness was then generated. This ratio was determined as throughout the cross-section of the briquettes, the core and surface layers varied in thickness.

Table 4.5 – Average of the core and briquette thickness for the fired samples in an oxidising atmosphere.

Sample	Average Briquette Thickness (mm)	Average Core Thickness (mm)	Average Core/Briquette Thickness Ratio
63_500_120_Oxi	4.86 ± 0.32	2.09 ± 0.27	0.43 ± 0.04
63_700_30_Oxi	5.04 ± 0.13	2.43 ± 0.34	0.48 ± 0.06
63_700_120_Oxi	5.45 ± 0.06	1.74 ± 0.20	0.32 ± 0.09
63_900_30_Oxi	6.03 ± 0.10	4.73 ± 0.06	0.78 ± 0.02
63_900_120_Oxi	5.80 ± 0.15	3.70 ± 0.14	0.64 ± 0.02
125_900_120_Oxi	5.95 ± 0.19	4.36 ± 0.39	0.73 ± 0.04

Figure 4.20 shows a bar chart depicting the relationship between soaking time and core thickness for all the briquettes fired in an oxidising atmosphere. The 63_500_30_Oxi briquette was not plotted as this was the weakest briquette from all the samples and as a result, it broke up during the grinding procedure and the whole sample was not recovered.

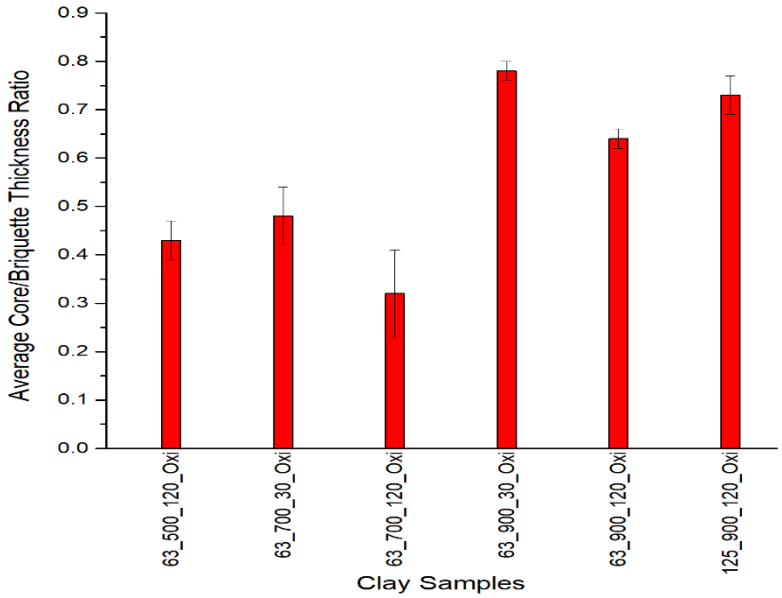

Figure 4.20 – Bar graph showing ratio of average core thickness over average briquette thickness of the fired clay samples.

From Figure 4.20, it is evident that on increasing the soaking time, the ratio of average core/briquette thickness, decreases.

4.2.2 Munsell Chart Data

Table 4.6 shows the results obtained from the Munsell Chart recording.

Table 4.6 – Munsell Chart data.

Samples	Pre-Firing	After Firing			Visible Inclusions	Observations
	Colour	Surface Colour	Core Colour	Margin Colour		
63_500_30_Oxi	2.5Y 6/3 light yellowish brown	5YR 5/4 reddish brown	Gley1 2.5/N black	5YR 5/4 reddish brown (same as surface)	N/A	Softer briquette as the plier left a light mark on the margin
63_500_30_Red	2.5Y 6/3 light yellowish brown	Gley1 2.5/N black	Gley1 2.5/N black (same as surface)	Gley1 2.5/N black (same as surface)	Sparse visible white inclusions	No visible cracks
63_500_120_Oxi	2.5Y 6/3 light yellowish brown	5YR 5/6 yellowish red	Gley2 3/10B very dark bluish grey	5YR 5/6 yellowish red (same as surface)	N/A	No visible cracks
63_500_120_Red	2.5Y 6/3 light yellowish brown	Gley1 3/N very dark grey	Gley1 3/N very dark grey (same as surface)	Gley1 3/N very dark grey (same as surface)	White inclusions	No visible cracks
63_700_30_Oxi	2.5Y 6/3 light yellowish brown	5YR 5/6 yellowish red	Gley2 4/10B very dark bluish grey	10YR 7/3 very pale brown	No visible inclusions but one void visible after break	No visible cracks
63_700_30_Red	2.5Y 6/3 light yellowish brown	Gley1 4/N dark grey	Gley1 4/N dark grey (same as surface)	Gley1 4/N dark grey (same as surface)	No visible inclusions	No visible cracks
63_700_120_Oxi	2.5Y 6/3 light yellowish brown	2.5YR 6/6 light red - 5/6 red	7.5YR 5/1 grey	7.5YR 6/4 light brown	Very sparse small inclusions	No visible cracks
63_700_120_Red	2.5Y 6/3 light yellowish brown	Gley1 4/N dark grey	Gley1 4/N dark grey (same as surface)	Gley1 4/N dark grey (same as surface)	N/A	No blisters and very hard to break
63_900_30_Oxi	2.5Y 6/3 light yellowish brown	2.5YR 5/8 red	Gley1 5/N grey	Gley1 3/N very dark grey	Visible voids	Crack visible in the middle

63_900_30_Red	2.5Y 6/3 light yellowish brown	Gley1 4/N dark grey	Gley1 5/N grey	Gley1 4/N dark grey (same as surface)	N/A	Swallowed in middle of briquettes, small blisters on surface
63_900_120_Oxi	2.5Y 6/3 light yellowish brown	2.5YR 4/8 - 5/8 red	Gley1 5/N grey	2.5YR 4/8 - 5/8 red (same as surface)	Small sparse whitish/yellowish inclusions	Possible air bubble in the middle and voids are visible
63_900_120_Red	2.5Y 6/3 light yellowish brown	Gley2 2.5/10B bluish black	Gley2 6/5PB light bluish grey	Gley2 2.5/10B bluish black (same as surface)	Sparse small inclusions and white inclusions on surface (like glitter)	Possible air bubble in the middle and voids are visible
125_900_120_Oxi	2.5Y 6/3 light yellowish brown	2.5 YR 5/8 Red	Gley1 5/N Grey	Gley1 3/N very dark grey	Very small inclusions white (looks like glitter)	one blister and a small crack on one corner, in section visible voids and visible blister

Gley refers to the Hue card used in the Munsell Chart. From the above table, it can be observed that on increasing the firing temperature, the surface and core colour of the briquettes varies. The core and surface colour change slightly when soaking time varies, however, the margin colour alters. It was also noted that when a temperature of 900 °C was reached, more visible inclusions, blisters, cracks and voids were present on the samples.

4.3 Microscopy

4.3.1 Optical Microscopy

The fired briquettes were viewed under a stereomicroscope at a magnification of x50. The inclusions and voids present in the clay matrix were recorded and tabulated using Figures 3.8-3.10 and Tables 3.6-3.8. Some inclusions and voids in the two images are labelled the same. This is because they appear to be the same. Figures 4.21 and 4.22 show the microscope image of the 63_500_30_Red briquette viewed at x50 magnification.

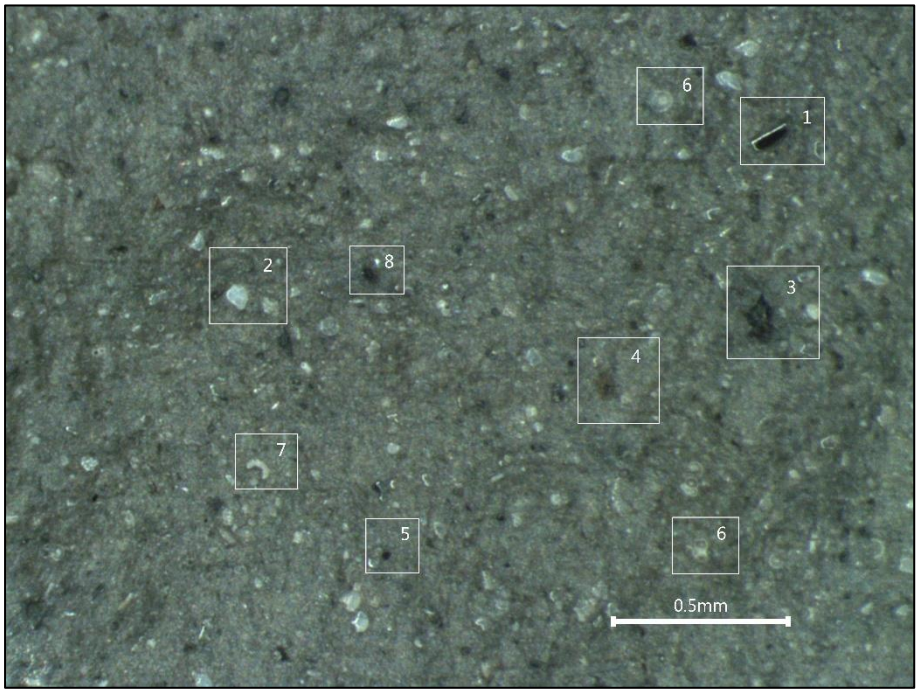

Figure 4.21 – Area 1 of 63_500_30_Red briquette viewed at x50 magnification.

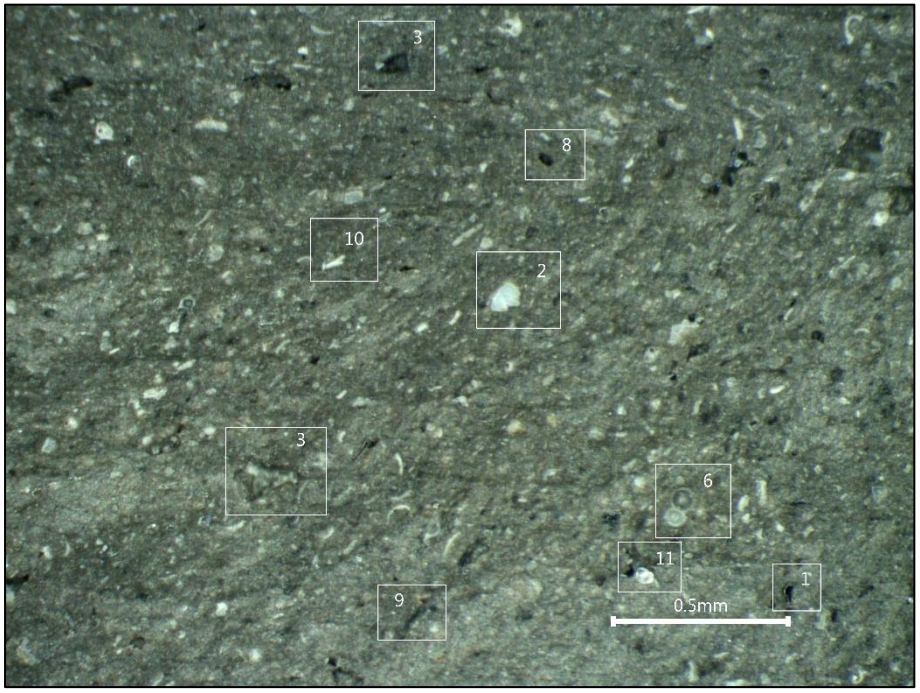

Figure 4.22 – Area 2 of 63_500_30_Red briquette viewed at x50 magnification.

Table 4.7 shows the Visual Comparison Chart (VCC) used to label the voids and inclusions present in the clay sample.

Table 4.7 – VCC for 63_500_30_Red sample.

Phase	Type	Size (Maximum Length)	Sorting	Shape	Frequency	Colour	Comments
1	Inclusion	0.12mm (Fine)	Very Poorly Sorted	Elongate Sub-Rounded	Very Rare (<0.5%)	Black	
2	Inclusion	0.09mm (Fine)	Moderately Sorted	Equant Angular	Few (5-15%)	Greyish white	
3	Void	0.13mm (Meso)	/	Vugh	/	/	
4	Inclusion	0.08mm (Fine)	Very Poorly Sorted	Equant Sub-Angular	Very Rare (<0.5%)	Dark brown	
5	Inclusion	0.02mm (Very Fine)	Moderately Sorted	Equant Rounded	Very Few (2-5%)	Black	Potentially magnetite...reduced form of iron oxide or glauconite
6	Inclusion	0.08mm (Fine)	Poorly Sorted	Equant Rounded	Few (5-15%)	Greyish white	Potential *Foraminifera*
7	Inclusion	0.07mm (Fine)	Very Poorly Sorted	Elongate Sub-Angular	Very Rare (<0.5%)	Greyish white	Probably a crushed microfossil
8	Inclusion	0.03mm (Very Fine)	Poorly Sorted	Elongate Rounded	Few (5-15%)	Black	
9	Void	0.12mm (Meso)	/	Planar Void	/	/	
10	Inclusion	0.07mm (Fine)	Poorly Sorted	Elongate Angular	Common (15-30%)	White	
11	Inclusion	0.07mm (Fine)	Poorly Sorted	Equant Sub-Rounded	Very Rare (<0.5%)	Shiny	

This sample had an abundance of inclusions estimated to be around 40% of the area of the matrix, by using Figure 3.7.

Figures 4.23 and 4.24 present the microscope image of the 63_700_30_Red briquette viewed at x50 magnification.

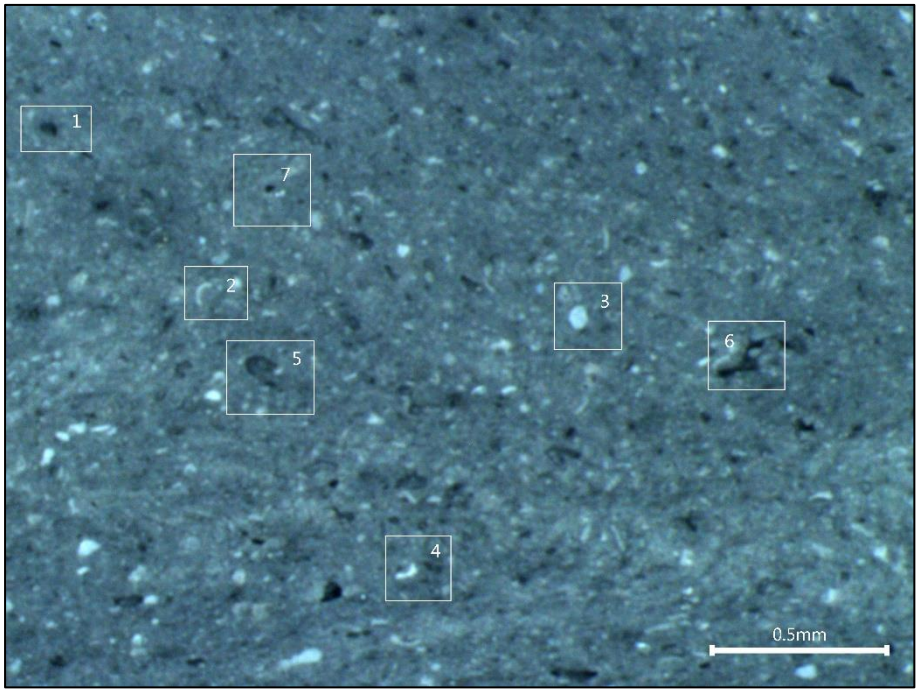

Figure 4.23 – Area 1 of 63_700_30_Red briquette viewed at x50 magnification.

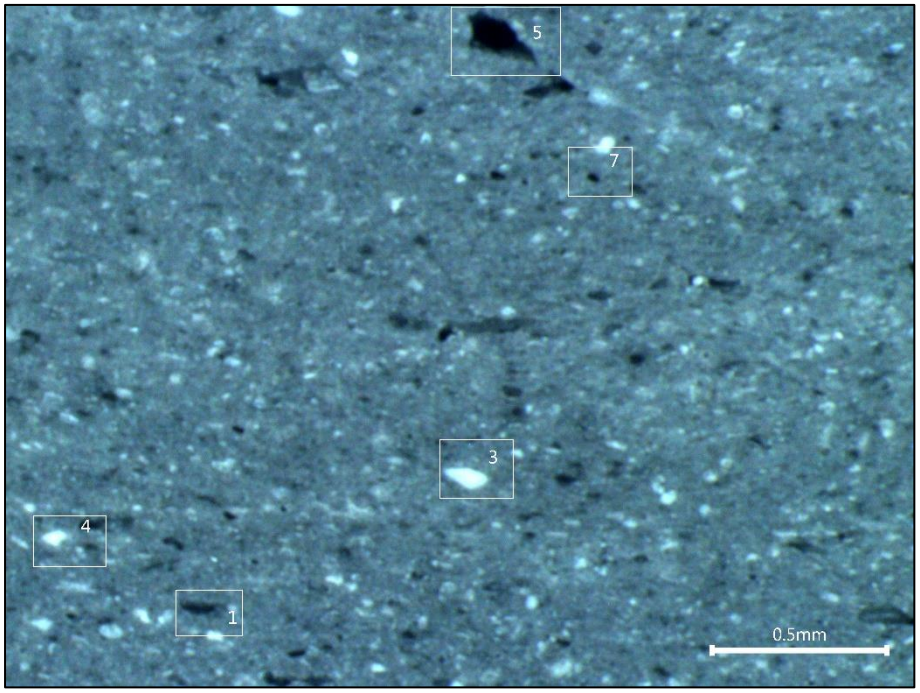

Figure 4.24 – Area 2 of 63_700_30_Red briquette viewed at x50 magnification.

Table 4.8 presents the Visual Comparison Chart (VCC) used to label the voids and inclusions present in the clay sample.

Table 4.8 – VCC for 63_700_30_Red sample.

Phase	Type	Size (Maximum Length)	Sorting	Shape	Frequency	Colour	Comments
1	Inclusion	0.04mm (Very Fine)	Very Poorly Sorted	Equant Sub-Angular	Few (5-15%)	Black	Possibly magnetite or glauconite
2	Inclusion	0.06mm (Very Fine)	Very Poorly Sorted	Elongate Sub-Angular	Very Rare (<0.5%)	Greyish white	Possible shell
3	Inclusion	0.09mm (Fine)	Poorly Sorted	Equant Sub-Rounded	Common (15-30%)	Greyish white	
4	Inclusion	0.06mm (Very Fine)	Poorly Sorted	Elongate Sub-Angular	Rare (0.5-2%)	White	
5	Void	0.10mm (Meso)	/	Vugh	/	/	
6	Void		/	Elongated Void (Channel + Planar)	/	/	
7	Void	0.01mm (Micro)	/	Vesicle	/	/	

This sample had an abundance of inclusions estimated to be around 40% of the area of the matrix, by using Figure 3.7.

Figures 4.25 and 4.26 show the microscope image of the 63_700_120_Oxi briquette viewed at x50 magnification.

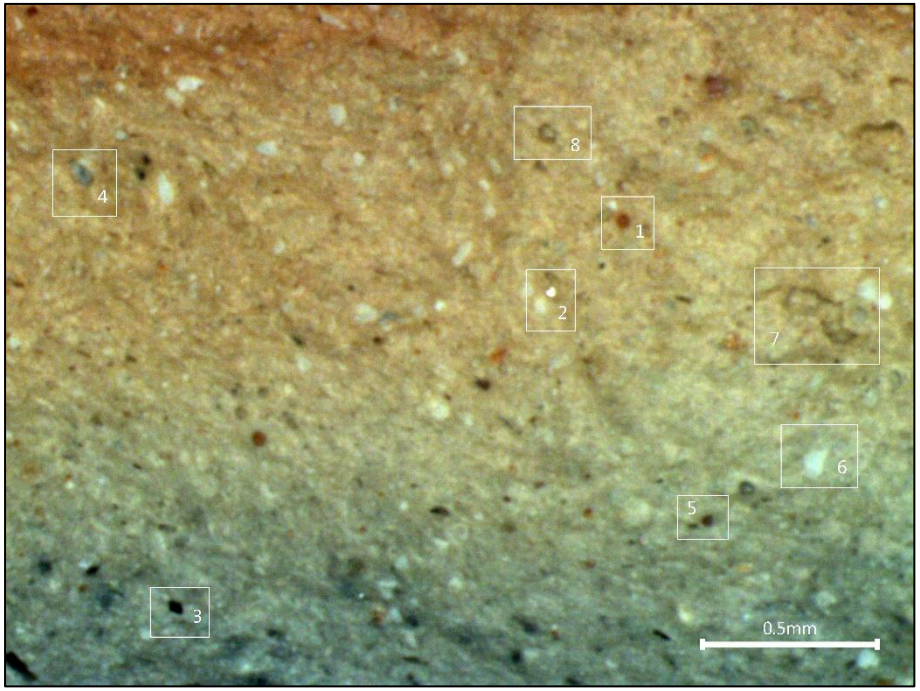

Figure 4.25 – Area 1 of 63_700_120_Oxi briquette viewed at x50 magnification.

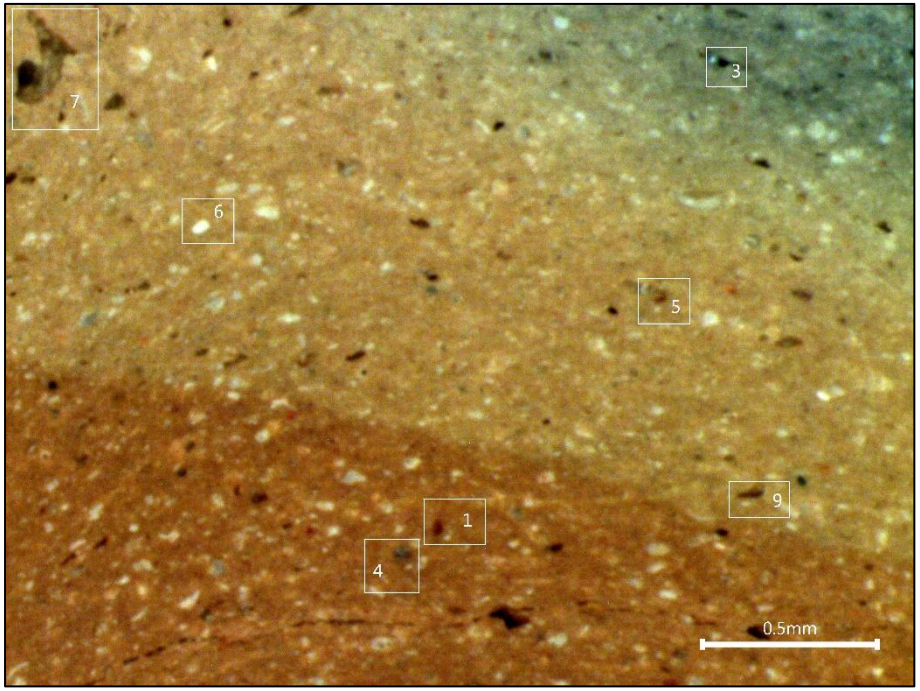

Figure 4.26 – Area 2 of 63_700_120_Oxi briquette viewed at x50 magnification.

Table 4.9 shows the Visual Comparison Chart (VCC) used to label the voids and inclusions present in the clay sample.

Table 4.9 – VCC for 63_700_120_Oxi sample.

Phase	Type	Size (Maximum Length)	Sorting	Shape	Frequency	Colour	Comments
1	Inclusion	0.03mm (Very Fine)	Moderately Sorted	Equant Rounded	Very Few (2-5%)	Reddish Brown	Possible glauconite
2	Inclusion	0.02mm (Very Fine)	Poorly Sorted	Equant Sub-Rounded	Very Rare (<0.5%)	Shiny	Possible quartz
3	Inclusion	0.05mm (Very Fine)	Very Poorly Sorted	Elongate Sub-Rounded	Few (5-15%)	Black	
4	Inclusion	0.07mm (Fine)	Very Poorly Sorted	Elongate Rounded	Very Few (2-5%)	Greyish Black	
5	Inclusion	0.03mm (Very Fine)	Poorly Sorted	Equant Sub-Rounded	Very Few (2-5%)	Brown	
6	Inclusion	0.08mm (Fine)	Moderately Sorted	Equant Angular	Frequent (30-50%)	Greyish White	Possible calcium carbonate
7	Void	0.23mm (Meso)	/	Vugh	/	/	
8	Void	0.07mm (Meso)	/	Vesicle	/	/	
9	Void	0.06mm (Meso)	/	Channel	/	/	

This sample had an abundance of inclusions estimated to be around 40% of the area of the matrix, by using Figure 3.7.

Figures 4.27 and 4.28 present the microscopic image of the 63_900_120_Oxi briquette viewed at x50 magnification.

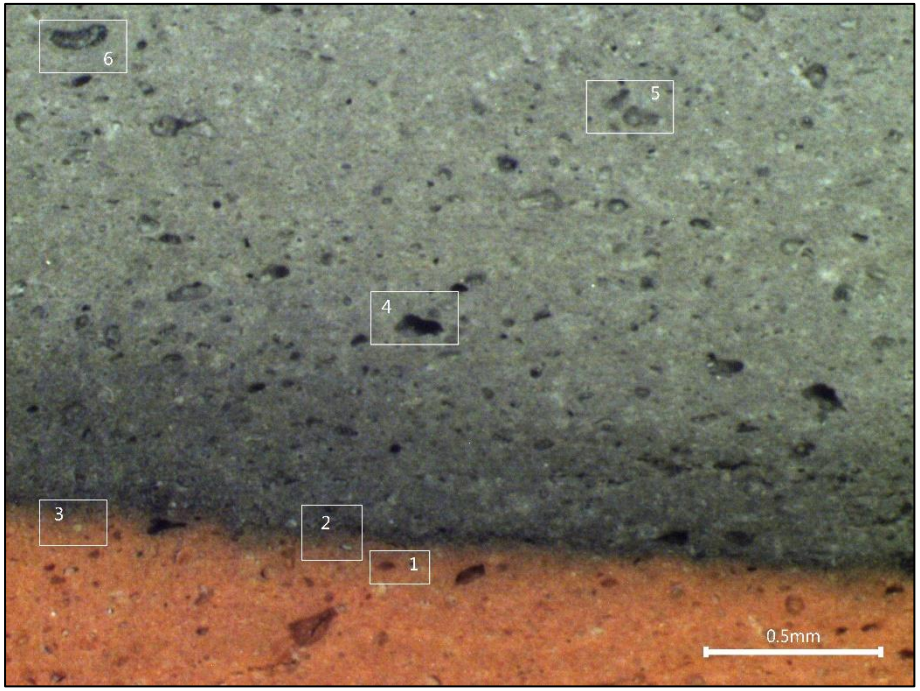

Figure 4.27 – Area 1 of 63_900_120_Oxi briquette viewed at x50 magnification.

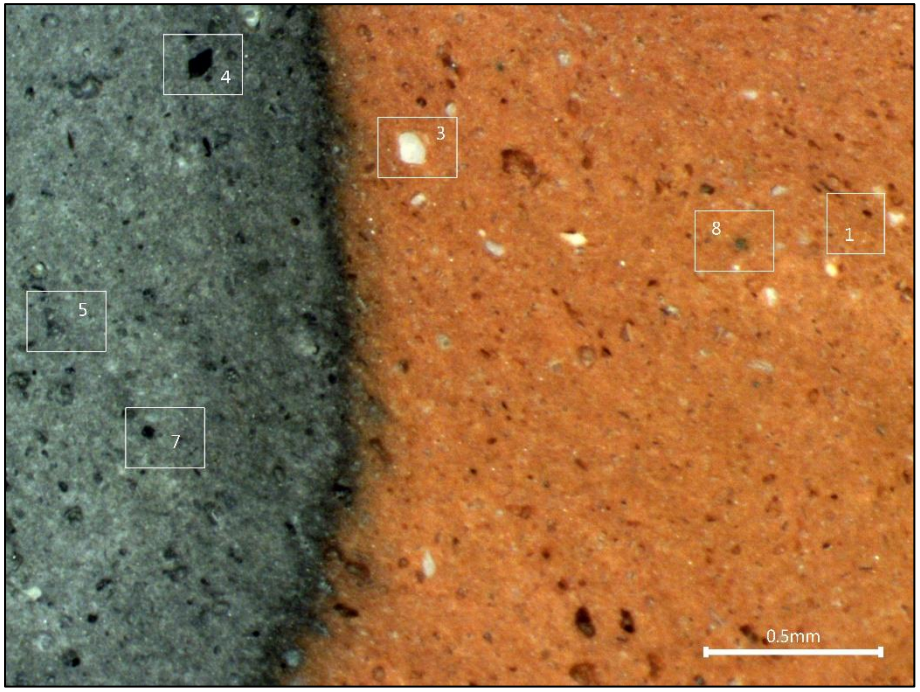

Figure 4.28 – Area 2 of 63_900_120_Oxi briquette viewed at x50 magnification.

Table 4.10 presents the Visual Comparison Chart (VCC) used to label the voids and inclusions present in the clay sample.

Table 4.10 – VCC for 63_900_120_Oxi sample.

Phase	Type	Size (Maximum Length)	Sorting	Shape	Frequency	Colour	Comments
1	Inclusion	0.05mm (Very Fine)	Very Poorly Sorted	Elongate Sub-Rounded	Rare (0.5-2%)	Brown	
2	Inclusion	0.03mm (Very Fine)	Very Poorly Sorted	Elongate Rounded	Rare (0.5-2%)	Greyish Black	
3	Inclusion	0.02mm (Very Fine)	Poorly Sorted	Equant Sub-Rounded	Few (5-15%)	Whitish Grey	Possible wollastonite
4	Void	0.13mm (Meso)	/	Vugh	/	/	
5	Void	0.05mm (Meso)	/	Vesicles	/	/	
6	Void	0.15mm (Meso)	/	Channel	/	/	
7	Inclusion	0.03mm (Very Fine)	Very Poorly Sorted	Equant Rounded	Very Few (2-5%)	Black	
8	Inclusion	0.04mm (Very Fine)	Very Poorly Sorted	Equant Sub-Rounded	Rare (0.5-2%)	Light Grey	

This sample had an abundance of inclusions estimated to be around 40% of the area of the matrix, by using Figure 3.7.

Figures 4.29 and 4.30 show the microscopic image of the 125_900_120_Oxi briquette viewed at x50 magnification.

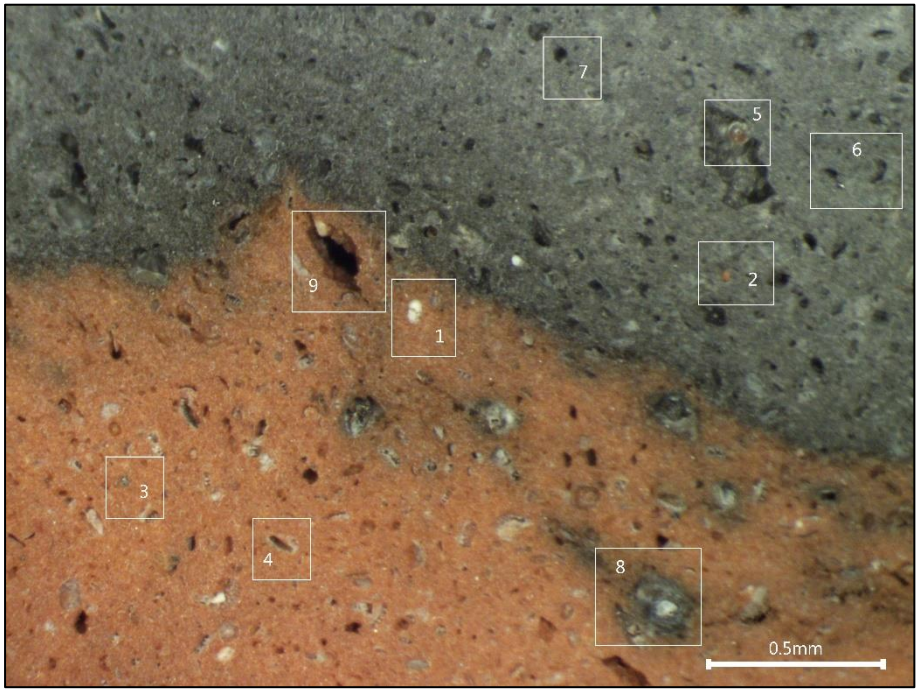

Figure 4.29 – Area 1 of 125_900_120_Oxi briquette viewed at x50 magnification.

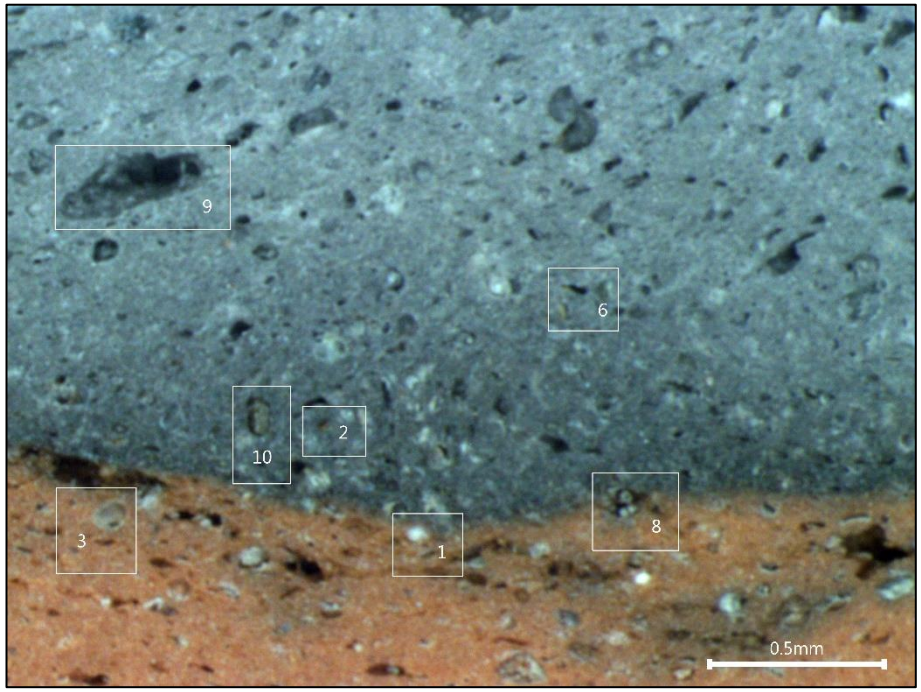

Figure 4.30 – Area 2 of 125_900_120_Oxi briquette viewed at x50 magnification.

Table 4.11 shows the Visual Comparison Chart (VCC) used to label the voids and inclusions present in the clay sample.

Table 4.11 – VCC for 125_900_120_Oxi sample.

Phase	Type	Size (Maximum Length)	Sorting	Shape	Frequency	Colour	Comments
1	Inclusion	0.07mm (Fine)	Very Poorly Sorted	Elongate Sub-Rounded	Few (5-15%)	White	Possible wollastonite
2	Inclusion	0.04mm (Very Fine)	Very Poorly Sorted	Equant Sub-Angular	Rare (0.5-2%)	Reddish Brown	
3	Inclusion	0.02mm (Very Fine)	Very Poorly Sorted	Equant Rounded	Rare (0.5-2%)	Grey	
4	Void/Inclusion	0.08mm (Fine)	Very Poorly Sorted	Elongate Sub-Rounded	Rare (0.5-2%)	White outer layer with brown core	Possible $CaCO_3$ around the void
5	Inclusion	0.08mm (Fine)	Very Poorly Sorted	Equant Sub-Rounded	Rare (0.5-2%)	Grey outer layer and brown core	
6	Void	0.07mm (Meso)	/	Planar Voids	/	/	
7	Void	0.03mm (Micro)	/	Vesicle	/	/	
8	Void	0.23mm (Meso)	/	Vugh	/	/	Possibly due to $CaCO_3$ decomposition
9	Void	0.26mm (Meso)	/	Vugh	/	/	
10	Inclusion	0.11mm (Fine)	Very Poorly Sorted	Elongate Sub-Rounded	Very Rare (<0.5%)	Brownish Grey	

This sample had an abundance of inclusions estimated to be around 40% of the area of the matrix, by using Figure 3.7.

4.3.2 SEM-EDS

SEM-EDS analysis was performed on the virgin clay greens to see if there were any differences in chemical composition between the sieved fractions. Three different areas were taken over each sample and then an average was obtained. Table 4.12 presents the average elemental composition (wt%) of the unfired clay samples sieved to 63 μm and 125 μm.

Table 4.12 – Average elemental composition (wt%) of unfired samples sieved to 63 μm and to 125 μm.

Element	Clay sample sieved to 63 μm (Wt%)	Clay sample sieved to 125 μm (Wt%)
C	17.80 ± 5.66	10.97 ± 4.59
O	38.51 ± 3.28	42.73 ± 3.26
Na	0.18 ± 0.03	0.22 ± 0.05
Mg	0.85 ± 0.09	1.18 ± 0.04
Al	7.67 ± 1.08	9.04 ± 0.72
Si	16.84 ± 2.55	20.72 ± 0.83
P	0.07 ± 0.05	0.03 ± 0.03
S	0.09 ± 0.03	0.15 ± 0.03
Cl	0.11 ± 0.06	0.11 ± 0.05
K	2.26 ± 0.09	2.30 ± 0.13
Ca	7.75 ± 2.60	5.88 ± 1.30
Ti	0.72 ± 0.37	0.59 ± 0.09
Fe	7.16 ± 2.80	6.07 ± 0.53

From the results in Table 4.12, it can be observed that the clay sample sieved to 63 μm has a higher carbon, calcium and iron content but has a lower oxygen, aluminium and silicon content than the clay sample sieved to 125 μm. The other elements are more or less similar.

Figures 4.31 and 4.32 visualise the 63_500_120_Oxi and 63_500_120_Red briquettes at a magnification of x500, respectively.

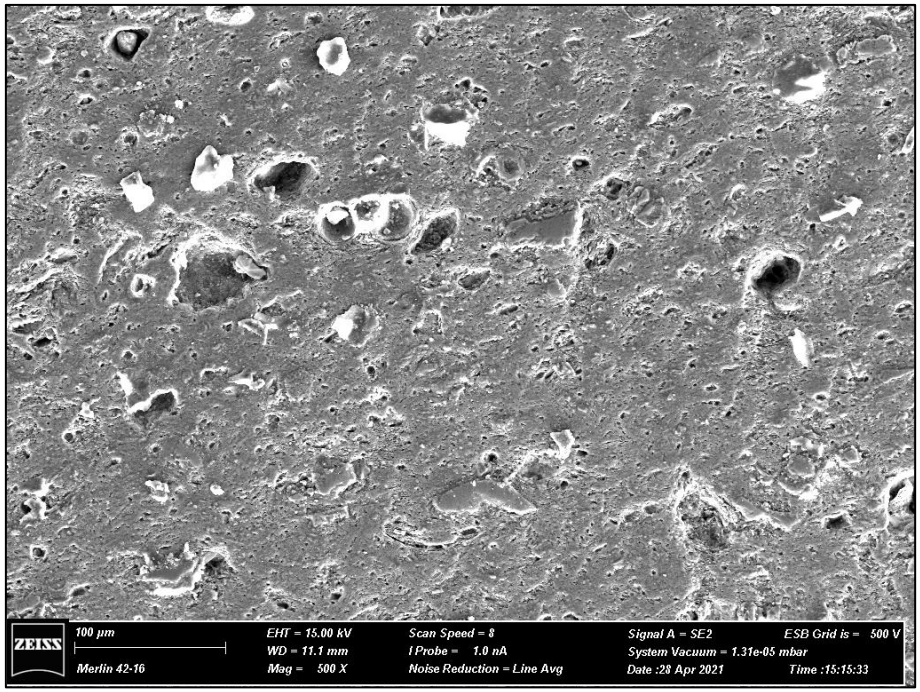

Figure 4.31 – 63_500_120_Oxi briquette viewed at a magnification of x500.

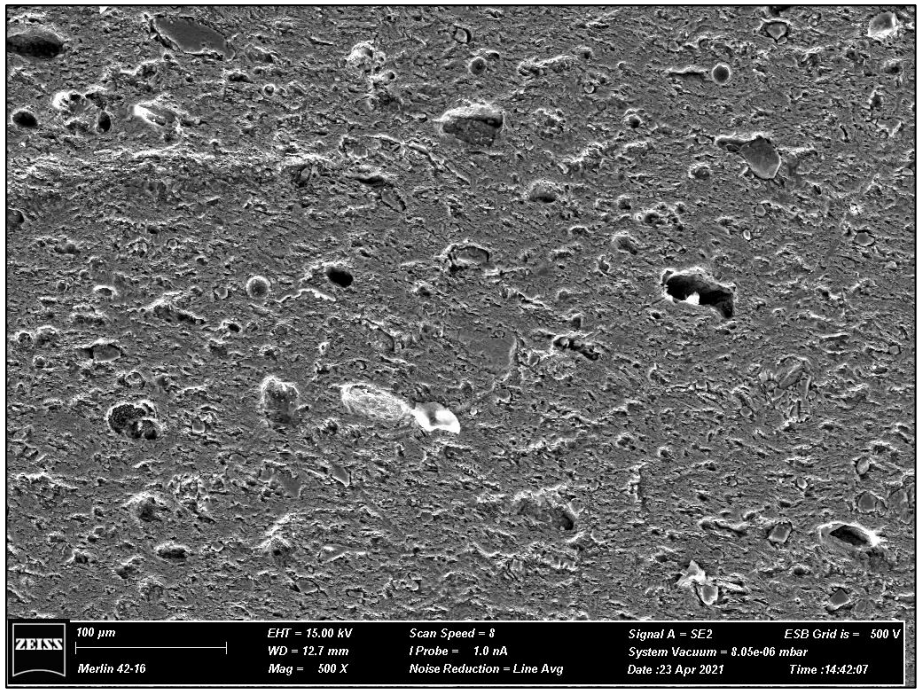

Figure 4.32 – 63_500_120_Red briquette viewed at a magnification of x500.

From these figures it can be observed that in a reducing atmosphere (Figure 4.32) more pores are present than in an oxidising atmosphere.

Figures 4.33 and 4.34 present the 63_900_120_Oxi and 63_900_120_Red briquettes at a magnification of x500, respectively.

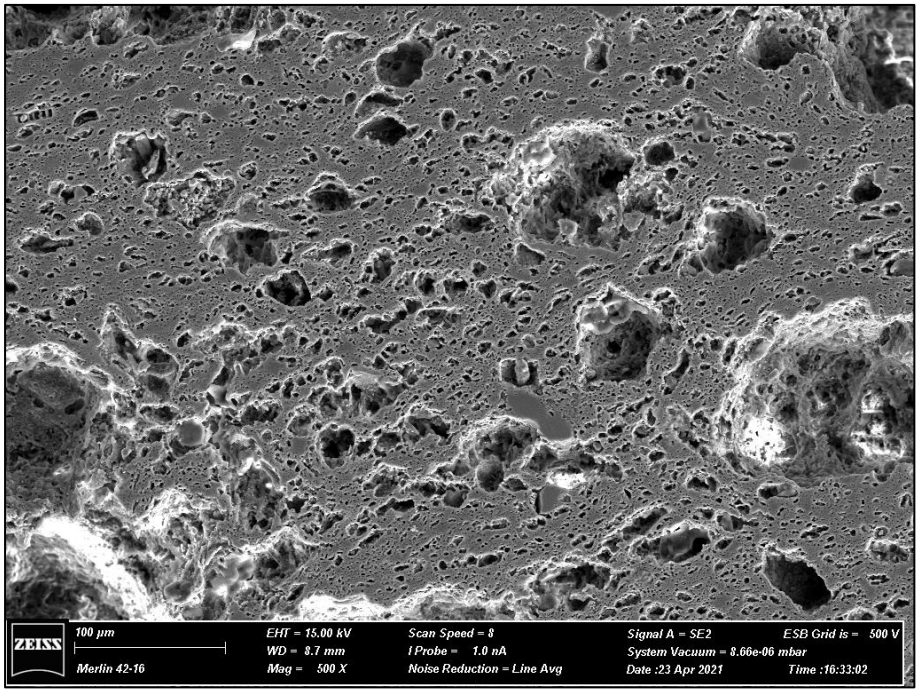

Figure 4.33 – 63_900_120_Oxi briquette viewed at a magnification of x500.

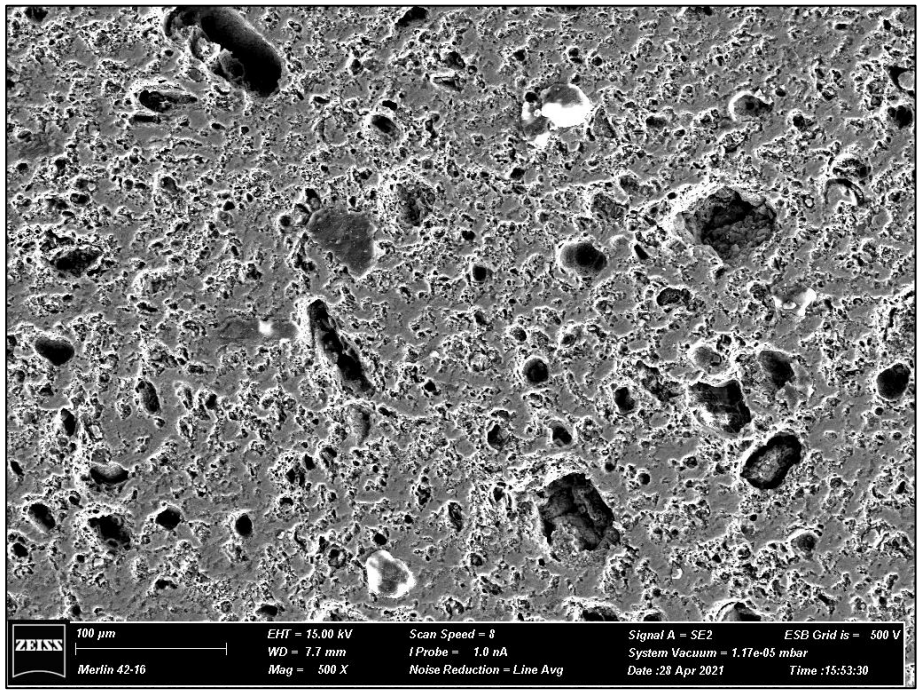

Figure 4.34 – 63_900_120_Red briquette viewed at a magnification of x500.

From these figures it can be observed that the briquette fired in an oxidising atmosphere (Figure 4.33), has a more porous and compact structure than that fired in a reducing atmosphere (Figure 4.34).

Figures 4.35 and 4.36 show the 63_500_120_Oxi and 63_500_120_Red briquettes at a magnification of x15000, respectively.

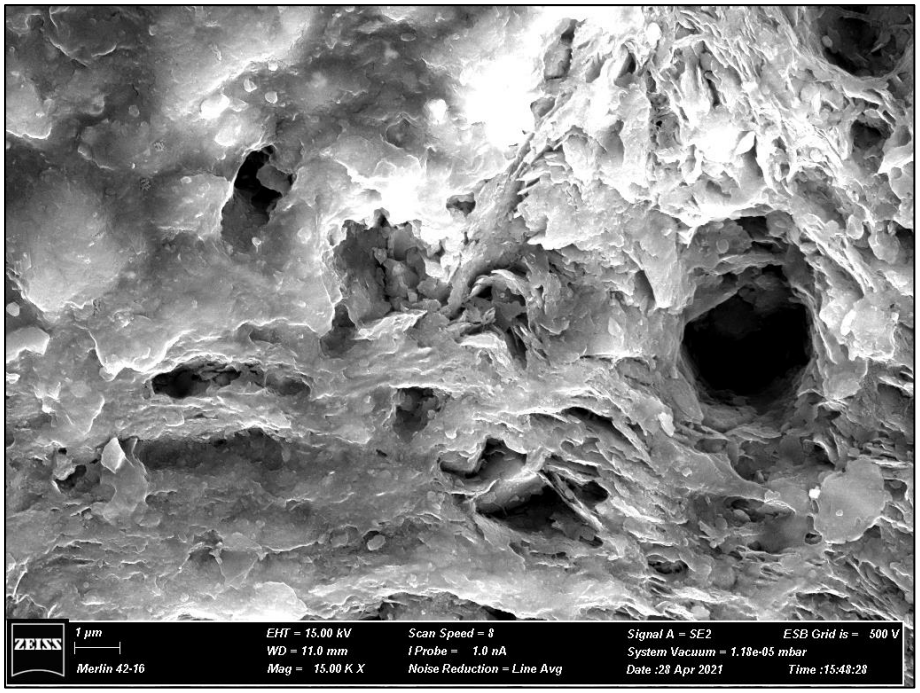

Figure 4.35 – 63_500_120_Oxi briquette viewed at a magnification of x15000.

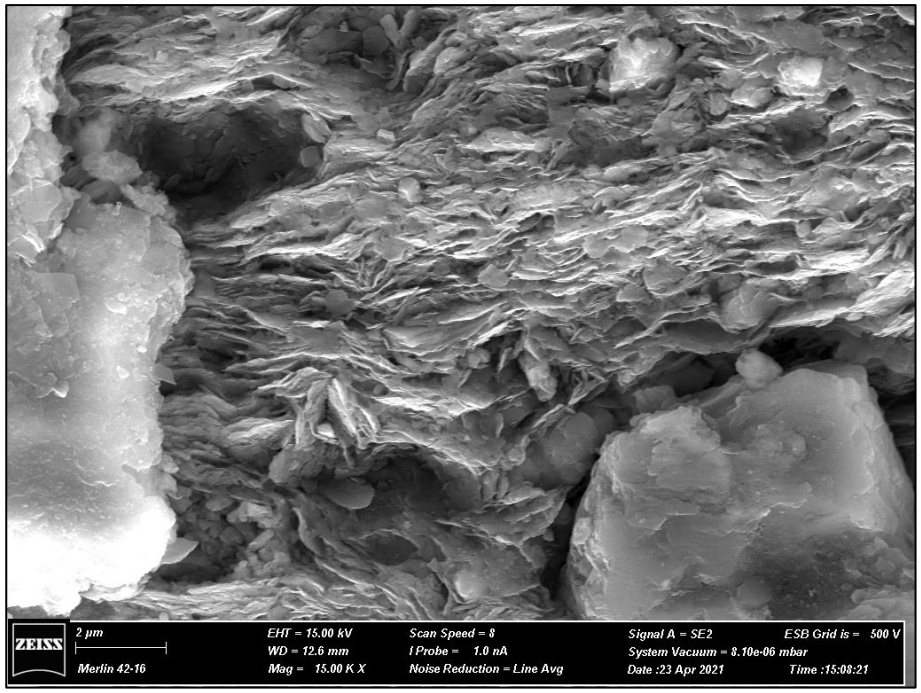

Figure 4.36 – 63_500_120_Red briquette viewed at a magnification of x15000.

From these figures it can be observed that kaolinite sheets are present in the microstructures of these briquettes.

Figures 4.37 and 4.38 visualise the 63_900_120_Oxi and 63_900_120_Red briquettes at a magnification of x15000, respectively.

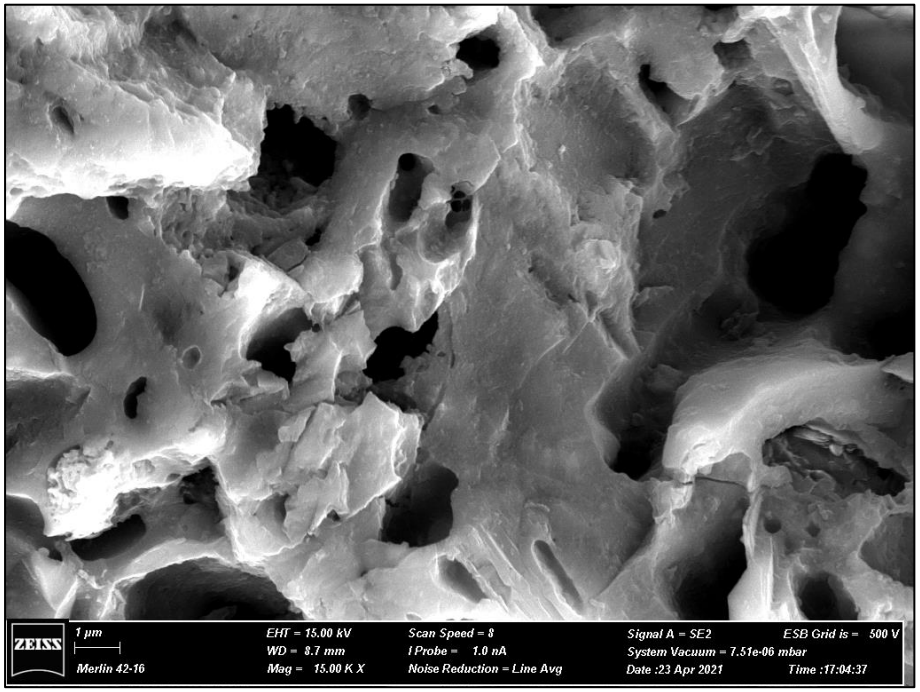

Figure 4.37 – 63_900_120_Oxi briquette viewed at a magnification of x15000.

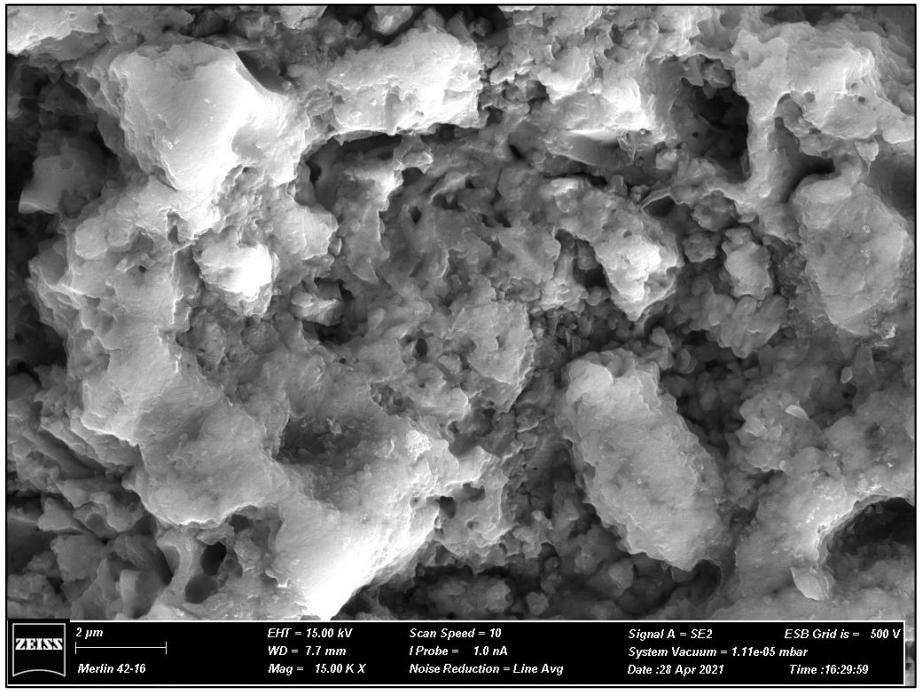

Figure 4.38 – 63_900_120_Red briquette viewed at a magnification of x15000.

From these figures it can be observed that kaolinite sheets are no longer present in the microstructures of these briquettes. However, the briquettes possess a more compact microstructure at elevated firing temperatures.

Figures 4.39 and 4.40 present the possible quartz inclusion embedded in the matrix at a magnification of x5000 and the EDS spectrum, respectively. Table 4.13 shows the elemental composition of the possible quartz inclusion.

Table 4.13 – Elemental composition (wt%) of possible quartz inclusion.

Element	Wt%	At%
O	51.48	63.50
Si	41.97	29.48

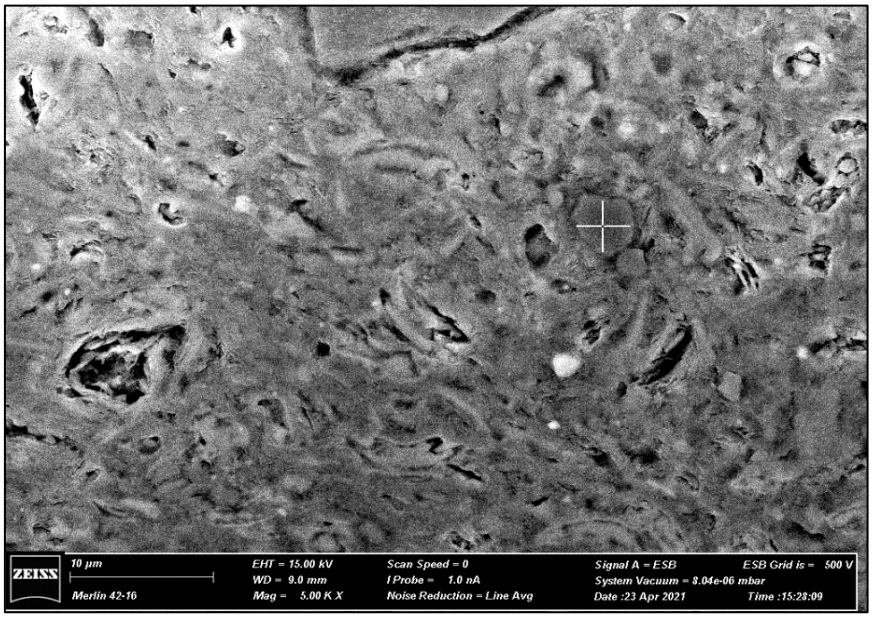

Figure 4.39 – Possible quartz inclusion viewed at a magnification of x5000, indicated with a cross.

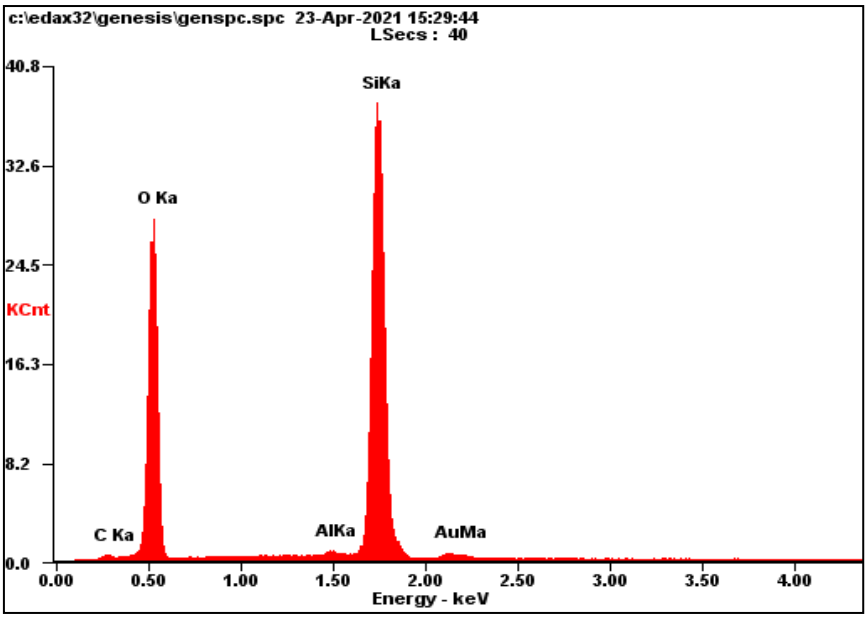

Figure 4.40 – EDS for possible quartz inclusion.

Figures 4.41 and 4.42 show the possible calcite inclusion embedded in the matrix at a magnification of x5000 and the EDS spectrum, respectively. Table 4.14 presents the elemental composition of the possible calcite inclusion.

Table 4.14 – Elemental composition (wt%) of possible calcite inclusion.

Element	Wt%	At%
C	17.69	28.39
O	44.90	54.10
Ca	28.13	13.53

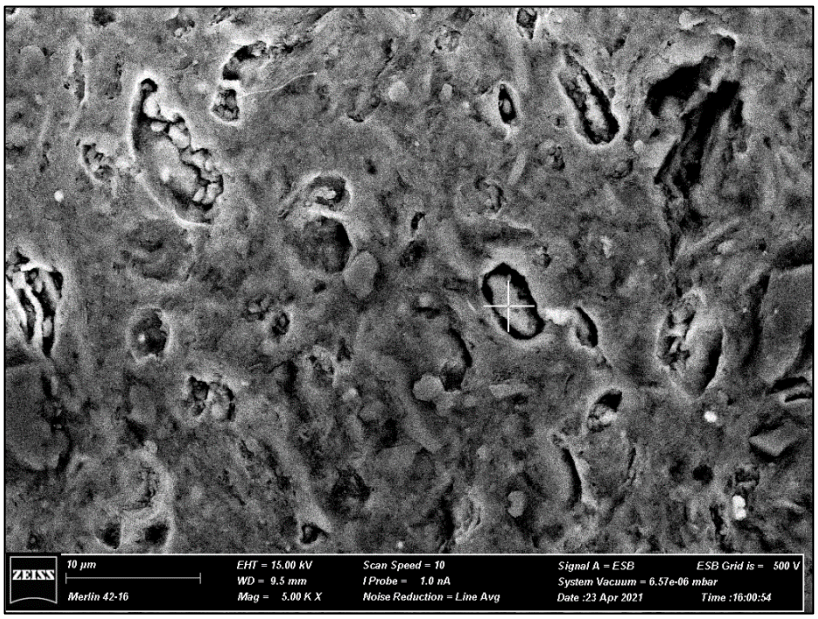

Figure 4.41 – Possible calcite inclusion viewed at a magnification of x5000, indicated with a cross.

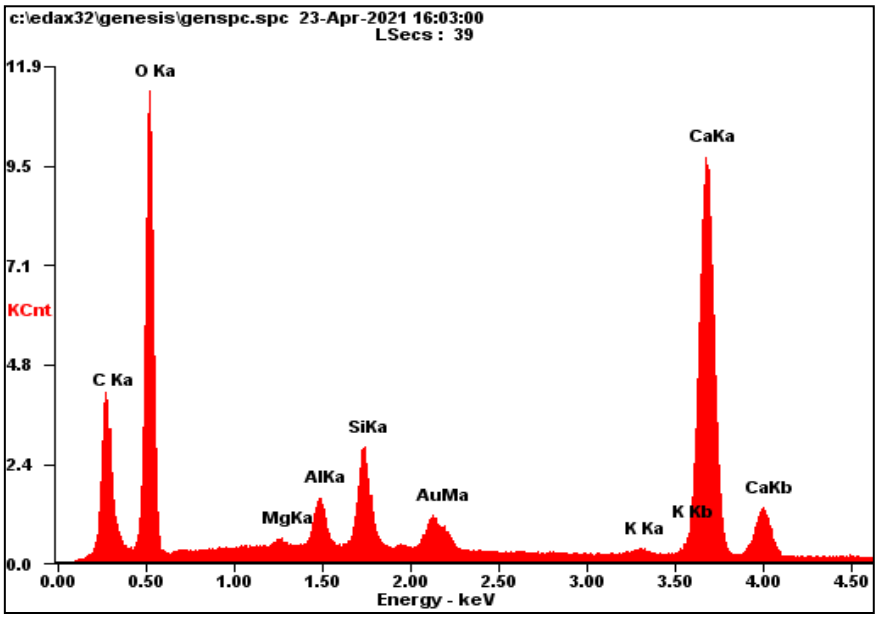

Figure 4.42 – EDS for possible calcite inclusion.

4.4 X-Ray Powder Diffraction (XRPD)

Diffractograms were produced for both the unfired and fired samples. The X-ray reflections were labelled with letters representing their mineral phase names, refer to Table 4.15.

Table 4.15 – Letters representing mineral phase names.

Letter	Mineral Phase Name
C	Calcite
G	Glauconite
H	Hematite
K	Kaolinite
Q	Quartz
T	Tridymite
W	Wollastonite
?	Unknown Mineral

The label ? was used to indicate peaks which could not be matched or identified.

4.4.1 Unfired Clay Samples

XRPD was conducted on the unfired clay samples sieved to 63 and 125 µm to see if there is any difference in the mineralogical content between the different clay mesh sizes. Figure 4.43 presents the diffractograms comparing the unfired briquettes.

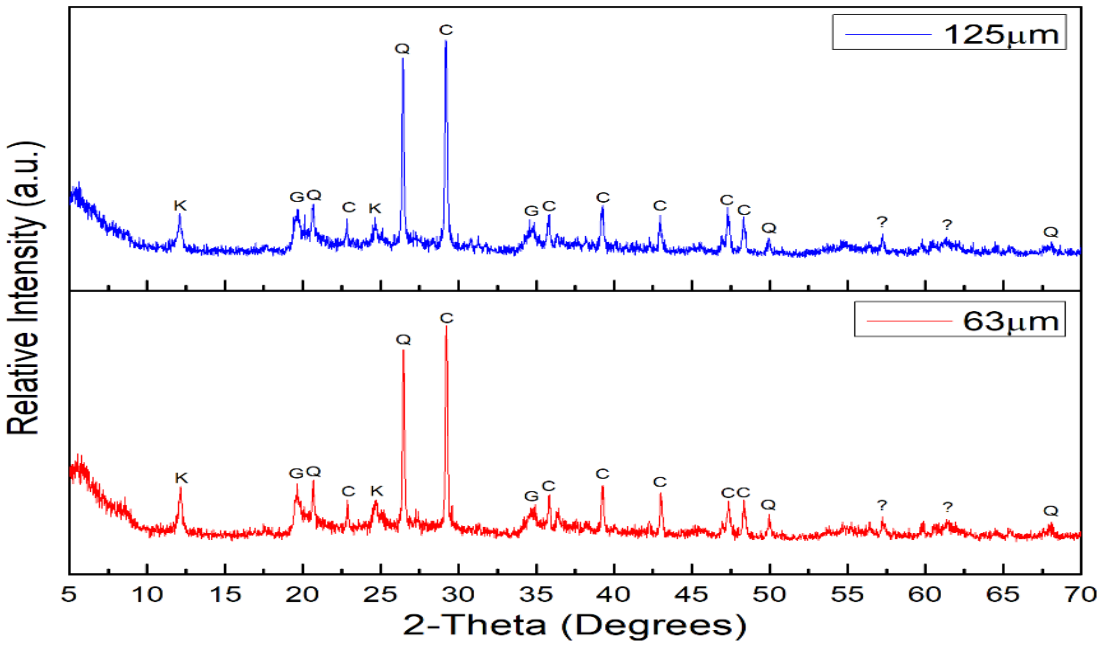

Figure 4.43 – XRPD diffractograms of the unfired clay samples sieved to 63 µm and 125 µm.

From the diffractograms in Figure 4.43 it can be observed that there are no differences between the clay mesh sizes. These unfired clay samples have an abundance of quartz, calcite, kaolinite and glauconite minerals.

4.4.2 Fired Clay Samples

Comparisons were made between the fired samples produced with different parameters, namely firing temperature, soaking time, firing atmosphere and mesh size.

4.4.2.1 Mineralogical Transformations with Increasing Firing Temperature

Figures 4.44 and 4.45 show the diffractograms comparing the fired briquettes with variation in firing temperature, at a soaking time of 120 minutes, in an oxidising atmosphere and reducing atmosphere, respectively. The briquettes fired at a soaking time of 30 minutes exhibited a similar behaviour to these diffractograms.

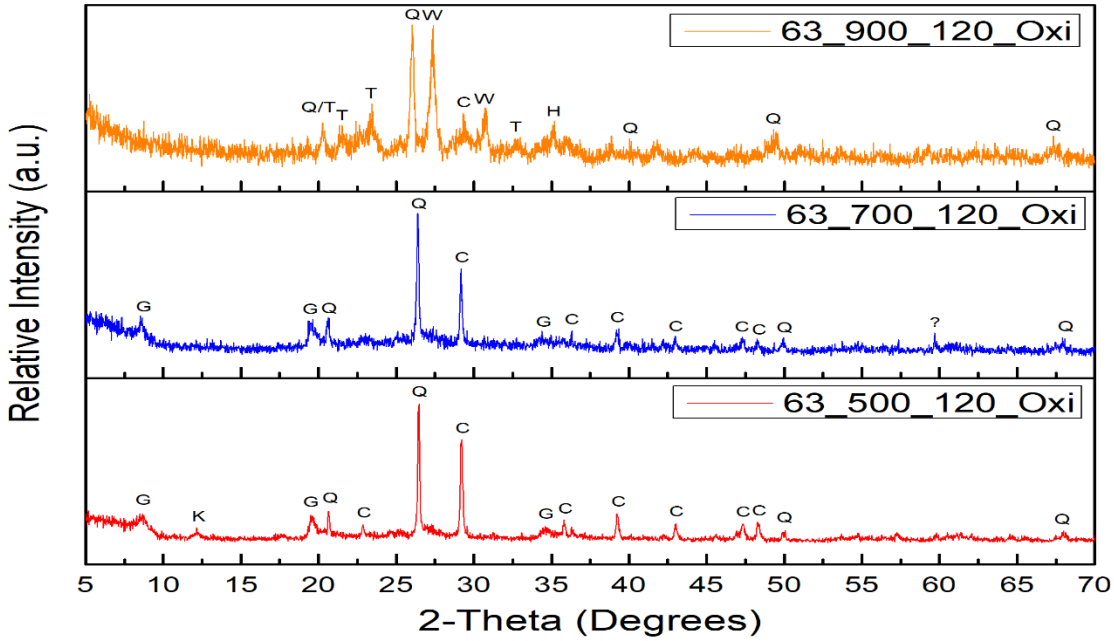

Figure 4.44 – XRPD diffractograms comparing the different firing temperatures in an oxidising atmosphere at 120 minutes.

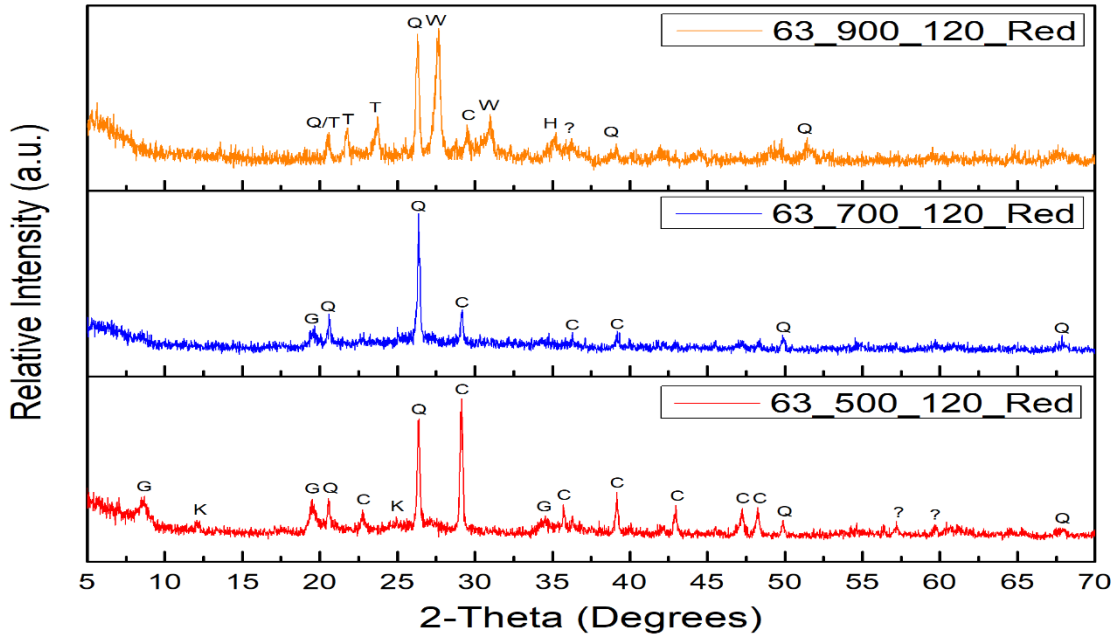

Figure 4.45 – XRPD diffractograms comparing the different firing temperatures in a reducing atmosphere at 120 minutes.

4.4.2.2 Mineralogical Transformations with Increasing Soaking Time

Figures 4.46 and 4.47 present the diffractograms comparing the fired briquettes with variation in soaking time at a firing temperature of 700 °C in an oxidising atmosphere and reducing atmosphere, respectively. The briquettes fired at 500 °C and 900 °C exhibited a similar behaviour to these diffractograms.

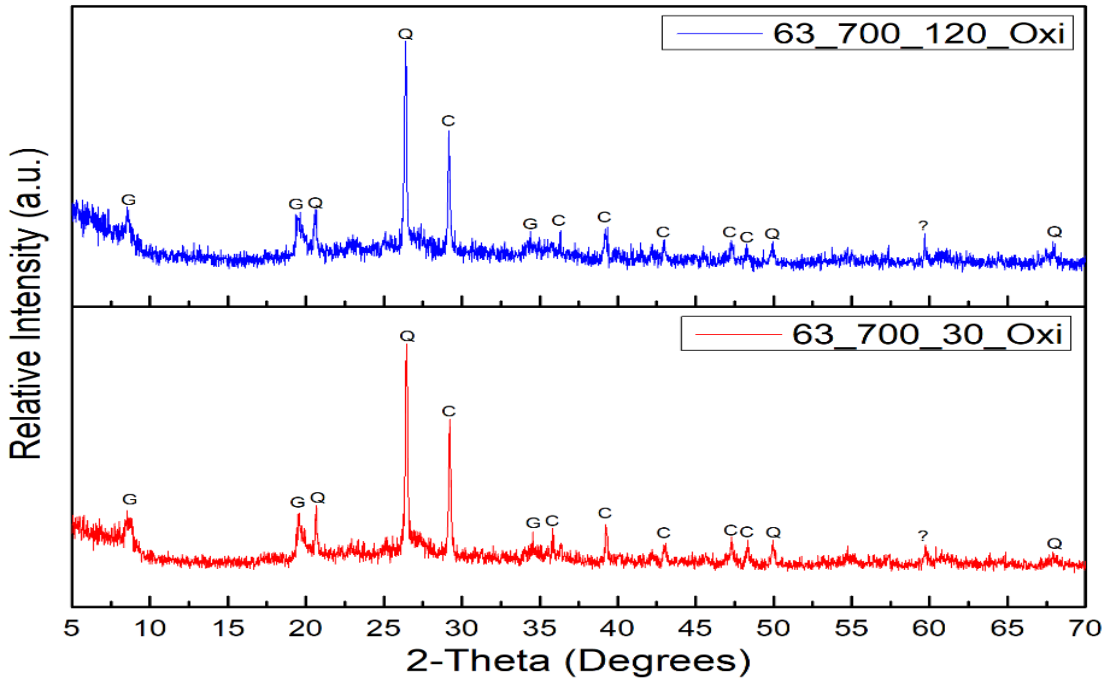

Figure 4.46 – XRPD diffractograms comparing the soaking times in an oxidising atmosphere at 700 °C.

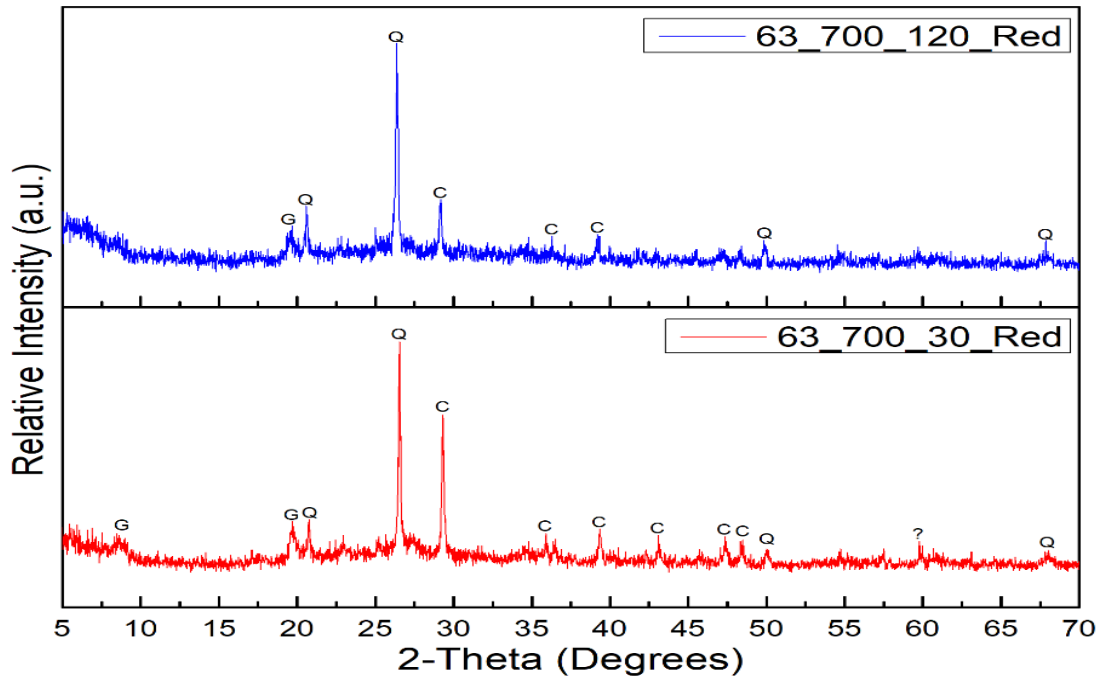

Figure 4.47 – XRPD diffractograms comparing the soaking times in a reducing atmosphere at 700 °C.

4.4.2.3 Mineralogical Transformations with Different Firing Atmospheres

Figures 4.48 and 4.49 show the diffractograms comparing the composition of fired briquettes with variation in firing atmosphere at a firing temperature of 500 °C at 30 minutes and 120 minutes, respectively. The briquettes fired at 700 °C and 900 °C exhibited a similar behaviour to these diffractograms.

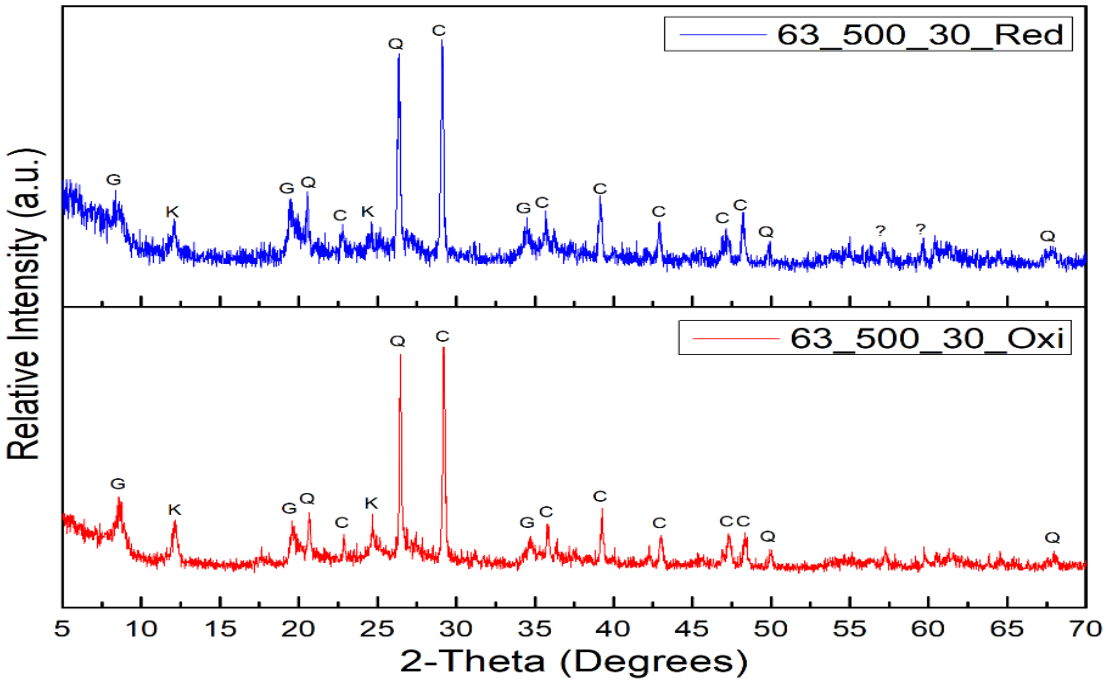

Figure 4.48 – XRPD diffractograms comparing the firing atmospheres at 500 °C at 30 minutes.

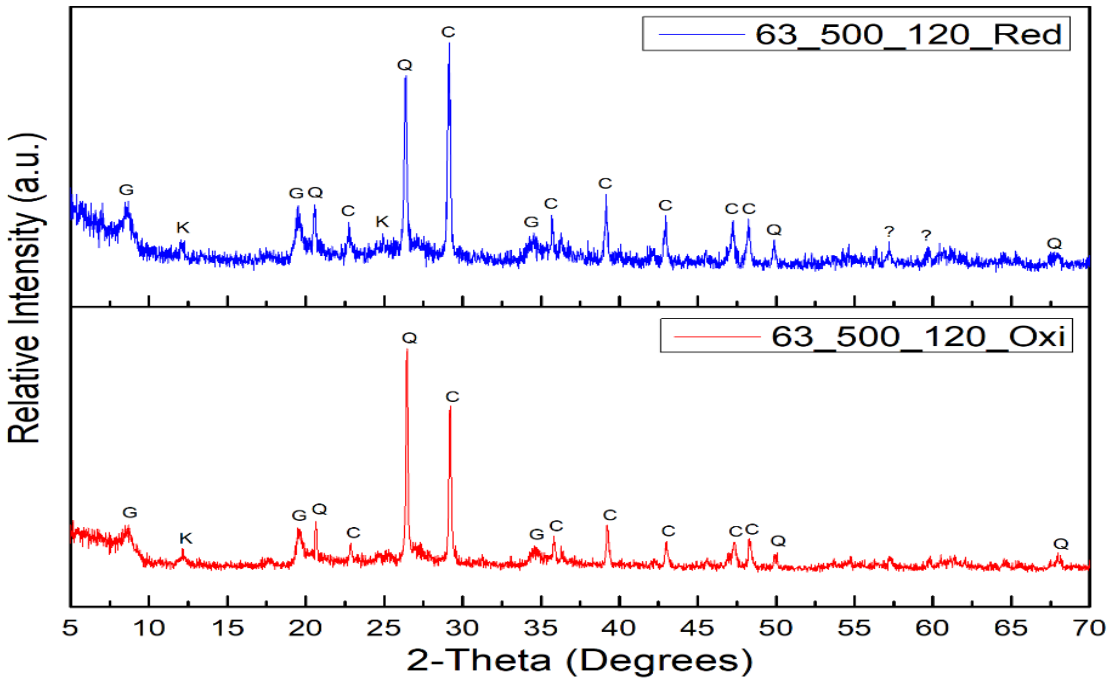

Figure 4.49 – XRPD diffractograms comparing the firing atmospheres at 500 °C at 120 minutes.

4.4.2.4 Mineralogical Transformations with Increasing Mesh Size

Figure 4.50 presents the diffractogram comparing the fired briquettes produced with clay sieved to different mesh sizes at a firing temperature of 900 °C for 120 minutes.

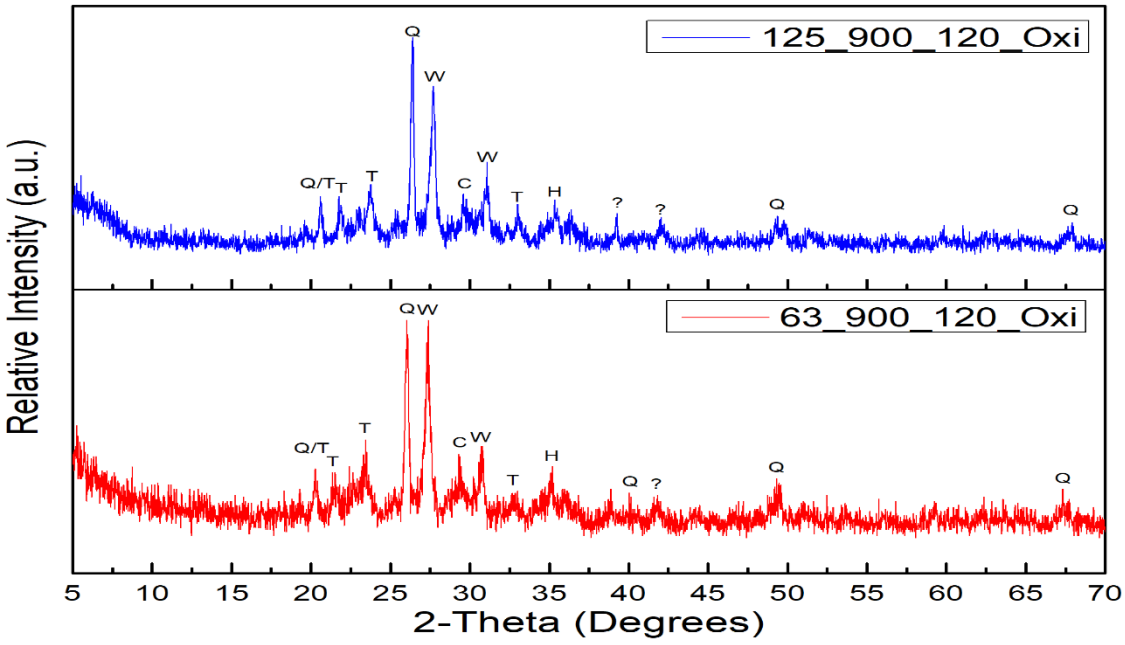

Figure 4.50 – XRPD diffractograms comparing the mesh sizes at 900 °C at 120 minutes.

The biggest difference in mineralogical transformations is when the firing temperature was altered. At 500 °C the minerals kaolinite, calcite, quartz and glauconite were present. When the temperature was increased to 700 °C, kaolinite was no longer present and both the calcite and glauconite peaks started to decrease. Finally, at a temperature of 900 °C, wollastonite, tridymite and hematite were present in the diffractograms (Figure 4.44 and 4.45).

When altering the soaking time, there was no transformation in mineralogy. The only difference was the intensity of the peaks, where a long soaking time yielded peaks with lower intensities (Figures 4.46 and 4.47). The same applied for the variation in firing atmospheres but the peaks remained more or less the same (Figures 4.48 and 4.49).

There were no difference in mineralogy of the fired samples when the mesh size was increased, as can be seen in Figure 4.50.

4.5 Hardness Testing

Tables 4.16 and 4.17 present the average Knoop hardness values ceramic sampled procured in this work for samples fired in an oxidising and reducing atmosphere, respectively. The 63_500_30_Red sample fell apart during the hardness test and was not included in the table below. Hardness values are averages of between x-y repeats. Knoop hardness was measured at the core and outer layer for the samples fired in an oxidising atmosphere.

Table 4.16 – Hardness results for samples fired in an oxidising atmosphere.

Sample	Average Outer Layer Hardness (HK)	Average Core Hardness (HK)
63_500_30_Oxi	25.1 ± 5.5	17.3 ± 2.8
63_500_120_Oxi	13.5 ± 3.1	17.7 ± 1.7
63_700_30_Oxi	36.0 ± 2.7	64.4 ± 2.9
63_700_120_Oxi	37.8 ± 1.7	44.3 ± 4.8
63_900_30_Oxi	169.0 ± 4.8	115.3 ± 16.5
63_900_120_Oxi	171.0 ± 40.6	131.1 ± 18.5
125_900_120_Oxi	180.8 ± 19.2	81.3 ± 12.2

Table 4.17 – Hardness results for samples fired in a reducing atmosphere.

Sample	Average Hardness (HK)
63_500_120_Red	16.4 ± 2.0
63_700_30_Red	39.7 ± 2.8
63_700_120_Red	37.1 ± 2.4
63_900_30_Red	40.2 ± 4.6
63_900_120_Red	44.5 ± 5.9

Figures 4.51 and 4.52 depict the bar graphs showing the tabulated hardness results for the oxidising and reducing atmosphere, respectively.

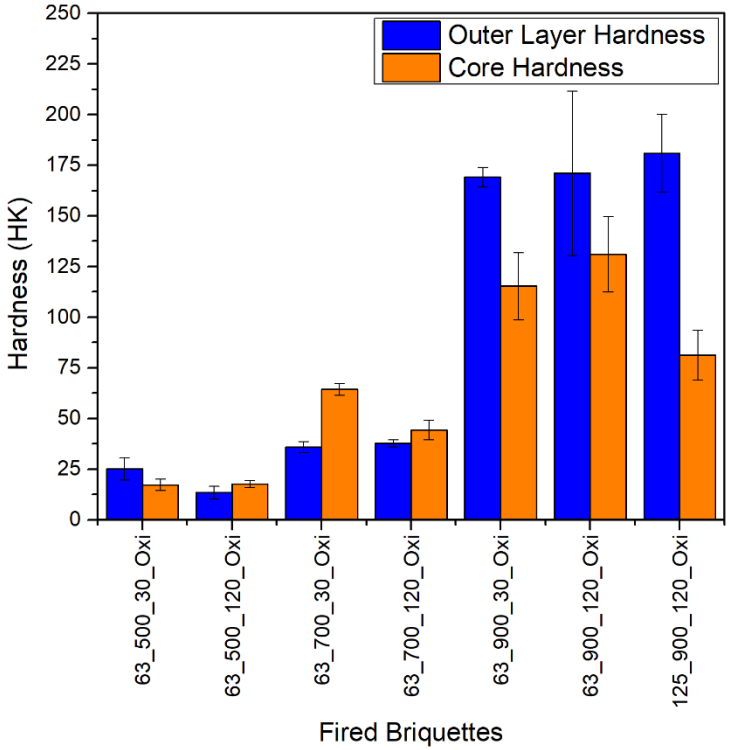

Figure 4.51 – Bar graph representing core and outer layer hardness of the briquettes fired in an oxidising atmosphere.

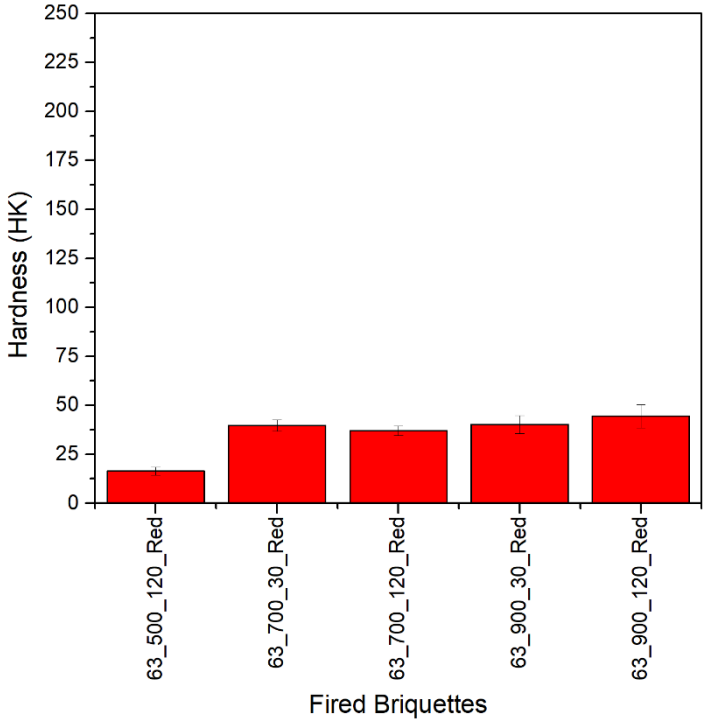

Figure 4.52 – Bar graph representing hardness of the briquettes fired in a reducing atmosphere.

From Figure 4.51 it can be observed that on increasing the firing temperature, both the outer layer and core hardness increase. Generally, the outer layer is harder than the core. From Figure 4.52 one can conclude that on increasing the temperature in a reducing atmosphere, hardness increases. However, from 700 °C onwards, the hardness values remain approximately the same. It was also noted that briquettes fired in an oxidising atmosphere were harder than the briquettes fired in a reducing atmosphere.

Figure 4.53 presents a graph of the hardness of the profile of the cross-section of the 63_900_120_Oxi and 63_900_120_Red briquettes.

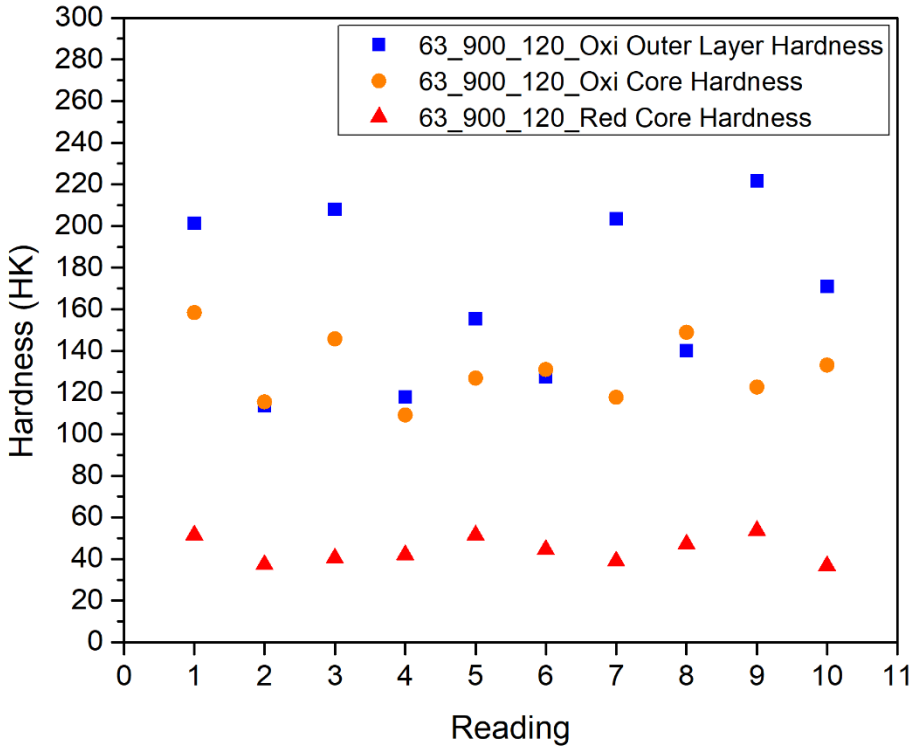

Figure 4.53 – Scattered plot of the variability of the profile of the 63_900_120_Oxi and 63_900_120_Red briquette cross-sections.

From the graph above it is clearly seen that there is a wide range in hardness results. This demonstrates the high variability achieved in these results.

5. Discussion

This Chapter provides the explanations and findings of Chapter 4 (Results) with the following topics/areas discussed further; linear drying shrinkage, colour change, porosity and voids, change in microstructure, change in mineralogy and change in hardness.

5.1 Linear Drying Shrinkage

Figures 4.1 and 4.2 show the graphs of mass of slabs (g) against drying time (hours) and length between marks (cm) against drying time (hours). Data points are averages of experimental batches 1 and 2, respectively. Figures 4.3 and 4.4 show the same graphs but for the averages of batches 3 and 4, respectively. From these Figures it can be observed that on increasing the drying time, more loss in weight and length between the slab marks was noted. After the 144^{th} hour of drying in air, the gradient increased and the largest loss in both weight and shrinkage was noted. This is because the briquettes were placed in a drying oven, which resulted in more shrinkage and weight loss. There also appeared to be a change in gradient after 96 hours. This could possibly be due to the change in environment since the samples were transported from one place to another. Hence, the humidity could have varied between one storage point/area and another, affecting both the shrinkage and weight loss as a result. This decrease in gradient could also correspond to the change in rate of loss of water vapour after the bulk water trapped inside the green was lost to evaporation.

The extracted clay sample was composed of different mineral phases including kaolinite and calcium carbonate. From this experiment it can be seen that the water of plasticity of the four batches ranged from approximately 38 to 44.5% by weight which is within range identified by Rice [16]. The author states that white sedimentary kaolin, which includes a high proportion of calcite mixed with kaolin, has a water of plasticity of between 29 and 56 wt% [16]. Most probably the clay in the Maltese Islands is made up of this type of kaolin since the Blue Clay formation is composed of both a high calcium carbonate content and kaolinite mineral [11-13].

It was also noted that clay sieved to 125 μm had a water of plasticity ranging from approximately 38 to 39.5% by weight, whereas clay sieved to 63 μm had a water of plasticity varying from 41 to 44.5% wt%. Therefore, clay sieved to the smaller mesh

size had a higher water of plasticity since the finer clay particles have a larger surface area-to-volume ratio. As a result, more water of plasticity is needed to work the clay. Therefore, it can be concluded that finer clays require more water than coarse clay to manufacture the briquettes [17]. In fact, it can be seen that batches 3 and 4 from Figures 4.3 and 4.4 exhibit more weight loss and more shrinkage due to the higher incorporated water of plasticity. Batch 4 however showed the greatest weight loss and most shrinkage since it had the highest water of plasticity.

From Tables 4.1 and 4.2 it can be seen that the clay sieved to 125 μm had a Linear Drying Shrinkage percentage (%LDS) of between 8.9 - 9%, whereas Tables 4.3 and 4.4 show that the clay sieved to 63 μm had a %LDS of between 8.9 - 10.7%. These findings are also in agreement with Rice [16] and Cuomo di Caprio [17]. These authors stated that kaolinite has a low unfired shrinkage of roughly 8 - 10%, which is within the range of this experiment. Batches 3 and 4 had a higher %LDS since more water was added during the manufacturing stage, hence, more water needs to evaporate to achieve drying, resulting in a higher shrinkage.

5.2 Colour Change

In Figure 4.5 it can be observed that the slabs have a light yellow-brown colour when the briquettes are still unfired. According to Cuomo di Caprio [17], this is the most common colour after the manufacturing stage. All the slabs had the same colour after the manufacturing process and no difference in colour was noted between the two samples sieved with different mesh sizes.

In Figure 4.6a it was noted that on increasing the firing temperature in an oxidising atmosphere, the briquettes turned red [29, 36, 47, 60]. However, on altering the soaking times, the colours only changed marginally. This shows that firing temperature is a parameter which affects the outcome more than the soaking time. These briquettes turned to a red colour due to the iron present in silicates such as glauconite [$(K^+, Na^+)(Fe^{3+}\ Al^{3+}, Mg^{2+})_2\ (Si, Al)_4O_{10}\ (OH)_2$]. Cuomo di Caprio [17] states that iron compounds have an effect on the briquettes as they develop a reddening action when the firing temperature is increased. However, as the temperature is increased in an oxidising atmosphere, these mentioned minerals rich in iron transform to hematite [35].

Increase in temperature when firing in a reducing atmosphere produced briquettes of a progressively lighter shade of grey, as can be seen in Figure 4.6b. This is possibly due to the decomposition and pyrolysis of organic matter present in the matrix which turns black, giving the grey colour to the matrix. Furthermore, oxidized iron compounds containing Fe^{3+} may also transform by reduction to Fe^{2+}compounds, such as for example the mineral magnetite (Fe_3O_4) which is a black coloured mineral or wurtzite (FeO) which is a brownish black coloured mineral.

Figures 4.7 - 4.13 present the cross-sections through briquettes fired in an oxidising atmosphere. From these images the margin (outer layer) and core can be clearly seen. The core forms due to the incomplete oxidation and reduction of carbonaceous matter [16, 17, 22]. According to De Bonis et al. [22], this core could originate from the short duration of firing, impeding the complete oxidation of the whole ceramic body in the process. It can be observed that on increasing the firing temperature, the briquettes that were fired at 500 °C had a black core (Figures 4.7 and 4.8); samples fired at 700 °C had a very dark bluish grey core (Figures 4.9 and 4.10); and briquettes fired at 900 °C had a grey core (Figures 4.11 - 4.13). The dark core signifies that carbon is present at the core of the briquettes. The core changes into a lighter colour due to the possible decomposition of organic matter with increasing firing temperature. It could also potentially be a result of the limited oxygen diffusion to the core. The same occurs to the briquettes fired in a reducing atmosphere. The core colour ranges from black at 500 °C (Figure 4.14 and 4.15) to dark grey at 700 °C (Figures 4.16 and 4.17) and finally to light bluish grey at 900 °C (Figures 4.18 and 4.19).

The briquettes fired at 700 °C and 900 °C in an oxidising atmosphere have a margin present in their cross-section as seen in Figures 4.9-4.13. This margin could have formed by two ways; firstly, upon firing, if the clay is rich in organic matter, this is decomposed and potentially forms this margin layer [60]; secondly, the fired ceramic could have a possible reducing atmosphere restricted to a local region of the briquette, possibly forming this outer margin layer.

From Figure 4.20 it can be observed that on increasing the soaking time, the ratio of average core/briquette thickness decreases, as confirmed by Pontikes and Angelopoulos [47] in their experiment. This is due to diffusion since longer soaking times allows oxygen to reach the core of the briquettes more than those fired at a shorter soaking

time. According to Cuomo di Caprio [17], short soaking time is not sufficient enough for oxygen to reach the core of the briquettes.

5.3 Porosity and Voids

Table 4.6 tabulates observations made during the macroscopic recording on the surface of the briquettes. The different briquettes fired at a temperature of 500 °C and 700 °C had no visible cracks present on the surface. However, the briquettes that were fired at 900 °C exhibited blisters, cores and pores which were present on the surface. The formation of these voids is probably due to the decomposition of calcium carbonate and organic material accompanied by a release of gaseous by-products, primarily CO_2. More voids were present at this firing temperature, providing more evidence that calcite has decomposed to form calcium oxide (CaO) and carbon dioxide. The number of pores increase during the firing stage due to the release of water vapour and of volatile gases as a result of the combustion of organic matter and decomposition of calcite [17, 47]. In fact, the briquettes fired at 500 °C do not have many voids present in their cross-section.

Air bubbles could have formed during the manufacturing stage, resulting in channel voids due to pressure applied on the mould. This pressure flattens and orientates the voids in the same direction [17]. An example of a channel void can be seen labelled as Phase 6 in Figure 4.27.

5.4 Changes in Microstructure

5.4.1 Optical Microscopy

Figures 4.21 - 4.30 show the microscopic images of the fired briquettes viewed at x50 magnification. From these images the major differences in inclusions and voids are visible when the firing temperature was altered. In fact, there were minimal differences when either the soaking time or firing atmosphere (oxidising-reducing) were changed in terms of voids and inclusions. In Section 4.3.1, inclusions and voids are referred to as phases, however, not all the inclusions could be properly identified. In this discussion, the focus will be on probable identified phases.

Phase 6 in Figures 4.21 and 4.22 shows potential *foraminifera*, which is composed mainly of calcium carbonate, that has survived the firing temperature of 500 °C. However, when briquettes were fired at higher temperatures, the foraminiferal structures

were no longer evident, suggesting that they were completely decomposed when exposed to higher temperatures.

Phase 7 in Figure 4.21 and Phase 2 in Figure 4.23 indicates shells present in the matrix up to a temperature of 700 °C. However, when briquettes were fired to a temperature of 900 °C, these shells were no longer present in the matrix. This is because on increasing the firing temperature, decarbonation occurs and, as a result, any shells, limestone fragments and non-plastic inclusions are volatilized in the process [5, 22].

Phase 1 in Figures 4.25 and 4.26 shows a potential glauconite inclusion in the briquette that was fired at 700 °C. The glauconite inclusions were not visible at 900 °C due to their decomposition to less noticeable phases [61]. Phase 5 in Figures 4.21 and 4.22 present a probable glauconite inclusion in a reducing atmosphere. According to Basso et al. [61], glauconite is black in colour in a reducing atmosphere and reddish-brown in an oxidising atmosphere. However, these inclusions could also be hematite in an oxidising atmosphere or magnetite in a reducing atmosphere. In this scenario, micro-Raman Spectroscopy can come in handy to determine the nature of these inclusions.

5.4.2 Electron Microscopy and Elemental Analyses

Table 4.12 shows the average elemental composition of three different areas of the unfired clay samples sieved to 63 and 125 μm. Major elements in the clay sample consisting of 63 μm particles are carbon (17.80 ± 5.66 wt%), calcium (7.75 ± 2.60 wt%), oxygen (38.51 ± 3.28 wt%), silicon (16.84 ± 2.55 wt%), aluminium (7.67 ± 1.08 wt%) and iron (7.16 ± 2.80 wt%). The elemental composition of the major elements in the clay sample sieved to 125 μm is as follows: carbon (10.97 ± 4.59 wt%), calcium (5.88 ± 1.30 wt%), oxygen (42.73 ± 3.26 wt%), silicon (20.72 ± 0.83 wt%), aluminium (9.04 ± 0.72 wt%) and iron (6.07 ± 0.53 wt%). From these results, it can be observed that the clay sample sieved to 63 μm has a marginally higher carbon, calcium and iron content but has a lower oxygen, aluminium and silicon content than the clay sample sieved to 125 μm. These differences could be due to compositional inhomogeneities and variations, that is, not necessarily real differences.

Figures 4.31, 4.32, 4.35 and 4.36 show the briquettes fired at a temperature of 500 °C at magnification of x500 and x15000. At the lower magnification, the microstructures are quite similar for both the oxidising and reducing atmosphere. It is evident that a number

of pores are present. At the higher magnification, probable kaolinite microsheets can be seen in the microstructures of these briquettes (Figures 4.35 and 4.36). At this temperature it is noted that no significant structural modification and no sintering has occurred to any great extent [22].

Figures 4.33, 4.34, 4.37 and 4.38 show the briquettes fired at a temperature of 900 °C and at magnifications of x500 and x15000. At the lower magnification it is clearly seen that the briquette fired in an oxidising atmosphere has less pores than the briquette fired in a reducing atmosphere. This shows that briquettes fired in oxidising conditions are predominantly characterised by interconnected pores, demonstrating that sintering has occurred. This causes the densification of the clay sample and as a result, porosity reduces drastically [17]. In this case, measurement of the degree of porosity can be carried out in the future to obtain a ratio of the volume of the voids or pore space divided by the total volume, as a percentage. It can be observed that sintering in an oxidising atmosphere appears more pronounced than in a reducing atmosphere, hence, a more reinforced body is produced in the process [6, 47, 62]. At the higher magnification, it is noted that kaolinite sheets are no longer present in both the oxidising and reducing atmosphere. This shows that the ceramic change has occurred. The briquettes fired in an oxidising atmosphere have a more compact microstructure than the microstructure generated under the reducing atmosphere. Figure 4.38 shows that the microstructure is not very compact which could possibly be due to the amount of organic matter present in the microstructure. Perhaps a longer soaking time or a higher firing temperature is needed to eliminate completely the organic material present in the microstructure when firing under reducing conditions.

5.5 Change in Mineralogy

Figure 4.43 shows the diffractograms of the unfired briquettes. No differences in the diffractograms were observed between the samples sieved to 63 μm and 125 μm. This indicates that the material remains the same in the two clay fractions. The mineralogy of the major diffraction peaks (i.e. the most intense reflection) of the samples include; kaolinite at 2-theta = 12.37°, glauconite at 2-theta = 19.71°, quartz at 2-theta = 26.65°, and calcite at 2-theta = 29.41°.

Differences in mineralogical content were recorded upon firing. Figures 4.44 and 4.45 demonstrate the change in phases when firing in an oxidising and reducing atmosphere, respectively. It can be observed that kaolinite is present at a temperature of 500 °C, with its major diffraction peak occurring at a 2-theta of 12.37°. However, on increasing the temperature to 700 °C and 900 °C, this mineral is completely transformed; this is because at the diffraction angle of 12.37°, kaolinite is no longer visible, showing that the ceramic change has occurred. Glauconite is also present after firing at 500 °C and 700 °C, with its major reflection at 2-theta of 19.71°. However, this mineral decomposes at a temperature of 900 °C since this diffracting angle (19.71°) is no longer visible. On increasing the temperature to 900 °C, quartz starts to transform to tridymite, having its major diffraction peak at 2-theta = 23.22° [19]. It is also noted that when firing at a higher temperature, calcite starts to reduce slowly. In fact at 900 °C only a fraction of the major diffraction peak of calcite at 29.41° is observed, showing that the mineral calcite present in the sample decomposes to lime, CaO. The products of decomposition of limestone, namely lime, then react with the mineral quartz to form Wollastonite, having its major diffraction peak at 2-theta = 27.52°. The reaction between lime and quartz to form Wollastonite is given below in Equation 5.1 [22]:

$$CaO(s) + SiO_{2(s)} \rightarrow CaSiO_{3(s)} \quad (5.1)$$

As explained previously, silicates or glauconites present in the microstructure have transformed to hematite at 900 °C [35]. This is supported by the presence of the major reflection for hematite at 2-theta of 33.16°.

Figures 4.46 and 4.47 show the diffractograms comparing the fired briquettes with variation in soaking time. The briquettes fired at 500 and 900 °C exhibited a similar behaviour to the diffractograms in these figures. X-ray reflections are more or less the same when varying the soaking time, with the exception that the peaks have a different intensity [47]. When firing for a duration of 30 minutes, the peaks have a higher intensity since the samples are exposed for a short amount of time and so this time is not sufficient enough for the mineralogical transformation to occur. In fact, it is clear that peaks of calcite diminished at a soaking time of 120 minutes, which shows that calcium carbonate decomposed more when left for a prolonged soaking time.

Figures 4.48 and 4.49 show the diffractograms comparing the fired briquettes with variation in firing atmosphere. The briquettes fired at 700 °C and 900 °C exhibited a similar behaviour to the diffractograms in these figures. There were no differences between these firing atmospheres in terms of mineralogical content [47]. However, the interesting part is that samples fired in an oxidising atmosphere at 500 °C resulted in less abundancy of quartz and a higher calcite peak. This is possibly due to the different firing parameters, particularly the firing atmosphere.

In Figure 4.50 it was noted that the 63_900_120_Oxi and 125_900_120_Oxi briquettes had no differences in mineralogical content which indicates that local variability of the material could have an effect on this. More Wollastonite and tridymite were present when the 63 μm sample was fired to a temperature of 900 °C in oxidizing conditions. This is most probably due to the fact that the 125 μm sample would almost certainly have more calcium carbonate retained, meaning that a different proportion of components was present at the firing stage. Also, since the 63 μm sample has smaller particles, there is more surface onto which reaction can take place. Therefore, the extent of reaction could be higher in the 63 μm clay even though the temperature is the same in both cases.

5.6 Change in Hardness

In Figure 4.51 it is evident that on increasing the temperature in an oxidising atmosphere, the hardness increases, thus confirming that the clay has transformed into a fired product/ceramic [6, 17]. The samples fired at 500 °C had a very low hardness when compared to samples fired at higher temperatures, showing that the ceramic change is far from complete at 500 °C. The highest hardness achieved in an oxidising atmosphere occurs at 900 °C which is possibly due to the transformation of minerals.

From the bar graph in Figure 4.51, it is observed that the outer layer is harder than the core layer due to the diffusion where the outer layer is transformed into a ceramic first. However, contrary to expectations, the core hardness was greater than the outer layer hardness, when samples were fired at 700 °C. This could be due to the high variability of the results obtained, as can be seen in Table 4.16. This high variability is also demonstrated in Figure 4.53 where it is clearly seen that certain hardness values of the outer layer and core overlap.

The 125_900_120_Oxi briquette had a slightly higher outer layer hardness than the fired sample sieved to 63_900_120_Oxi briquette. This could be due to the fired 125 μm sample having more inclusions embedded in the matrix. However, the 125 μm sample had a lower core hardness. This could potentially be due to the variability of results. It was also noted that the highest discrepancy was seen in the hardness results of the outer layer and core of the two samples with varying mesh size.

Figure 4.52 demonstrates the hardness results of the briquettes fired in a reducing atmosphere. From this figure, samples fired at 500 °C had the lowest hardness. This explains why the 63_500_30_Red sample fell apart during the hardness test and was thus not included. It was noticed that on increasing the temperature in reducing conditions, the hardness increased slightly, however, the different samples fired at 700 °C and 900 °C had roughly the same hardness, ranging from 37.1 – 44.5 HK. This is potentially due to the grey cross-section produced by the reducing atmosphere. From this experiment, there was no difference between the observable effects in relation to hardness between the samples treated for different soaking times in a reducing atmosphere.

From this experiment it is evident that samples fired in an oxidising atmosphere are harder than those fired in a reducing atmosphere. Although these briquettes have the same minerals, there could potentially be a problem with the association of minerals in a reducing atmosphere. This is demonstrated in Figures 4.37 and 4.38, where the sample fired in a reducing atmosphere (Figure 4.38) is less compact than the briquette fired in an oxidising atmosphere (Figure 4.37).

6. Conclusion

This Chapter summarises the findings from the research carried out as part of the dissertation work. This Chapter also includes scope for future work that can be carried out to develop further this study.

6.1 Concluding Remarks

The main conclusions that can be drawn from this study are summarised below:

- The samples sieved to 63 μm needed more water of plasticity to manufacture the clay sample into briquettes, resulting in a higher %LDS.
- Colour, porosity and voids, microstructure, mineralogy, and material hardness were all observed to alter with increasing firing temperature. This shows that firing temperature is a parameter which affects the outcome of the end product more than the range of parameters considered.
- In an oxidising atmosphere, an increasing in firing temperature resulted in the briquettes turning more red. On increasing the firing temperature in a reducing atmosphere, the briquettes turned from black to grey. Change in core colour was also noted as well as the thickness of the core where it was found that when the samples were fired for prolonged soaking times, the thickness was lower. Briquettes fired at the highest temperature in both oxidising and reducing conditions had the most voids present in the microstructure.
- At 500 °C it was observed that the fired samples in an oxidising and reducing atmosphere had a similar frequency of pores present in the microstructure. The kaolinite sheets are evident under the scanning electron microscope, showing that sintering has not occurred yet and the ceramic change is yet to occur. At 900 °C, there were differences in the microstructure between the samples fired using different atmospheres. The briquette fired in an oxidising atmosphere had less porosity, thus showing that the sample has been sintered in oxidising conditions. From SEM imaging it was also noted that at this temperature, a more compact structure was observed, demonstrating that the ceramic transformation has occurred.

- On increasing the firing temperature, calcite decomposed almost completely, forming calcium oxide, which reacted with quartz present in the microstructure to form wollastonite in the process. Also, quartz started to transform into tridymite. Hematite was also detected at this firing temperature.
- In an oxidising atmosphere, an increase in firing temperature resulted in a harder ceramic. On the other hand, ceramics produced in a reducing atmosphere, had a lower hardness and this hardness roughly remained the same. Generally for oxidising conditions, the outer layer hardness is harder than the core hardness, demonstrating that the core layer has not transferred to a ceramic yet.

Coming back to the research question in Chapter 1 (Introduction), '*Can sourced clay from the Maltese Islands be converted into pottery?*', it can be concluded that the answer is affirmative since a ceramic was produced from locally sourced clay. The aim to produce a ceramic from sourced Maltese clay by experimental firings, as described in Chapter 1, was achieved in this dissertation.

6.2 Future Work

Below are some suggestions for possible future work to improve the results obtained and to gain more information on the fired samples:

- Micro Raman Spectroscopy could be used to help in the identification of inclusions such as magnetite and hematite since these could not be identified with optical microscopy, EDS or XRPD analysis.
- This research could be extended to lower or higher firing temperatures, ranging from 200 to 1400 °C. This is because it would be interesting to see what happens at both lower and elevated temperatures.
- Finally, the clay samples can be sieved to different fractions to verify if a change in mesh size has an effect on the firing procedure. Hence, a wider range on the Wentworth Scale Chart is to be chosen.

References

[1] J. Hunter and I. Ralston, *The archaeology of Britain*. London: Routledge, 2009.

[2] M. Richards, R. Schulting and R. Hedges, "Sharp shift in diet at onset of Neolithic", *Nature*, vol. 425, no. 6956, pp. 366-366, 2003. [Accessed 27 July 2020].

[3] T. Lewis and B. Collins, *Near Eastern Archaeology*. Atlanta: American Schools of Oriental Research, 2004.

[4] H. Baccour, M. Medhioub, F. Jamoussi and T. Mhiri, "Influence of firing temperature on the ceramic properties of Triassic clays from Tunisia", *Journal of Materials Processing Technology*, vol. 209, no. 6, pp. 2812-2817, 2009. [Accessed 17 August 2020].

[5] C. Sinopoli, "Book Review of The Oxford Handbook of Archaeological Ceramic Analysis, edited by Alice M.W. Hunt", *American Journal of Archaeology*, vol. 122, no. 4, 2018. [Accessed 19 August 2020].

[6] V. Lee and T. Yeh, "Sintering effects on the development of mechanical properties of fired clay ceramics", *Materials Science and Engineering: A*, vol. 485, no. 1-2, pp. 5-13, 2008. [Accessed 21 August 2020].

[7] "CORDIS | European Commission", *Cordis.europa.eu*, 2020. [Online]. Available: https://cordis.europa.eu/project/id/795633/reporting. [Accessed 17 September 2020].

[8] C. John, M. Mutti and T. Adatte, "Mixed carbonate-siliciclastic record on the North African margin (Malta)—coupling of weathering processes and mid Miocene climate", *Geological Society of America Bulletin*, vol. 115, pp. 217-229, 2003. [Accessed 5 October 2020].

[9] R. Gauci and J. Schembri, *Landscapes and landforms of the Maltese islands*. [Place of publication not identified]: SPRINGER NATURE, 2019, pp. 31-41.

[10] House, M.R., Dunham, K.C. and Wigglesworth, J.C., “Geology and structure of the Maltese Islands”, *Malta: Background for development. University of Durham*, pp. 24-33, 1961 [Accessed 7 October 2020].

[11] M. Pedley, M. Clarke and P. Galea, *Limestone isles in a crystal sea*. San Gwann, Malta: Publishers Enterprises Group, 2002, pp. 35-59.

[12] O. Magri, "A Geological and Geomorphological Review of the Maltese Islands with Special Reference to the Coastal Zone", *Territoris*, vol. 6, pp. 9-26, 2006. [Accessed 15 October 2020].

[13] M. Soldati, M. Barbieri, S. Biolchi and F. Buldrini, "Multidisciplinary geological excursion in the open-air laboratory of the Island of Malta 11-18 November 2010", *Dipartimento di Scienza della Terra*, pp. 7-8, 2010. [Accessed 15 October 2020].

[14] H. PEDLEY, "Miocene bioherms and associated structures in the Upper Coralline limestone of the Maltese Islands: their lithification and palaeoenvironment", *Sedimentology*, vol. 26, no. 4, pp. 577-591, 1979. [Accessed 20 October 2020].

[15] J. Murray, "The Maltese Islands, with special reference to their geological structure", *Scottish Geographical Magazine*, vol. 6, no. 9, pp. 449-488, 1890. [Accessed 20 October 2020].

[16] P. Rice, *Pottery analysis*, 2nd ed. Chicago, Illnois: University of Chicago Press, 2015.

[17] N. Cuomo di Caprio, *Ceramics in archaeology Volume 1*. 2017.

[18] C. Orton and M. Hughes, *Pottery in archaeology*, 2nd ed. Cambridge: Cambridge University Press, 2013.

[19] D. Santacreu, *Materiality, Techniques and Society in Pottery Production*. Warsaw/Berlin: De Gruyter Open Ltd, 2014.

[20] W. Callister and D. Rethwisch, *Materials science and engineering*, 9th ed. Wiley, 2014.

[21] A. Cordell, N. Wallis and G. Kidder, "Comparative Clay Analysis and Curation for Archaeological Pottery Studies", *Advances in Archaeological Practice*, vol. 5, no. 1, pp. 93-106, 2017. [Accessed 4 November 2020].

[22] A. De Bonis, G. Cultrone, C. Grifa, A. Langella and V. Morra, "Clays from the Bay of Naples (Italy): New insight on ancient and traditional ceramics", *Journal of the European Ceramic Society*, vol. 34, no. 13, pp. 3229-3244, 2014. [Accessed 13 November 2020].

[23] L. Beuselinck, G. Govers, J. Poesen, G. Degraer and L. Froyen, "Grain-size analysis by laser diffractometry: comparison with the sieve-pipette method", *CATENA*, vol. 32, no. 3-4, pp. 193-208, 1998. [Accessed 17 November 2020].

[24] J. Grech, "Characterisation of Roman Pottery from Malta", Undergraduate, University of Malta, 2019.

[25] I. Bernal, H. Cabezas, C. Espitia, J. Mojica and J. Quintero, "ANÁLISIS PRÓXIMO DE ARCILLAS PARA CERÁMICA", Revista de la Academia Colombiana de Cencias, vol. 27, no. 105, pp. 569-578, 2003. [Accessed 17 November 2020].

[26] S. Ferrari and A. Gualtieri, "The use of illitic clays in the production of stoneware tile ceramics", Applied Clay Science, vol. 32, no. 1-2, pp. 73-81, 2006. [Accessed 17 November 2020].

[27] R. Alonso Alcalde, J. Baena Preysler and D. Canales, *Playing with the time. Experimental archaeology and the study of the past*, 1st ed. [Madrid]: Servicio de Publicaciones de la UAM, 2017, pp. 231-235.

[28] K. Harry, L. Frink, C. Swink and C. Dangerfield, "An Experimental Approach to Understanding Thule Pottery Technology", *North American Archaeologist*, vol. 30, no. 3, pp. 291-311, 2009. [Accessed 5 December 2020].

[29] S. Karaman, S. Ersahin and H. Gunal, "Firing temperature and firing time influence on mechanical and physical properties of clay bricks", *Journal of Scientific and Industrial Research*, vol. 65, pp. 153-159, 2005. [Accessed 13 December 2020].

[30] M. Webb and F. de Laguna, "Travels among the Dena: Exploring Alaska's Yukon Valley", The Western Historical Quarterly, vol. 33, no. 1, p. 95, 2002. [Accessed 17 December 2020].

[31] I. Žuŝihovskaâ, Prehistoric pottery-making of the Russian Far East. Oxford: Archaeopress, 2005.

[32] D. Arnold, "Ceramic Theory and Cultural Process after 25 Years", *Ethnoarchaeology*, vol. 3, no. 1, pp. 63-98, 2011. [Accessed 17 December 2020].

[33] J. Skibo, M. Schiffer and K. Reid, "Organic-Tempered Pottery: An Experimental Study", American Antiquity, vol. 54, no. 1, pp. 122-146, 1989. [Accessed 17 December 2020].

[34] M. Carter, "Prehistoric Ceramic Production: Raw Materials and Firing Methods of La Crosse Locality Oneota.", *Joural of Undergraduate Research*, vol. 5, pp. 261-280, 2002. [Accessed 4 February 2021].

[35] M. Jordán, A. Boix, T. Sanfeliu and C. de la Fuente, "Firing transformations of cretaceous clays used in the manufacturing of ceramic tiles", *Applied Clay Science*, vol. 14, no. 4, pp. 225-234, 1999. [Accessed 19 February 2021].

[36] F. Tencariu, M. Alexianu, V. Cotiugă, V. Vasilache and I. Sandu, "Briquetage and salt cakes: an experimental approach of a prehistoric technique", *Journal of Archaeological Science*, vol. 59, pp. 118-131, 2015. [Accessed 13 March 2021].

[37] D. Albero, "Pastas desgrasadas con calcita y pastas desgrasadas con materia vegetal: aproximación experimental", Boletín del Laboratorio de Petrología y Conservación Cerámica, vol. 2, no. 2, pp. 18-34, 2010. [Accessed 17 March 2021].

[38] D. Papadopoulou, M. Lalia-Kantouri, N. Kantiranis and J. Stratis, "Thermal and mineralogical contribution to the ancient ceramics and natural clays characterization", Journal of Thermal Analysis and Calorimetry, vol. 84, no. 1, pp. 39-45, 2006. [Accessed 17 March 2021].

[39] A. Khalfi and P. Blanchart, "Desorption of water during the drying of clay minerals. Enthalpy and entropy variation", Ceramics International, vol. 25, no. 5, pp. 409-414, 1999. [Accessed 17 March 2021].

[40] W. Worrall, Clays and ceramic raw materials. London: Elsevier applied Science, 1986.

[41] R. Thér and M. Gregor, "Experimental Reconstruction of the Pottery Firing Process of Late Bronze Age Pottery from North-Eastern Bohemia", *Archaeological Ceramics: A Review of Current Research. BAR international Series 2193*, pp. 128-142, 2011. [Accessed 24 March 2021].

[42] S. Harrison, "An Experimental Prehistoric Pottery Firing at Harray, Orkney", *Antiquity*, vol. 82, p. 317, 2008. [Accessed 24 March 2021].

[43] M. Maggetti, C. Neururer and D. Ramseyer, "Temperature evolution inside a pot during experimental surface (bonfire) firing", *Applied Clay Science*, vol. 53, no. 3, pp. 500-508, 2011. [Accessed 24 March 2021].

[44] R. Thér, "Experimental Pottery Firing in Closed Firing Devices from the Neolithic —Hallstatt Period in Central Europe", *EuroREA*, vol. 1, pp. 35-82, 2004. [Accessed 24 March 2021].

[45] O. Gosselain, "Bonfire of the enquiries. Pottery firing temperatures in archaeology: What for?", *Journal of Archaeological Science*, vol. 19, no. 3, pp. 243-259, 1992. [Accessed 24 March 2021].

[46] A. Livingstone Smith, "Bonfire II: The Return of Pottery Firing Temperatures", *Journal of Archaeological Science*, vol. 28, no. 9, pp. 991-1003, 2001. [Accessed 24 March 2021].

[47] Y. Pontikes and G. Angelopoulos, "Effect of firing atmosphere and soaking time on heavy clay ceramics with addition of Bayer's process bauxite residue", Advances in Applied Ceramics, vol. 108, no. 1, pp. 50-56, 2009. [Accessed 4 April 2021].

[48] "Munsell Soil Color Charts | Munsell Soil Color charts | Online-Shop | Dr. F. Krantz, Rheinisches Mineralien-Kontor", *Krantz-online.de*, 2009. [Online]. Available:https://www.krantzonline.de/en/onlineshop/___product/411/___showCat/146/___pageid/16/munsell_soil_color_charts.html. [Accessed: 4 April 2021].

[49] D. Albero Santacreu and G. Mateu Vicens, "Raw Materials and Pottery Production at the Late Bronze and Iron Age Site of Puig de Sa Morisca, Mallorca, Spain", *Geoarchaeology*, vol. 27, no. 4, pp. 285-299, 2012. [Accessed 4 April 2021].

[50] G. Asciak, "Characterisation and identification of fossil and mineral inclusions in Roman pottery from one site in Victoria, Gozo", Postgraduate, University of Malta, 2018.

[51] P. Quinn, *Ceramic petrography*. Oxford: Archaeopress, 2013.

[52] D. Clinton and R. Morrell, "Hardness testing of ceramic materials", *Materials Chemistry and Physics*, vol. 17, no. 5, pp. 461-473, 1987. [Accessed 21 April 2021].

[53] D. Arnold, *Ceramic theory and cultural process*. Cambridge: Cambridge University Press, 1985.

[54] A. Bonanno, *Malta: Phoenician, Punic, and Roman*. [Valletta (Malta)]: Midsea books, 2005, pp. 215-216.

[55] E. Richard-Tremeau, A. Humann and L. Xuereb, "Wet Sieving of Clay Samples for Archaeological Research", University of Malta, Msida, 2021.

[56] F. Andreatta et al., "Degradation of PTFE non-stick coatings for application in the food service industry", *Engineering Failure Analysis*, vol. 115, p. 104652, 2020 [Accessed 24 April 2021].

[57] J. Betts, "Low Magnification Micrographs of Pottery with Meiji Techno Stereomicroscope and Microtec Camera", University of Malta, Msida, 2018.

[58] W. Saputra, *A new roundness scale for sedimentary particles (after Powers)*, 2016 [Accessed 26 April 2021].

[59] ASTM International, "Standard Test Method for Knoop Indentation Hardness of Advanced Ceramics", C1326 − 13, 2013.

[60] E. Ndreçka, N. Civici, E. Beqiraj and I. Gjipali, "Results from Multi Technique Investigation of Pottery from Different Early Neolithic Sites in Albania", *Journal of Materials Science and Chemical Engineering*, vol. 05, no. 09, pp. 10-26, 2017. [Accessed 5 May 2021].

[61] E. Basso, C. Capelli, M. Riccardi and R. Cabella, "A particular temper: mineralogical and petrographic characterisation of ceramic fabrics with glauconitic inclusions", *ArchéoSciences*, no. 32, pp. 93-97, 2008. [Accessed 5 May 2021].

[62] S. Gualtieri, "Ceramic raw materials: how to establish the technological suitability of a raw material", *Archaeological and Anthropological Sciences*, vol. 12, no. 8, 2020. [Accessed 5 May 2021].